Journal of Controlled Release 359 (2023) 161–174

Contents lists available at ScienceDirect

Journal of Controlled Release

journal homepage: www.elsevier.com/locate/jconrel

Temozolomide-fatty acid conjugates for glioblastoma multiforme: *In vitro* and *in vivo* evaluation

Reena Jatyan [a], Deepak Kumar Sahel [a], Prabhjeet Singh [a], Rajeev Sakhuja [b], Anupama Mittal [a], Deepak Chitkara [a,*]

[a] Department of Pharmacy, Birla Institute of Technology and Science Pilani, Vidya Vihar, Pilani 333031, Rajasthan, India
[b] Department of Chemistry, Birla Institute of Technology and Science Pilani, Vidya Vihar, Pilani 333031, Rajasthan, India

ARTICLE INFO

Keywords:
Temozolomide
Glioblastoma multiforme
Fatty-acid conjugates
Blood-brain barrier

ABSTRACT

Glioblastoma multiforme (GBM) is the deadliest brain tumor with a poor prognosis and limited therapeutic options. Temozolomide (TMZ) is the first-line chemotherapeutic agent used for the treatment of GBM; however, it suffers from several limitations, including short half-life, rapid metabolism, <1% brain bioavailability, methyl guanine methyl transferase (MGMT) based chemoresistance, and hematological toxicities. Several approaches have been adopted to overcome these limitations, particularly by using nanotechnology-based systems, but its physicochemical properties make TMZ challenging to load into these nanocarriers. In the current research, we conjugated TMZ with different fatty acids, i.e., linoleic acid (LA), oleic acid (OA), and palmitic acid (PA), to obtain TMZ-fatty acid conjugates, which are comparatively hydrophobic, less prone to degradation and potent. These conjugates were thoroughly characterized using ^{1}H NMR spectroscopy, high-resolution mass spectrometry (HR-MS), and reverse phase-high performance liquid chromatography (RP-HPLC). The synthesized conjugates, namely Temozolomide-oleic acid (TOA,**6R$_1$**), Temozolomide-linoleic acid (TLA, **6R$_2$**), and Temozolomide-palmitic acid (TPA, **6R$_3$**), showed an IC_{50} of 101.4, 67.97, and 672.04 μM, respectively in C_6 cells and 428.257, 366.43 and 413.69 μM, respectively in U87-MG cells. On the other hand, the free TMZ showed an IC_{50} of >1000 μM and 564.23 μM in C_6 and U87-MG, respectively. Further, the *in vivo* efficacy of the TMZ-fatty acid conjugates was evaluated in the C_6-induced orthotropic rat glioblastoma model, wherein the TMZ-fatty acid conjugate showed improved survival rate (1.6 folds) and overall health of the animals. Collectively, the conjugation of fatty acids with TMZ improves its anticancer potential against glioblastoma multiforme (GBM).

1. Introduction

Glioblastoma multiforme (GBM) is the most challenging brain tumor that occurs in primary astrocytes and accounts for 60% of all primary brain tumors in adults [1]. Despite the availability of chemotherapies for the treatment of GBM, the median survival rate for glioma tumor patients is <14 months [2]. WHO classified brain tumors into four major grades, namely I to IV, based on the severity and histopathological observations. Grade IV is the most aggressive and may penetrate, proliferate, and exist in an undifferentiated, difficult-to-treat form [3,4]. GBM is an uncommon kind of tumor with a worldwide incidence of 10 per 100,000 persons regardless of age [5]; however, males are more likely than women to get brain tumors [6].

Temozolomide (TMZ), an imidazotetrazine derivative of dacarbazine, is a first-line drug for the treatment of patients with GBM [7]. TMZ is given *via* oral and intravenous routes. The marketed formulations of Temozolomide (TMZ) are capsule (Temodal Capsules (100 mg/Capsule), Temoside (100 mg/capsule) and injection formulations (Temodar for injection (100 mg/vial), The specific dose of TMZ varies depending on the treatment regimen, but it is typically given in daily doses ranging from 75 to 150 mg/m^2. Most tumor cells are innately resistant to TMZ at pharmacotherapeutic doses or quickly develop resistance. Further, due to the overexpression of MGMT, 50% of TMZ-treated patients do not respond to this treatment [7]. On administration, TMZ spontaneously converts into 5-(3-methyltriazen-1-yl) imidazole-4-carboxamide (MTIC) form at physiological pH by releasing the $-CO_2$ from the imidazotetrazine ring, a six-membered ring that further gets open to convert into MTIC [8]. MTIC form is unstable and

* Corresponding author at: Department of Pharmacy, Birla Institute of Technology and Science (BITS)-Pilani, Pilani Campus, Vidya Vihar, Pilani 333 031, Rajasthan, India.
E-mail address: deepak.chitkara@pilani.bits-pilani.ac.in (D. Chitkara).

https://doi.org/10.1016/j.jconrel.2023.05.012
Received 28 October 2022; Received in revised form 6 April 2023; Accepted 9 May 2023
Available online 8 June 2023

converts into AIC, resulting in the release of methyl diazonium ions. The cation reacts with the nucleophile site and performs the methylation at the DNA to induce autophagy [9]. TMZ is a potent anticancer drug with 100% oral bioavailability [10] and causes apoptosis *via* autophagy [11]. There are several limitations associated with TMZ viz., short half-life (1.8 h) [12], rapid metabolism at physiological pH (>7.0) [9], only 1% of the administered dose reaches the brain in intact form, hydrophilicity, and development of chemo-resistance [13]. Attempts have been made to improve the TMZ efficacy using nanocarrier-mediated delivery approaches. Several nanocarriers viz., liposomes, solid lipid nanoparticles, polymer-drug conjugate,and polymeric micelles were screened in recent research [14]. The water solubility of the TMZ limits the loading efficiency into the hydrophobic core of nanocarriers and therefore makes it difficult to achieve therapeutic outcomes. In 2015, Gao et al. prepared TMZ-loaded liposomes by the conventional proliposome method. The prepared nano formulation showed a narrow range particle size of 156.70 ± 11.40 nm with a PDI of 0.29 ± 0.04. The reported encapsulation efficiency was 35.45 ± 1.48% at a theoretical loading of 2.81 ± 0.20% *w/w* [15]. The conjugation strategy is also an important way to overcome the delivery difficulties wherein TMZ was conjugated to polymers or small molecules. TMZ–Perillyl alcohol conjugate (TMZ–POH) is a new TMZ analog synthesized by conjugating TMZ with POH, a naturally occurring monoterpene that enhances TMZ's cytotoxicity in several cancers [16,17]. According to Song et al., TMZ-POH suppressed MGMT that was dependent on the proteasomal pathway, and this inhibition was a key contributor to the improvement in its overall efficiency. [16]. Ward et al., synthesized a polymer (methacryloyloxyethyl phosphorylcholine) using reversible addition-fragmentation chain-transfer (RAFT) polymerization and conjugated it with TMZ using a disulfide linker. The resulting polymer-TMZ conjugate enhanced TMZ stability in terms of half-life to the extent of 19 folds, along with improved cytotoxicity in glioma cells [18]. In 2020, Du et al. reported a novel conjugate of TMZ with doxorubicin [19] to exert a synergistic effect on conformational changes in the DNA. A nanocarrier containing copper-bound apoferritin was developed with 83% *w/w* loading efficiency for TMZ-DOX conjugate [19]. Further, Peng et al. developed a folate-targeted triblock polymer (Fa-PEG-PEI-PCL, Fa-PEC) and loaded TMZ along with surface decoration with siRNA targeting BCL-2 [20]. Collectively, the nano carrier-based approaches showed a better effect than the free TMZ.

Fatty acids are saturated or unsaturated long-chain hydrocarbons with a –COOH terminal group. In addition, they possess other properties such as antioxidant, anticancer, antiproliferative action, etc. Recently, fatty acids have been used to make prodrugs by conjugating them with small molecules [21]. We have earlier reported lisofylline-linoleic acid conjugate for the treatment of diabetes mellitus. The outcomes of the study showed that the conjugate had self-assembling potential with modified pharmacokinetic properties (5-fold) [22]. Ke et al., reported a linoleic acid-conjugated paclitaxel, which enhanced the anticancer, and anti-proliferative potential along with brain tumor targeting *via* improving BBB permeability. Further, the conjugate showed higher cellular uptake due to inhibition of p-gp efflux, improved *in vivo* kinetic behavior, and antitumor efficacy in tumor-bearing animals [23]. Fatty acids were also explored for their MGMT depletion property, for example, Goder et al. stated that lipoic acid downregulated MGMT expression and induces an autophagy-like response in colorectal tumor cells [24].

In the current study, we have synthesized TMZ-fatty acid conjugates **($6R_{1-3}$)**, namely TMZ-oleic acid **(TOA, $6R_1$)**, TMZ-linoleic acid **(TLA, $6R_2$)**, and TMZ-palmitic acid **(TPA, $6R_3$)**, with a hydrazine linkage (-NH-NH-). The conjugates **($6R_{1-3}$)** were thoroughly characterized using ^{1}H NMR spectroscopy and mass spectrometry. The purity of the conjugates (**$6R_{1-3}$**) was determined using RP-HPLC and further evaluated for *in vitro* cell culture in U87-MG and C_6 cells for cytotoxicity, cell migration, and apoptosis-inducing potential. The expression of MGMT protein was evaluated using western blotting. Further, the *in vivo* efficacy of **($6R_1$)** was evaluated in the C_6 cells induced orthotropic rat glioma model, wherein the overall survival rate, change in body weight, tumor load, brain weight, histological evaluation, and metastasis were evaluated. Collectively, the aim of the present study is to investigate both the physiochemical property and biological effect of the conjugates with respect to free drug. The outcomes demonstrated that fatty acid conjugates improved the physiochemical property of TMZ, such as plasma stability and hydrophobicity. Furthermore, the biological effects were also found to improve, as indicated by lower IC_{50} value and higher apoptosis, improved pharmacokinetic, and overall *in vivo* efficacy.

2. Materials

Temozolomide (TMZ) was purchased from Carbanio, India. Oleic acid, Linoleic acid, and Palmitic acid were purchased from ACME synthetic chemicals (India). Acetyl chloride, Hydrazine hydrate (80%), and *N*,*N*-diisopropylethylamine (DIPEA) were purchased from TCI Chemicals India Pvt. Ltd. (Chennai, India). *N*-(3-Dimethylaminopropyl)-*N*′-ethyl carbodiimide hydrochloride (EDC.HCl) and Hydroxy benzotriazole (HOBt) were purchased from Spectrochem Ltd. (Mumbai, India). Dulbecco's Modified Eagle's medium (DMEM), Fetal Bovine Serum (FBS), BCA kit, Annexin V Alexa fluor 488 conjugates, and annexin binding buffer were purchased from Thermo Fisher Scientific (MA, USA). 3-(4,5-dimethyl-thiazol-2-yl)-2,5-diphenyl tetrazolium bromide (MTT) was purchased from Sisco Research Laboratories (Mumbai, India). Bovine Serum Albumin (BSA), Dimethyl Sulfoxide (DMSO), and Phosphate Buffered Saline (PBS) pH 7.4 were purchased from Hi-Media Laboratories. All other reagents and solvents used in this research were purchased from local vendors.

3. Methodology

3.1. Synthesis and characterization of TMZ-acid (2)

A previously reported method was used to convert the amide group (-CO-NH_2) of TMZ **(1)** to a free –COOH end group [19] (Fig. 1). Briefly, TMZ (1.0 g) **(1)** was dissolved in 8 mL of concentrated sulphuric acid (H_2SO_4) and kept for continuous stirring for 30 min. at room temperature. Further, the reaction was transferred to a cold condition, and sodium nitrite (2.6 g) in 11.2 mL water was added dropwise under continuous nitrogen purging. The resulting solution was kept on stirring at room temperature overnight, which was followed by the addition of 10 mL of ice-cold water to precipitate the product. The crude TMZ-acid **(2)** was obtained by vacuum filtration and characterized using ^{1}H NMR, FT-IR, and mass spectrometry.

3.2. Synthesis of the hydrazide-modified fatty acids ($5R_{1-3}$)

A two-step chemical reaction was adopted for the -COOH end group modification of fatty acid to hydrazide (−NH−NH_2) group. Firstly, the fatty acid (1.0 g) **($3R_{1-3}$)** was dissolved in 15 mL of dry ethanol and kept on stirring for 10 min. at room temperature. Further, 500 μL of acetyl chloride was added dropwise to the reaction mixture and kept for 3 h at room temperature. The reaction was quenched by adding sodium bicarbonate (2.0 g), followed by celite filtration to get the crude esterified fatty acid **($4R_{1-3}$).** The resulting product was directly used in the next reaction to obtain a hydrazide-modified fatty acid **($5R_{1-3}$)** (Fig. 1). Briefly, 800 mg of the esterified fatty acid **($4R_{1-3}$)** in 15 mL of dry ethanol was taken in a 50 mL round-bottom flask, followed by the addition of 1 mL of 80% hydrazine hydrate dropwise at room temperature. Further, the reaction was refluxed for 6 h and monitored using TLC with a solvent system comprising ethyl acetate and hexane (50:50). The reaction was quenched by adding 15 mL of ice-cold water, and the product was extracted using ethyl acetate. The organic layer was separated, dried over sodium sulfate, and concentrated using a rotary evaporator to get a yellow/whitish semisolid hydrazide-modified fatty

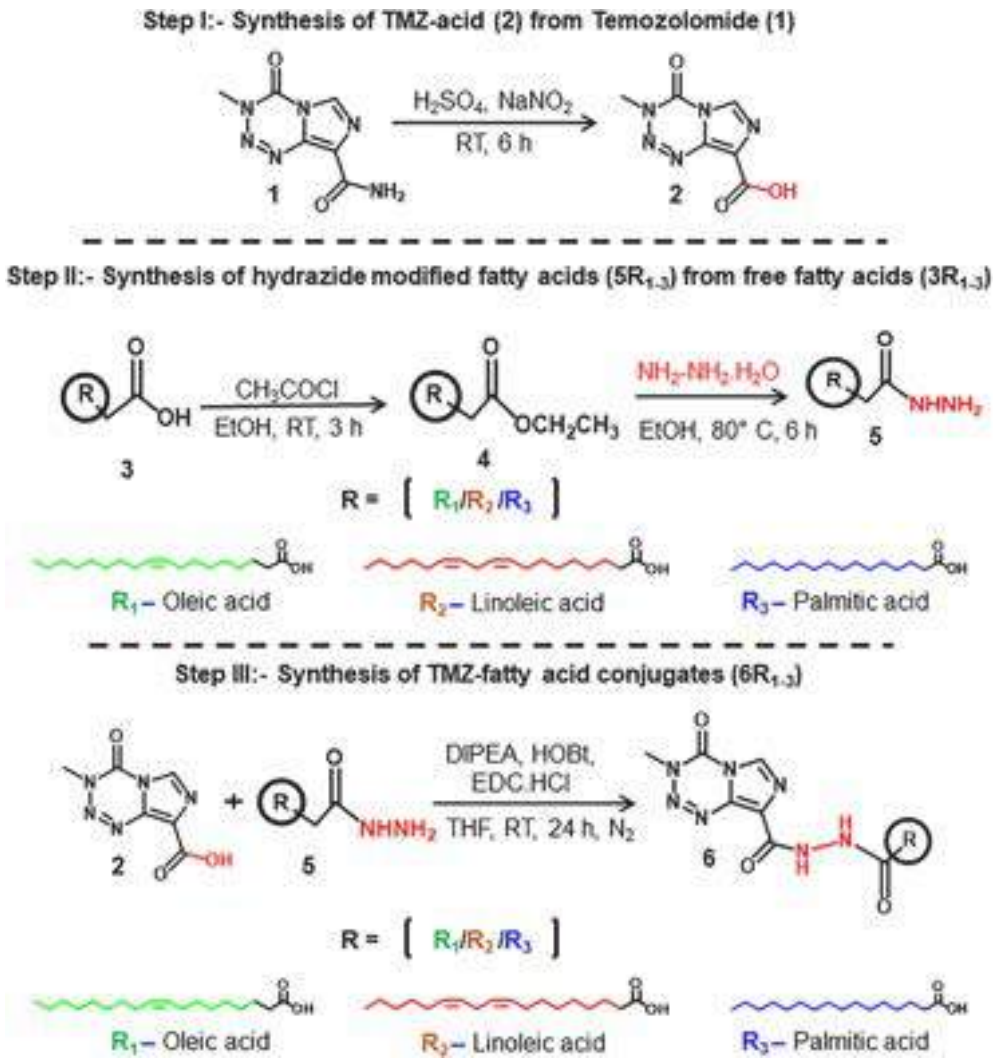

Fig. 1. Synthetic scheme to obtain TMZ-fatty acid conjugates **($6R_{1-3}$)**, Step I: Conversion of TMZ **(1)** to TMZ-Acid **(2)**; Step II: Synthesis of hydrazide-modified fatty acids **($5R_{1-3}$)** from fatty acids **($3R_{1-3}$)**; and Step III: Synthesis of TMZ-fatty acid conjugates **($6R_{1-3}$)** by coupling TMZ-Acid **(2)** and hydrazide modified fatty acids **($5R_{1-3}$)** by means of EDC/HOBt reaction.

acid **($5R_{1-3}$)**. The same protocol was utilized to synthesize all three hydrazide-modified fatty acids (**$5R_1$**, **$5R_2$**, and **$5R_3$**). The resulting products were characterized using ^{1}H NMR spectroscopy and mass spectrometry.

3.3. Synthesis of TMZ-fatty acid conjugates ($6R_{1-3}$)

The TMZ-fatty acid conjugates **($6R_{1-3}$)** were synthesized using EDC/HOBt-mediated amide coupling between TMZ-acid **(2)** and hydrazide-modified fatty acids **($5R_{1-3}$)**. Briefly, TMZ-acid **(2)** (500 mg) and fatty acid hydrazide **($5R_{1-3}$)** (~800 mg) were dissolved in tetrahydrofuran (THF, 10 mL) followed by the addition of DIPEA (400 μL), and the reaction was stirred at room temperature for 15 min. to activate the –COOH group of TMZ-acid **(2)**. Thereafter, the reaction mixture was kept at 0 °C and HOBt (346 mg) followed by EDC.HCl (476.81 mg) in 5 mL of THF was subsequently ad,ded and the mixture was stirred at room temperature for 24 h under an inert atmosphere of nitrogen. After this, 20 mL of ice-cold water was added to the reaction mixture, and the desired product was extracted using dichloromethane (DCM). The organic layer was separated, dried over anhydrous $NaSO_4$, and concentrated using rotary evaporator to obtain crude products. Further, TMZ-Fatty acid conjugates **($6R_{1-3}$)** were purified by column chromatography using DCM and methanol as mobile phase in a ratio of 95:05. The final products **($6R_{1-3}$)** were characterized using ^{1}H NMR spectroscopy, and mass spectrometry. The purity of the conjugates was determined using RP-HPLC with a mobile phase comprising ACN/MilliQ (0.1% formic acid) in a proportion of 95:05.

3.4. Cell culture assays

Glioma cells (C_6 and U87-MG) were obtained from the National Centre for Cell Science (NCCS, Pune) and were maintained in Dulbecco's Modified Eagle's medium (DMEM) supplemented with 10% fetal bovine serum (FBS) and 1% penicillin/streptomycin antibiotics under a humid environment at 37 °C with 5% CO_2. The cells were allowed to grow up to 80% confluency before seeding for experimentation.

3.5. Cytotoxicity assay

C_6 or U87-MG glioma cells were seeded in a 96-well culture plate with a density of 5×10^3 cells/well and allowed to grow overnight in a humid environment with 5% CO_2 at 37 °C temperature. Afterward, cells were treated with 25 uM to 1000 μM concentration of free TMZ, free OA, free LA, free PA, TMZ + OA, TMZ + LA, TMZ + PA, TOA **($6R_1$)**, TLA **($6R_2$)**, and TPA **($6R_3$)** in 0.05% DMSO. Herein, cells treated with 0.05% DMSO in DMEM media were taken as the negative control. After

treatment, cells were incubated for 72 h followed by replacement of media with fresh DMEM media containing 0.5 mg/mL of 3-(4,5-dimethyl thiazolyl-2)-2,5-diphenyl tetrazolium bromide (MTT) and incubated for 4 h. Further, the MTT-containing media was discarded, and 200 μL of dry DMSO was added to each well to dissolve the formazan crystals. The metabolic activity of cells as a function of cell viability was determined by reading the absorbance at 630 nm using an Epoch microplate spectrophotometer (Biotek Instruments, USA). Herein, the absorbance at 630 nm was subtracted from the absorbance at 570 nm to minimize the background absorbance. The following formula was used to determine the % viability [25].

$$\%\text{Cell viability} = \frac{\text{OD (570 - 630 nm) of treatment group}}{\text{OD (570 - 630 nm) of control group}} \text{X } 100$$

3.6. Migration assay

Briefly, C_6 or U87-MG cells were seeded in 6 well plates and incubated overnight. The next day, the straight-line scratch was made in the monolayer of the cells, and then the debris was removed by washing thrice with PBS followed by the addition of fresh media containing TMZ, TOA, TLA, and TPA with concentrations equivalent to their respective IC_{50} values. Herein, the untreated cells, added with DMSO only, were taken as a negative control. After 48 h, the cells were observed under a microscope (Zeiss, Germany) for tracking the migration of the cells in the scratched area and compared with negative control cells.

3.7. Apoptosis assay

For the analysis of the apoptotic status of C_6 and U87-MG cells treated with TMZ **(1)** and its fatty acid conjugates **($6R_{1-3}$)**, an Annexin V/PI kit-based flow cytometry assay was performed. Briefly, C_6 or U87-MG glioma cells were seeded in 6 well plates with a density of 1×10^5 cells/well followed by overnight incubation at 37 °C with 5% CO_2 in a humid environment. Further, the cells were incubated with different treatments i.e., free TMZ, TMZ + OA, TMZ + LA, TMZ + PA, TOA **($6R_1$)**, TLA **($6R_2$)**, and TPA **($6R_3$)** in 0.05% DMSO for 24 h at their respective IC_{50}. Herein, cells treated with DMSO were taken as a negative control. The cells were trypsinized, centrifuged, and redispersed in Annexin binding buffer followed by the addition of Annexin V/PI, incubated for 5 min in dark, and analyzed using flow cytometry (CytoFlex, Beckman Coulter, USA). Data were interpreted using CytExpert 3.0 software [26].

3.8. Western blotting

Briefly, C_6 or U87-MG cells were seeded in a petri dish with a density of 5×10^5 followed by incubation at 37 °C/5% CO_2 under a humid environment. The next day, the cells were treated with free TMZ, TOA **($6R_1$)**, TLA **($6R_2$)**, and TPA **($6R_3$)** in 0.05% DMSO with a concentration equivalent to their IC_{50} value and incubated for 48 h. Ice-cold RIPA buffer along with protease inhibitor was used to extract the protein from C_6 or U87-MG cells. The protein concentration was determined using a BCA kit (Thermo Scientific, USA), and 25 μg of total protein was loaded and resolved in 12% SDS-PAGE at 95 V for 1.5 h. The protein bands were transferred to nitrocellulose membrane followed by incubation with primary antibody (MGMT, GAPDH) overnight at 4 °C. The membrane was washed with TBST buffer and incubated with 1:1000 times diluted secondary antibody for 1 h at room temperature. Further, the Pierce™ ECL Western Blotting Substrate (Thermo Scientific, USA) was poured over the membrane and observed under the ChemiDoc system (Bio-Rad, USA).

3.9. Plasma stability study

The plasma stability study of the TMZ and its fatty acid conjugates (**$6R_{1-3}$**) was evaluated using a previously reported HPLC-based method with slight modification [27]. Firstly, a stock solution of 30 mg/mL of TMZ (**1**), TOA (**$6R_1$**), TLA (**$6R_2$**), and TPA (**$6R_3$**) was prepared separately in a solvent system (5% dimethylacetamide (*v*/v), 10% ethanol (v/v), and 5% tween 80 (*w/v*)). Further, 3 mL of fresh rat plasma was taken in a 5 mL glass vial, and 100 μL of TMZ (**1**), TOA (**$6R_1$**), TLA (**$6R_2$**), and TPA (**$6R_3$**) from the stock was spiked. Next, the samples were kept under stirring at 37 °C temperature, and 100 μL of plasma was taken after predetermined time points (0, 0.25, 0.5, 1, 2, 4, 6, 8, 12, and 24 h). The collected plasma samples were acidified by adding 5 μL of 0.1 mM of ascorbic acid, followed by the addition of 900 μL of ACN. The resulting samples were vortexed for 3 min followed by centrifugation at 10,000 rpm for 30 min. The supernatant was collected, vacuum dried, and resuspended in the mobile phase (ACN: Acetate buffer, 95:05), and analysis was done using HPLC based method. The data was presented as % drug remaining, and the concentration at t_0 was considered as 100%.

3.10. Development of C_6 cells induced orthotropic glioblastoma in Sprague Dawley rats

For orthotropic glioma model development, Sprague Dawley (SD) rats were used after the approval of protocol from the Institutional Animal Ethics Committee (IAEC) of BITS Pilani, Pilani Campus *(Protocol number: IAEC/RES/29/04)*. All the experimental procedures were carried out in accordance to the guidelines of the Committee for the Purpose of Control and Supervision of Experiments on Animals (CPCSEA). To anesthetize rats ($n = 05$; 4–6 weeks of age), ketamine (80 mg/kg) and xylazine (4.5 mg/kg) were intraperitoneally injected, and then the head of the rats was shaved, and an incision of about 3–4 cm was made to expose the skull, followed by a burr hole at 2 mm anterior and 3 mm lateral to the bregma. The rat was fixed with a stereotaxic apparatus, and 2×10^6 of C_6 cells suspended in 10 μL of PBS were injected through the burr hole using Hamilton's syringe at a flow rate of 3 μL/min at a depth of 4 mm. The burr hole was sealed using biodegradable wax, and the incision was sutured [28]. Animals were placed back in the home cages and were kept under physical and behavioral observations as an indication of tumor development.

3.11. Pharmacokinetic study

Briefly, SD rats bearing C_6 cells-based orthotropic glioma tumors were randomly divided into four groups ($n = 04$), namely TMZ (**1**) and TOA (**$6R_1$**), treated with 25 mg/kg of dose. For the injection, free TMZ (**1**) was dissolved in the normal saline, and TOA was dissolved in the 5% dimethylacetamide(*v*/v), 10% ethanol (v/v), and 5% Tween 80 (*w/v*) in normal saline and injected intravenously. At predetermined time points (i.e., 0.25, 0.5, 0.75, 1, 2, 4, 6, 8, 12, 24, and 48 h), 200 μL of blood was collected in EDTA containing microcentrifuge tubes followed by centrifugation at 10,000 rpm for 10 min to collect the plasma. The plasma was acidified immediately using 5 uL of 0.1 M ascorbic acid, and TMZ (**1**) and its fatty acid conjugate (**$6R_1$**) was extracted from the plasma by liquid-liquid extraction method. Firstly, 50 μL of plasma was taken and 5 μL of 0.1 M ascorbic acid was added into it and mixed thoroughly after the addition of IBMX (5 μL of 250 ng/mL; internal standard) and vortexed for 15 min. After that, 1.2 mL of tertiary butyl methyl ether (TBME) was added, and the mixture was vortexed for 3 min, followed by centrifugation for 4 min at 10000 rpm. The organic layer (1 mL) was separated and evaporated to drynes to obtain a residue. The residue was reconstituted in 100 μL of the mobile phase (A: 10 mM Ammonium Acetate +0.1% Formic Acid; B: Methanol+0.1% Formic Acid), and 10 μL was injected into LC-MS/MS system (Waters, Xevo TQD). Phoenix 2.1 Winolin software was used to determine various pharmacokinetic parameters viz., $t_{1/2}$ (half-life), C_{max} (maximum plasma concentration), $AUC_{0\text{-}t}$, and $AUC_{0\text{-}\infty}$, MRT (mean residence time), V_d (volume of distribution) and C_L (clearance) by using the non-compartment model approach.

3.12. Efficacy study

Briefly, after glioma cell inoculation, animals were kept for 7 days and randomly divided into three groups (n = 05), namely positive control (PBS treated), free TMZ treated, and TOA **(6R$_1$)** treated group. The animals were treated thrice a week with 10 mg/kg dose of TMZ (in normal saline) or TOA (**6R$_1$**) (in normal saline containing 5% Dimethylacetamide(*v*/v), 10% ethanol (v/v), and 5% tween 80 (*w/v*)) *via* the intravenous route. The positive control animal received normal saline containing 5% dimethylacetamide (v/v), 10% ethanol (v/v), and 5% Tween 80 (w/v) administered *via* the intravenous route. The animals were monitored continuously for their body weight, locomotion activity, and overall health score for 80 days. Further, the brain of all animals was isolated and examined for physical appearance, total weight (g), hemisphere width (mm), and histological characteristics, The lungs of the animals were collected and fixed with Bouin's solution (75% picric acid, 25% formalin, 5% glacial acetic acid) for 6 h followed by incubation in 70% alcohol to examine the metastasis of glioma within the lungs.

3.13. Statistics

All of the data are shown as the mean ± standard deviation or standard error of mean. Analysis of variance (ANOVA) followed by Tukey's multiple comparison test was used to compare the differences between the groups, and (*$P \leq 0.05$, ***$P \leq 0.01$, ***$P \leq 0.005$, and ****$P \leq 0.001$) was considered statistically significant.

4. Results

4.1. Synthesis and characterization of TMZ-Acid (2)

Dropwise addition of $NaNO_2$ to a TMZ solution in H_2SO_4 resulted in the synthesis of TMZ-acid **(2)** as a white floppy powder with >80% practical yield. Characterization of the synthesized TMZ-acid was done using FT-IR spectroscopy, where the disappearance of –NH_2 peak of amide at 3300–3500 cm^{-1} and the appearance of –OH peak of carboxylic acid at 2700–3300 cm^{-1} confirmed the synthesis of TMZ-acid **(2)** (Fig. 2a). Additionally, the mass of the TMZ-acid **(2)** was determined as a final confirmation where a $[M + 1]^+$ peak at 196.0448 ($C_6H_5N_5O_3$, Cal. $[M + 1]^+ = 196.0470$) was observed (Fig. 2b).

4.2. Synthesis and characterization of the hydrazide-modified fatty acids (5R$_{1–3}$)

The free-COOH end group of the fatty acids (3**R$_1$, 3R$_2$, and 3R$_3$**) could be used as a potential site for conjugation with other moieties. Esterification of the free–COOH was performed with acetyl chloride to get yellowish, oily esterified fatty acids (**4R$_{1–3}$**) with a practical yield >90%. The resulting product was modified to get a yellow-colored semisolid product with an 85% practical yield. Fig. 3 showed hydrazide-modified oleic acid [^{1}H NMR (400 MHz, $CDCl_3$) δ 6.73 (brs, 1H), 5.41–5.31 (m, 2H), 2.17 (d, J = 7.6 Hz, 2H), 2.07–1.97 (m, 4H), 1.71–1.59 (m, 2H), 1.37–1.25 (m, 20H), 0.90 (t, J = 6.8 Hz, 3H)]. Fig. 4 showed hydrazide-modified linoleic acid [^{1}H NMR (400 MHz, $CDCl_3$) δ 7.12 (brs, 1H), 5.42–5.26 (m, 4H), 2.76 (t, J = 6.4 Hz, 2H), 2.15 (t, J = 8.0 Hz, 2H), 2.08–2.00 (m, 2H), 1.68–1.56 (m, 2H), 1.40–1.27 (m, 16H), 0.89 (t, J = 6.8 Hz, 3H)]. Fig. 5 showed hydrazide-modified palmitic

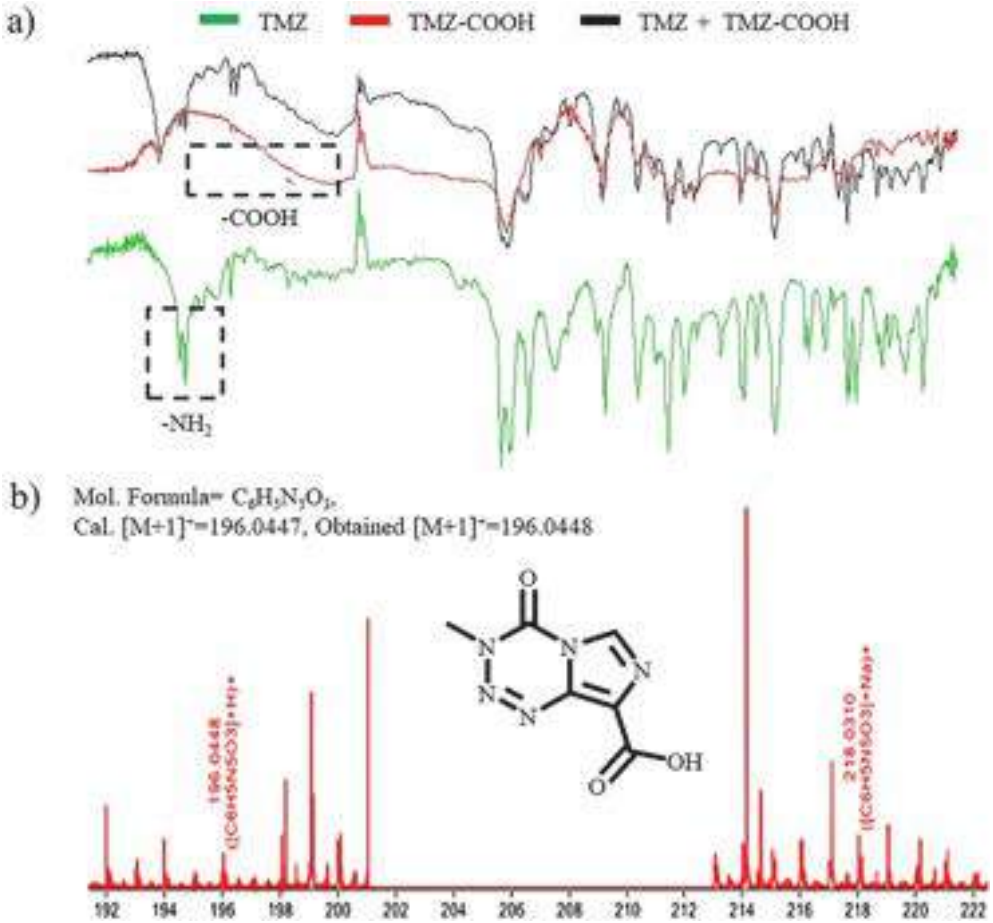

Fig. 2. Characterization of acid derivative of TMZ *i.e* TMZ-acid **(2)**, a) FTIR spectra, and b) ESI-TOF mass spectrometry peak.

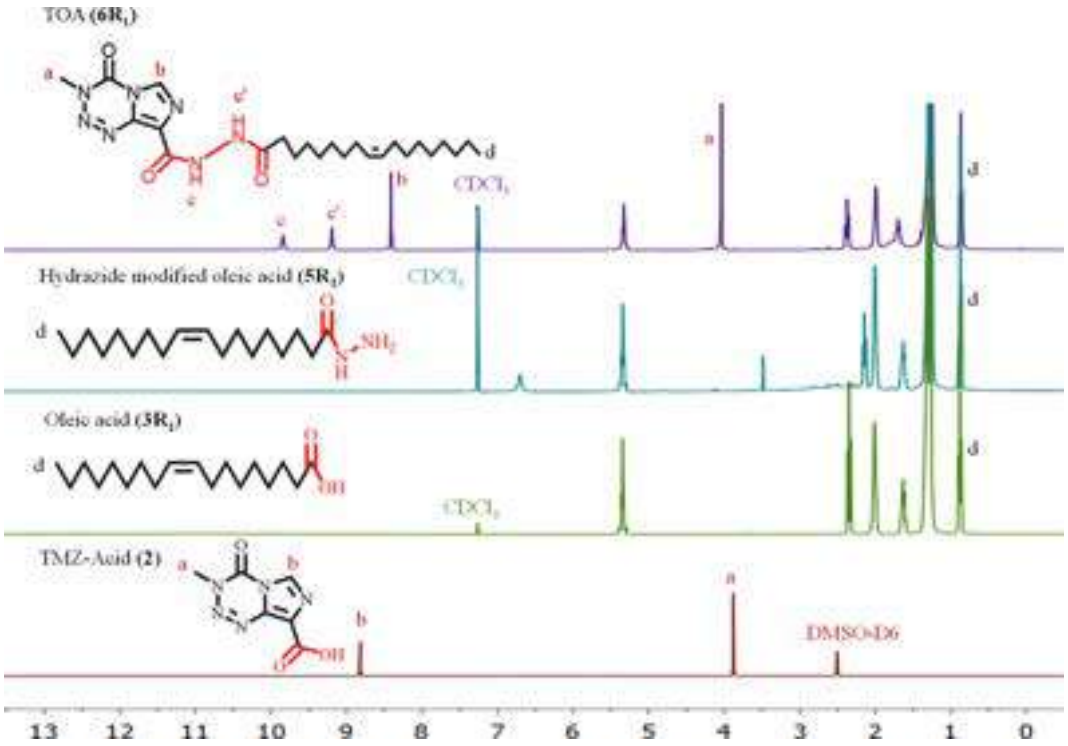

Fig. 3. ^{1}H NMR spectra of oleic acid **($3R_1$)**, hydrazide-modified oleic acid **($5R_1$)**, TMZ-Acid **(2),** and TOA **($6R_1$)** conjugate.

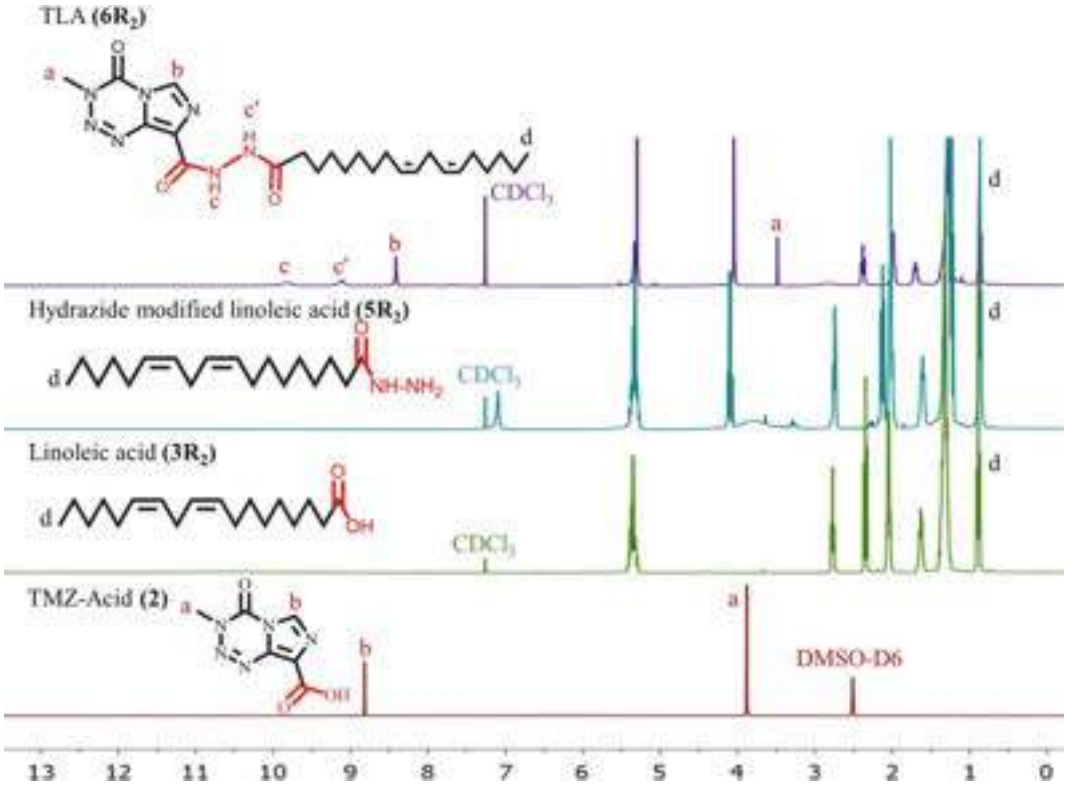

Fig. 4. Characteristic ^{1}H NMR spectra of linoleic acid **($3R_2$)**, hydrazide derivative of linoleic acid **($5R_2$)**, TMZ-Acid **(2)** and TLA ($6R_2$) conjugate.

acid [(400 MHz, $CDCl_3$) δ 3.67 (brs, 3H), 2.31 (t, J = 7.6 Hz, 2H), 1.68–1.55 (m, 2H), 1.34–1.24 (m, 24H), 0.89 (d, J = 7.2 Hz, 3H)], wherein the peak at 4.20–4.03 (m, 2H) and δ 7.12–7.30 (brs, 1H) confirmed the presence of hydrazine end group. Further, mass spectrometry ESI-TOF for hydrazide-modified linoleic acid (Mol. formula- $C_{18}H_{34}N_2O$; Cal. $[M + 1]^+ = 295.3$; obtained $[M + 1]^+ = 295.28$), for hydrazide-modified oleic acid (Mol. formula- $C_{18}H_{36}N_2O$; Cal. $[M + 1]^+ = 297.3$; obtained $[M + 1]^+ = 297.28$) and for hydrazide modified palmitic acid (Mol. formula- $C_{16}H_{34}N_2O$; Cal. $[M + 1]^+ = 271.27$; obtained $[M + 1]^+ = 271.27$) confirmed the successful synthesis of

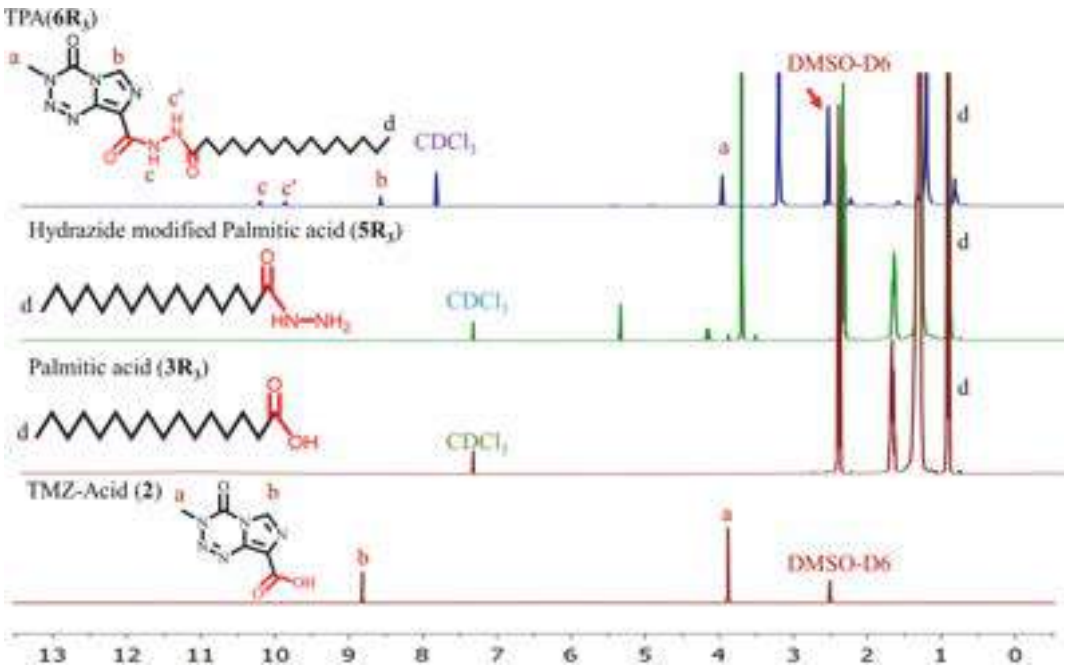

Fig. 5. ^{1}H NMR spectra of palmitic acid **(3R$_3$)**, hydrazide-modified palmitic acid **(5R$_3$)**, TMZ-COOH **(2),** and TPA **(6R$_3$)** conjugate.

hydrazide modified fatty acids.

4.3. Synthesis and characterization of TMZ-fatty acid conjugates *(6R$_{1-3}$)*

TMZ-Acid **(2)** and hydrazide-modified fatty acids **(5R$_{1-3}$)** were conjugated using EDC/HOBt-mediated amide coupling chemistry. The reaction was monitored using TLC with a solvent system containing DCM:MeOH (95:05), and the appearance of a bright yellow spot on TLC indicated the completion of the synthesis of the conjugate. The final product was purified using column chromatography with DCM:MeOH (95:05) as the mobile phase. The final yield of TOA (**6R$_1$**), TLA (**6R$_2$**), and TPA (**6R$_3$**) were 0.728 g (72%), 0.720 g (72%), and 0.500 g (50%), respectively. However, the conjugation reaction showed good reproducibility in terms of the final yield obtained. Fig. 3 showed ^{1}H NMR spectra of TOA **(6R$_1$)** [^{1}H NMR (400 MHz, $CDCl_3$) δ 9.86 (brs, 1H), 9.22 (brs, 1H), 8.43 (s, 1H), 5.39–5.30 (m, 2H), 4.06 (s, 3H), 2.40 (t, J = 7.2 Hz, 2H), 2.06–1.97 (m, 4H), 1.77–1.64 (m, 2H), 1.37–1.24 (m, 20H), 0.89 (t, J = 6.4 Hz, 3H)]. Fig. 4 showed ^{1}H NMR spectra of TLA **(6R$_2$)** [^{1}H NMR (400 MHz, $CDCl_3$) δ 9.83 (brs, 1H), 9.14 (brs, 1H), 8.44 (s, 1H), 5.38–5.30 (m, 4H), 4.07 (s, 3H), 2.40 (t, J = 7.6 Hz, 2H), 2.06–1.97 (m, 4H), 1.77–1.69 (m, 2H), 1.35–1.24 (m, 16H), 0.89 (t, J = 6.8 Hz, 3H)]. Fig. 5 showed ^{1}H NMR spectra of TPA **(6R$_3$)** [^{1}H NMR (400 MHz, $CDCl_3$, DMSO-d_6) δ 10.15 (brs, 1H), 9.82 (brs, 1H), 8.53 (s, 1H), 3.93 (s, 3H), 2.21 (t, J = 7.4 Hz, 2H), 1.63–1.52 (m, 2H), 1.27–1.13 (m, 24H), 0.81 (t, J = 6.8 Hz, 3H)]. The TMZ peaks at δ 4.0–4.2 (a, -CH_3, s, 3H), δ 8.2–8.5 (b, -CH, s, 1H), and hydrazide linker peaks at δ 9.0–9.2 (c', -NH, s, 1H), δ 9.7–10.5 (c, -NH, s, 1H) showed successful conjugation. Further, mass spectrometry data (Fig. 6b) of TOA **(6R$_1$)** (Mol. formula. $C_{24}H_{39}N_7O_3$; Cal. $[M + 1]^+ = 474.3192$; obtained $[M + 1]^+ = 474.3151$), TLA **(6R$_2$)** (Mol. formula. $C_{24}H_{37}N_7O_3$; Cal. $[M + 1]^+ = 472.3036$; obtained $[M + 1]^+ = 472.3033$), and TPA **(6R$_3$)** (Mol. formula. $C_{22}H_{37}N_7O_3$; Cal. $[M + 1]^+ = 448.3036$; obtained $[M + 1]^+ = 448.3007$) confirmed the synthesis of the conjugates. The purity of conjugates were determined using an RP-HPLC system with a mobile phase comprising ACN/water (0.1% formic acid) in a proportion of 95:05, wherein all the three conjugates showed a purity of >98% (Fig. 6a).

4.4. Cytotoxicity and migration assay

For the calculation of the % cell viability, DMSO-treated cells were taken as negative control. Results showed that the TOA **(6R$_1$)**, TLA **(6R$_2$)**, and TPA **(6R$_3$)** conjugates had an IC_{50} value of 101.4 μM, 67.97 μM, and 672.04 μM, respectively in C_6 cells (Fig. 7 a1). However, the physical mixtures of TMZ with fatty acids, i.e. TMZ + OA, TMZ + LA, TMZ + PA, and free fatty acids **(3R$_{1-3}$)** i.e. free OA, free LA, and free PA showed IC_{50} of 331.88 μM, 198.34 μM, 1000 μM and 628.03 μM, 377.5 μM, 293.84 μM, respectively in C_6 cells (Fig. 7 a1). Similarly, in U87-MG cells the TOA **(6R$_1$)**, TLA **(6R$_2$)**, and TPA **(6R$_3$)** conjugates showed an IC_{50} value of 428.25 μM, 366.42 μM, and 413.69 μM, respectively (Fig. 7 b1). Further, the physical mixtures i.e. TMZ + OA, TMZ + LA, TMZ + PA, and free fatty acids **(3R$_{1-3}$)** i.e. free OA, free LA, and free PA showed IC_{50} of 367.99 μM, 352.2 μM, 188.58 μM, and 306.01 μM, 248.01 μM, and 289.10 μM, respectively in U87-MG cells (Fig. 7 b1). Additionally, the migration properties of C_6 and U87-MG cells was determined in the presence of TMZ **(1)**, TOA **(6R$_1$)**, TLA **(6R$_2$)**, and TPA **(6R$_3$)**. As shown in Fig. 7 a2 & b2, the migration potential of both the cells was seen to be reduced significantly when cells were treated with TMZ-fatty acid conjugates **(6R$_{1-3}$)** as compared to the free TMZ **(1)**.

4.5. Apoptosis assay

Annexin/PI staining-based flow cytometric assay was used to determine the apoptotic potential of TMZ **(1)**, TOA **(6R$_1$)**, TLA **(6R$_2$)**, TPA **(6R$_3$)**, TMZ + OA, TMZ + LA, and TMZ + PA in C_6 and U87-MG cells. Fig. 8a&b represented the apoptosis data, where C_6 cells treated with free TMZ **(1)** showed total apoptosis of 18.28% (early apoptosis, 4.96%; late apoptosis, 13.32%). While conjugates i.e. TOA **(6R$_1$)** showed 83.19% (early apoptosis, 14.32%; late apoptosis, 68.87%), TLA **(6R$_2$)** showed 52.2% (early apoptosis, 16.39%; late apoptosis, 35.81%), and TPA **(6R$_3$)** showed 63.39% (early apoptosis, 26.61%; late apoptosis, 36.78%). The physical mixture i.e. TMZ + OA showed 70.68% (early apoptosis, 20.54%; late apoptosis, 50.14%), TMZ + LA showed 35.37% (early apoptosis, 1.89%; late apoptosis, 33.48%) and TMZ + PA showed 53.04% (early apoptosis, 5.28%; late apoptosis, 47.76% (Fig. 8a&b). Similarly, in U87-MG cells, TMZ **(1)** showed apoptosis of 25.32% (early apoptosis, 6.80%; late apoptosis, 18.52%). The conjugates i.e., TOA

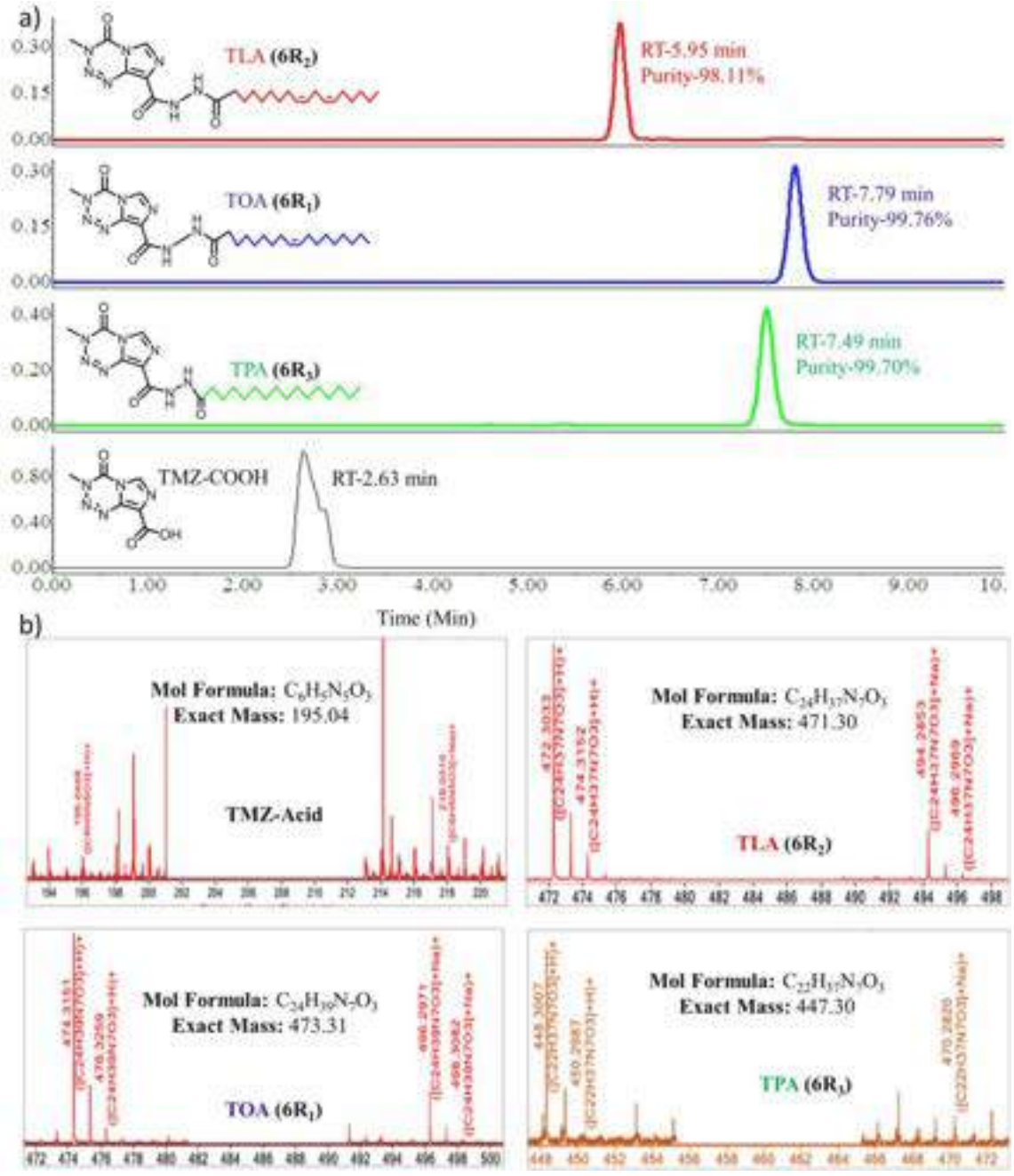

Fig. 6. Characteristics HPLC and mass spectra (HRMS) of TOA **($6R_1$)**, TLA **($6R_2$)**, TPA **($6R_3$)** conjugates, and TMZ-Acid **(2)**.

($6R_1$) showed 52.44% (early apoptosis, 31.70%; late apoptosis, 20.74%), TLA **($6R_2$)** showed 60.82% (early apoptosis, 31.44%; late apoptosis, 29.38%), and TPA **($6R_3$)** showed 56.93% (early apoptosis, 28.30%; late apoptosis, 28.63%). The physical mixtures i.e., TMZ + OA showed 59.38% (early apoptosis, 34.04%; late apoptosis, 25.34%), TMZ + LA showed 48.97% (early apoptosis, 20.86%; late apoptosis, 28.11%), and TMZ + PA showed 26.53% (early apoptosis, 10.40%; late apoptosis, 16.13%) (Fig. 8d&e).

4.6. Western blotting

The expression of MGMT was determined at the protein level in both C_6 and U87-MG cell lines using the western blot analysis. As shown in Fig. 8c, the C_6 cells inherently have the expression of MGMT protein without any treatment and after treatment with free TMZ **(1)**, the expression of MGMT was further increased. Interestingly, after the treatment with TOA **($6R_1$)**, TLA **($6R_2$)** and TPA **($6R_3$)** expression of MGMT get reduced in the C_6 cell lines. Similarly, the U87-MG cells showed an increase in expression of MGMT after the treatment with free TMZ **(1)** and the expression of MGMT get reduced when the cells were treated with TOA **($6R_1$)**, TLA **($6R_2$)** and TPA **($6R_3$)** (Fig. 8f).

4.7. Plasma stability study

The plasma stability study was performed at a different time interval as shown in Fig. 9, the percentage of TMZ was about 26.14% after 1 h. On the other hand, the TOA **($6R_1$)**, TLA **($6R_2$)**, and TPA **($6R_3$)** were found 59.21%, 55.79%, and 76.53%, respectively. After 2 h, only 0.16% of the TMZ was remaining. However, interestingly, there was 42.52%, 43.37%, and 76.53% of TOA **($6R_1$)**, TLA **($6R_2$)**, and TPA **($6R_3$)**,

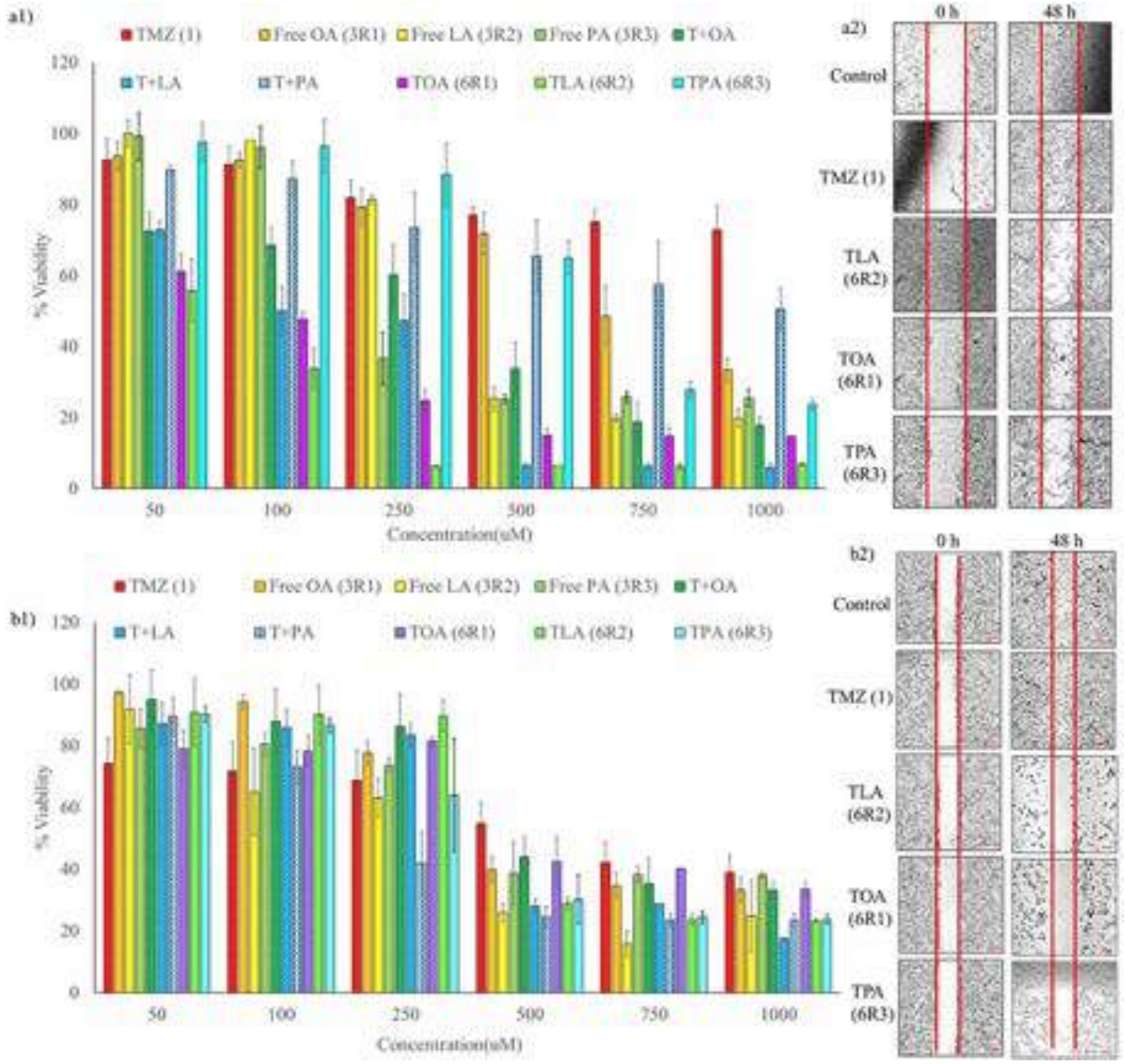

Fig. 7. *In vitro* evaluation of TMZ-Fatty acid conjugates in C_6 and U87-MG cells, a1&b1) cells viability assay in C_6 and U87-MG cells respectively, and a2&b2) migration assay in C_6 and U87-MG cells respectively.

respectively, were observed. Moreover, after 6 h, the remaining % of TOA (**$6R_1$**), TLA (**$6R_2$**), and TPA (**$6R_3$**) was 23.6%, 5.43%, and 41.6%, respectively. However, there was no detectable amount was observed after 12 h.

4.8. Pharmacokinetic study

The plasma concentration profile of the samples is shown in Fig. 10, and different PK parameters are shown in Table 1 wherein there was an improvement in the pharmacokinetic profile of the TOA (**$6R_1$**) compared to free TMZ. Interestingly, there was a 7.7-fold increase in half-life of TOA (**$6R_1$**) with respect to the TMZ, which has a half-life of 1.5 h. Similarly, the observed mean residence time (MRT) of TOA (**$6R_1$**) was found to be increased ~3.8-fold in comparison to free TMZ, which has an MRT of 2.59 h.

4.9. Efficacy study

C_6 cells-induced orthotopic glioma model in Sprague Dawley rats was used to evaluate the *in vivo* efficacy of synthesized TOA **($6R_1$)** conjugate. The treatment was carried out for 80 days and as per the Kaplan Meier survival rate analysis (Fig. 11a), the animals in the positive control group died within 18 days, while in the TMZ **(1)** treated group, the survival rate was 40% after 80 days. Interestingly, a 100% of survival rate was observed in TOA **($6R_1$)** treated group and the overall health was also found to be good. After C_6 cells injection, a sudden weight loss was observed in all the animals but once the treatment started the animals showed recovery in their overall weight (g). As shown in Fig. 11b, the positive control group animals showed continuous weight loss, while TMZ **(1)** and TOA **($6R_1$)** treated animals showed better recovery. The morphological images of the brain of different groups of animals are shown in Fig. 11c. In positive control group, animals tumor growth was observed at the injection site, while a significantly less affected area was observed in TMZ **(1)** and TOA **($6R_1$)** treated groups. To confirm the physical tumor, the right/left hemisphere width (mm) ratio (Fig. 11d) and total brain weight (Fig. 11e) were examined. As per the observation, the ratio of right/left hemisphere width was found to increase in the positive control animals w.r.t the normal control group. Interestingly, the ratio of right/left hemisphere width in the animals treated with TOA **($6R_1$)** was significantly lesser than in the TMZ **(1)** treated group. A

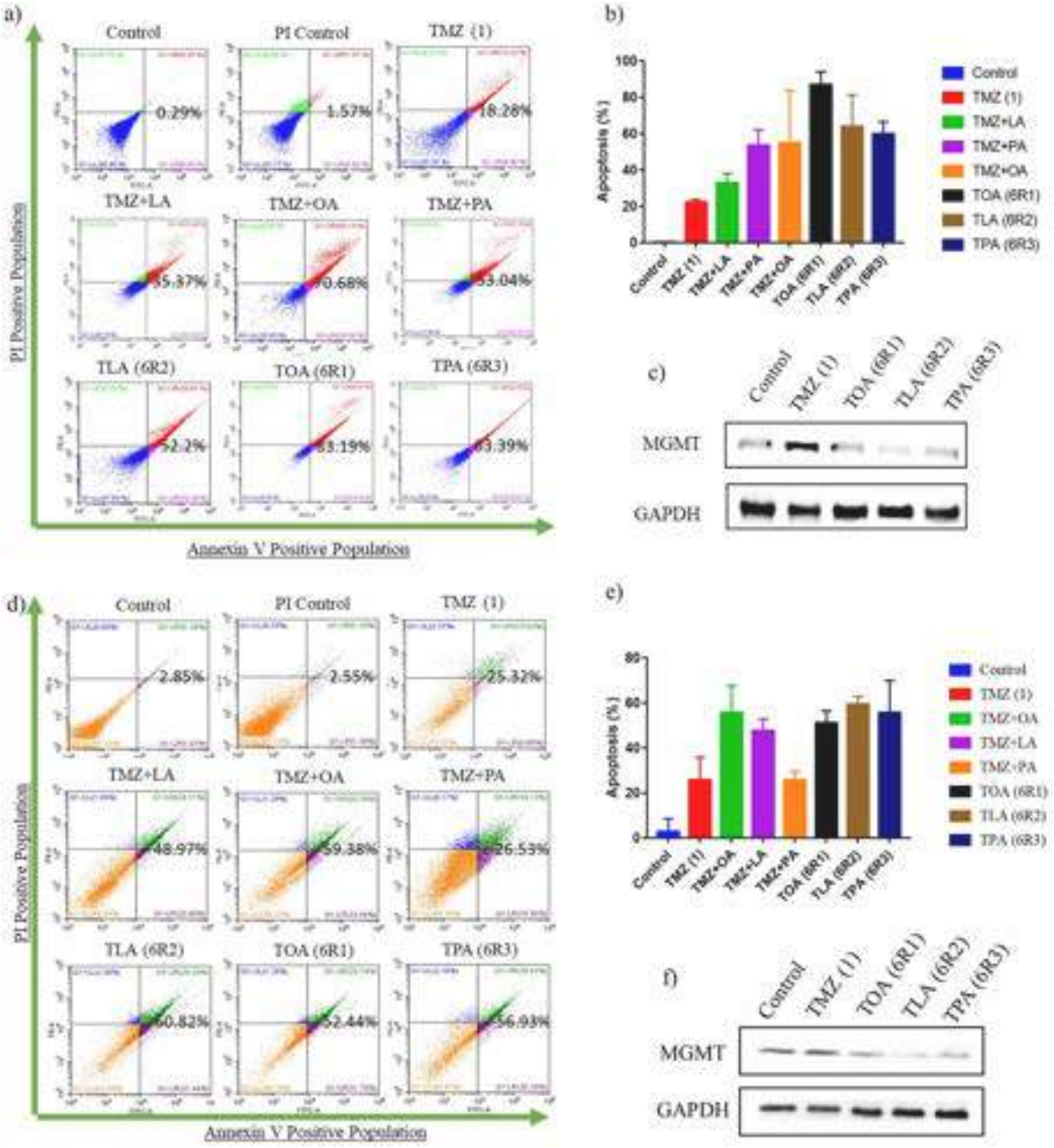

Fig. 8. *In vitro* evaluation of TMZ-fatty acid **($6R_{1-3}$)** conjugates in C_6 and U87-MG cells, a&d) apoptosis status in C_6 and U87-MG cells respectively, b&e) quantitative apoptotic of C_6 and U87-MG cells respectively, and c&f) MGMT expression in C_6 and U87-MG cells respectively after different treatments.

similar kind of result was observed when the total brain weight (g) was measured. The weight of the brain in the positive control group was significantly higher than that of the negative control group, while after treatment with TMZ **(1)** and TOA **($6R_1$)** the brain weight (g) was significantly decreased as compared to positive control group. H&E staining was carried out for histological evaluation at the injection site. Fig. 12a shows the H&*E*-stained whole brain sections at higher magnification, the right lobe (C_6 cells injected) shows the tumor growth (red outline) while the left lobe (un-injected) shows normal vasculature. Overall, after treatment with TMZ **(1)** and TOA **($6R_1$)**, the tumor volume got reduced as compared to the positive control group. The TOA **($6R_1$)**, on the other hand, was more effective than TMZ **(1)** alone. The same can be seen in the high-resolution images of the tumor area obtained using a bright field inverted light microscope Fig. 12b. It has been reported that metastasis can be seen and to evaluate the same, the lungs of the animals were isolated after the completion of the study and fixed in Bouin's solution to see the metastatic nodules. As shown in Fig. 12c, the metastatic nodules were observed in positive control animals, but the number of nodules in TMZ **(1)** and TOA **($6R_1$)** treated animals were significantly lower.

5. Discussion

GBM has been considered as the most aggressive brain tumor [29], with TMZ as the first line treatment given orally as well as *via* parenteral route [30]. Although, TMZ is a potent molecule, it suffers from limitations including a short half-life [31], rapid metabolism [32], lesser accumulation in brain tissues (~1%) [13], and development of chemo-

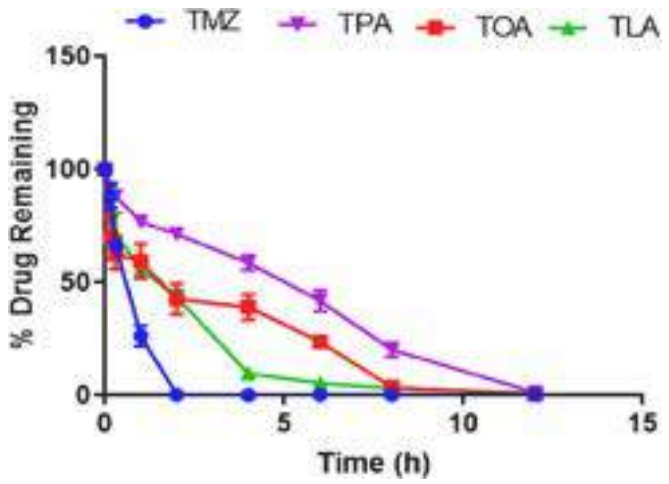

Fig. 9. The stability study of TMZ **(1)** and TMZ-fatty acid conjugates **($6R_{1-3}$)** in rat plasma ($n = 05$).

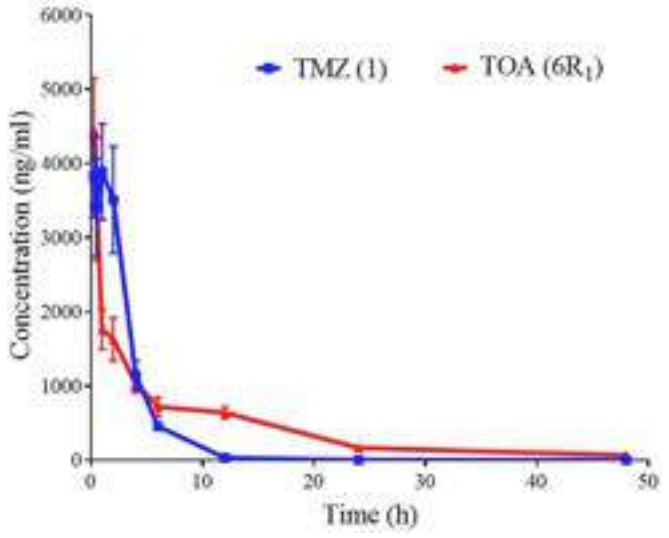

Fig. 10. Pharmacokinetic studies of free TMZ and TOA **($6R_1$)** conjugate after intravenous (i.v.) administration in glioma-bearing SD rats. Each point represents a mean ± SEM ($n = 04$) at a dose of 25 mg/kg.

Table 1
The non-compartmental pharmacokinetic parameters for TMZ and TOA in SD rat plasma ($n = 04$) after i.v. bolus at a dose of 25 mg/kg.

Parameters	TMZ	TOA
C_{max} (ng/mL)	4298.506	5634.895
$t_{1/2}$ (h)	1.531	11.81
$AUC_{0\text{-last}}$ (ng.h/mL)	15,441.3	21,360.32
$AUC_{0\text{-}\infty}$ (ng.h/mL)	15,445.11	22,501.43
$AUMC_{0\text{-last}}$ (ng.h/mL)	40,054.76	211,031.1
$AUMC_{0\text{-}\infty}$ (ng.h/mL)	40,246.14	285,254.2
MRT (h)	2.59	9.87
V_z (mL/kg)	1430.12	7574.84
CL (mL/h/kg)	647.45	444.41

resistance caused by overexpression of MGMT [33]. In past few years, efforts have been made to improve its efficiency utilizing nano carrier-based approaches, wherein some success has been seen. Among various strategies, hydrophobization of hydrophilic chemotherapeutic agent using a fatty acid is considered highly promising for enhancing their efficiency [22]. For instance, Li et al. showed that the lipophilicity of doxorubicin was enhanced following conjugation with palmitic acid to create a prodrug with a pH-sensitive hydrazone linkage. Further, the prodrug was feasible to load into the hydrophobic core of polymeric micelles with a loading efficiency of 99.3 ± 5.7% [34]. We have earlier reported that conjugating lisofylline with linoleic acid increased its overall efficacy in treating diabetes with over a five-fold increase in half-life [22]. Due to hydrophobization, lisofylline-linoleic acid conjugate showed 75 ± 4.12% encapsulation efficiency with a practical drug loading of 9.29 ± 1.16% in mPEG-Poly-(carbonate-*co*-lactide) [mPEG-b-P(CB-co-LA)] polymer [35].

Interestingly, the fatty acids have also been explored for their anti-cancer activity in different types of cancers [36]. In 2017, Jiang et al. reported that oleic acid causes apoptosis in the TSCC cell line and effectively kills cancer cells *via* autophagy [36]. In the current study, we have conjugated TMZ with fatty acids to obtain three different conjugates i.e. TOA **($6R_1$)**, TLA **($6R_2$)**, and TPA **($6R_3$)**. For conjugation, the TMZ was first converted into an acid derivative i.e. TMZ-acid **(2)** and characterized using FTIR, ^{1}H NMR and mass spectrometry. Our results were in line with the previously reported synthesis of TMZ-acid [19]. The free -COOH group of fatty acids **($3R_{1-3}$)** was modified to -CO-NH-NH_2 (hydrazide derivative, **$5R_{1-3}$**) using a two-step reaction. The EDC/HoBt amide coupling under cold conditions has been reported for good yield and purity, and therefore used for conjugation [37]. However, the major concern during the synthesis experiments was related to the stability of the TMZ, since it is prone to hydrolysis at physiological pH. Therefore, the purified TMZ-fatty acid conjugates **($6R_{1-3}$)** were evaluated for the protons of -CH_3 at 3rd carbon by integrating the -CH_3 (3H) protons peak at δ 4.1 (a, -CH_3, s, 3H) in the ^{1}H NMR spectra. The integration was further confirmed with the ^{1}H proton at 6th carbon at δ 8.5 (b, -CH, s, 1H). The protons at both the carbons were found intact and therefore confirmed the intact form of TMZ in the final conjugate. The TMZ-fatty acid conjugates **($6R_{1-3}$)** showed a purity of >98% with an overall yield of >50%. To evaluate the potency of the conjugates, we performed a cell viability assay, wherein the conjugates showed ~5-fold decrease in the IC_{50} value indicating synergistic anticancer effect with fatty acids. These findings were consistent with the published literature, where fatty acids including oleic acid, palmitic acid and linoleic acid have shown anticancer activity [36,38,39]. Autophagy is a cellular process that could lead to apoptosis and oleic acid has been reported to induce autophagy in cancer cells [36]. Since, TMZ is also an autophagy inducer, therefore fatty acid has enhanced the overall anticancer effect of the TMZ. Zhu et al. have earlier reported the antiproliferation effect of the palmitic acid in PC3 and DU145 prostate cancer cell lines with IC_{50} values of 10.72 μM and 16.83 μM, respectively [38]. Similarly, Jiang et al. also showed OA significantly inhibited the cell growth in a dose and time-dependent manner with the IC_{50} values of 291 μM and 159 μM in CAL27 and UM1 cells, respectively after 24 h of incubation. Furthermore, the IC_{50} value was reduced to 228 μM and 78 μM in CAL27 and UM1 cells, respectively after 96 h of incubation. Overall, they concluded that OA could be used as a potent anticancer molecule by inducing apoptosis and autophagy by blocking the Akt/mTOR pathway [36]. Further, the cells treated with conjugates showed apoptosis and minimal necrosis as shown in Fig. 8. However, the major problem with glioma treatment using TMZ is resistance *via* MGMT upregulation. Kitenge et al. showed that the effect of TMZ in glioblastoma xenograft cells *in vivo* (GBM43 and GBM44) was not significant due to modulation in the MGMT expression [40]. Since we got a potent cytotoxic effect of TMZ when conjugated with a fatty acid, it needs to be explored more to understand the effect of conjugates on MGMT expression. Fatty acids have been previously reported for their effect on MGMT depletion. In western blotting data, we observed that the MGMT expression was increased when cells were treated with TMZ alone, while the expression was decreased when cells were treated with the conjugates. This confirmed that the fatty acid plays a significant role in MGMT depletion and therefore makes TMZ more potent, sensitive, and effective in killing C_6 and U87-MG cells. This could also be attributed to the lower IC_{50}

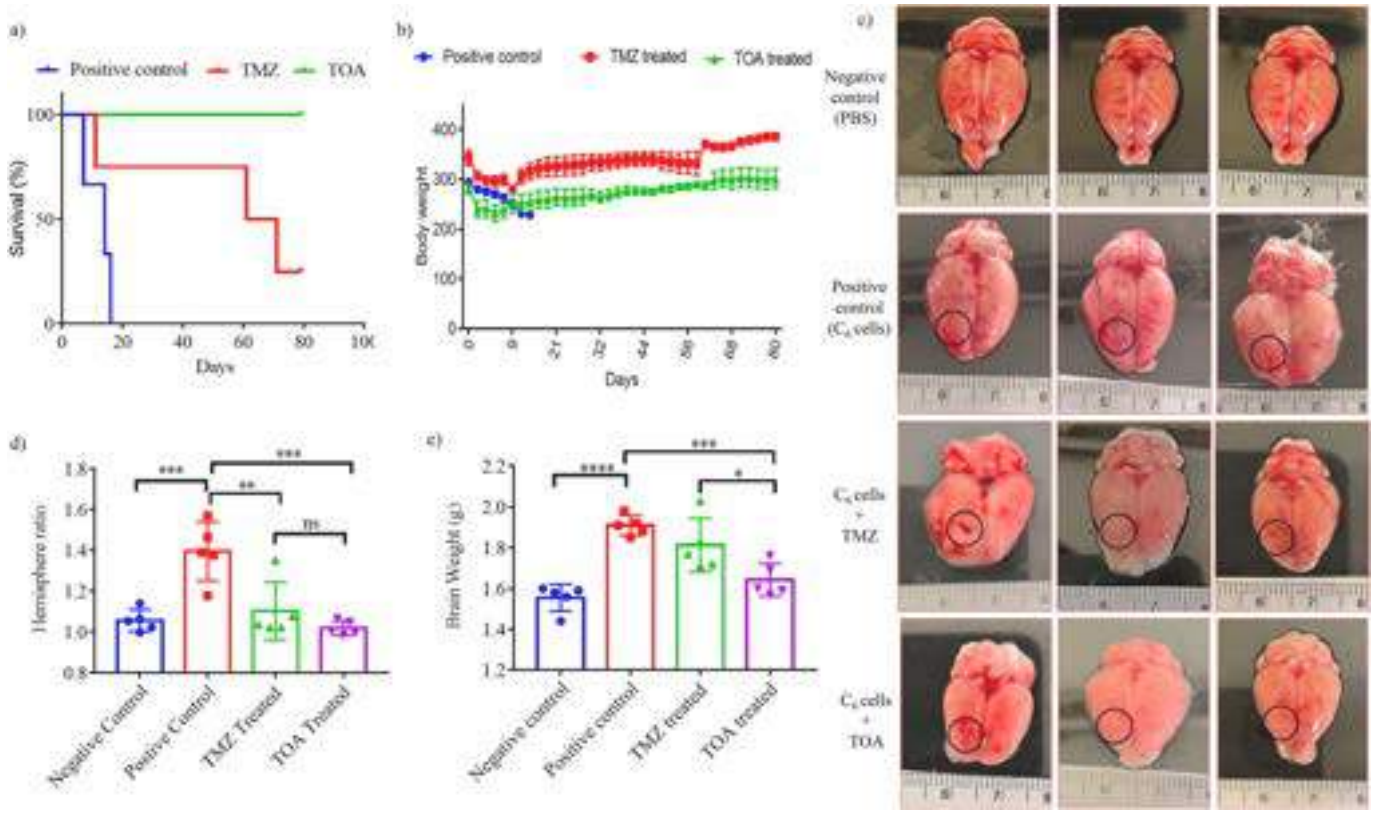

Fig. 11. *In vivo* efficacy study of TOA (**$6R_1$**) conjugate and free TMZ **(1)** in C_6 cell induced orthotropic glioma bearing SD rats, a) Kaplan Meier survival rate, b) total body weight, c) whole-brain images of animals from different treatment group, d) right/left hemisphere ratio, and e) total brain weight.

value in cells treated with TMZ fatty acid conjugates **($6R_{1-3}$)** [41]**.** It has also been reported previously that combination therapy sensitized the glioma cells toward TMZ. In 2011, Wang et al. reported the effect of docosahexaenoic acid (DHA) on the sensitization of brain tumor cells toward etoposide therapy. Additionally, the reported reason was the synergistic effect of DHA by suppressing DNA repair genes [42]. Collectively, the outcomes of the *in vitro* studies concluded that the fatty acid conjugates of TMZ are more effective. At physiological pH, the TMZ undergoes hydrolysis, by the means of decarboxylation at the C4 position of the six-membered ring, which results in the formation of MTIC and later forms AIC and a methyl diazonium ion. The effect of fatty acid conjugation on the degradation pattern of TMZ was examined using plasma stability studies, as shown in Fig. 9, the degradation of TMZ gets slowed down after conjugation and is dependent upon the degree of unsaturation of the fatty acid and maximum stability was observed in case of PA. Moreover, the unsaturation of fatty acid also contributes to the hydrophobicity of the final conjugate (Fig. 9), which could also be another reason for the sustained hydrolysis. Similar results were reported earlier by Singh et al., where the stability and efficiency of lysofylline depended upon the degree of unsaturation [43]. Moreover, the TOA **($6R_1$)** conjugate was chosen further for *in vivo* studies since it has shown better *in vitro* apoptosis as compared to other conjugates. Also, as per the MTT assay, the free palmitic acid has a cell viability of 37% at 250 μM concentration, while oleic acid has a cell viability of 79% at the same concentration which indicated that free palmitic acid could be cytotoxic. Moreover, Oleic acid conjugate is more stable in plasma than linoleic acid conjugate. A C_6 cells-based orthotropic glioma model was developed in SD rats as reported previously [28]. Due to the complex anatomical location of the brain, it is challenging to observe the growth of the brain tumor physically. However, as per the reported literature, some parameters could be observed to predict the onset of tumor growth. For example, the number of cells injected was kept constant i.e., 2×10^6 of C_6 cells, loss in body weight [44], right eye bulging, and reduced locomotion activity of the rat. The animal showing the above parameters were taken further and randomly divided into different groups. A pharmacokinetic study revealed the improved kinetic of fatty acid conjugate and the reason might be the improvement in the stability of the conjugate at the physiological pH of the blood after conjugation to a fatty acid. A similar observation has been reported by Jin et al. for prodrugs of gemcitabine prepared by conjugating it with lipid derivatives. As per their observations, PK parameters of gemcitabine get improved after conjugation with the lipids [45]. Similar reports were by Italia et al., wherein the conjugation of lysofylline with a lipid improved its *in vivo* stability and PK profile. More specifically, the LSF-LA prodrug exhibited reduced protein binding and showed a significantly higher half-life (5.7-fold), and higher apparent volume of distribution (5.3-fold) than free LSF [22].The TOA **($6R_1$)** conjugate showed better outcomes in terms of overall survival rate, brain weight, hemisphere width and reduction in tumor volume, which could be attributed to the improved efficacy after fatty acid conjugation. Similar observations were reported by Yu et al., where a series of temozolomide ester (TMZEs) prodrugs were synthesized, having different chain lengths, which lead to an increase in lipophilicity due to the esterification of the TMZ. The TMZEs showed stability in plasma and brain homogenates showed better cell uptake and cytotoxicity in the C_6 cell line at the lower dose, and showed ~2-fold improvement in survival rate [46]. Interestingly, the study demonstrated that the physicochemical and biological properties of TMZ get improved after esterification, which further increases lipophilicity, membrane absorption, and therapeutic effect [46]. In order to understand the metastasis, the lungs were stained with Bouin's solution. A higher number of metastatic nodules were present in the positive control group, while there was a reduction in the metastatic nodules in TMZ and TOA-treated animals. Collectively, the TOA conjugate is a better therapeutic option for the treatment of glioma, and further studies as warranted for its development. The TMZ is given orally and has 100% bioavailability, However, intravenous injections of TMZ

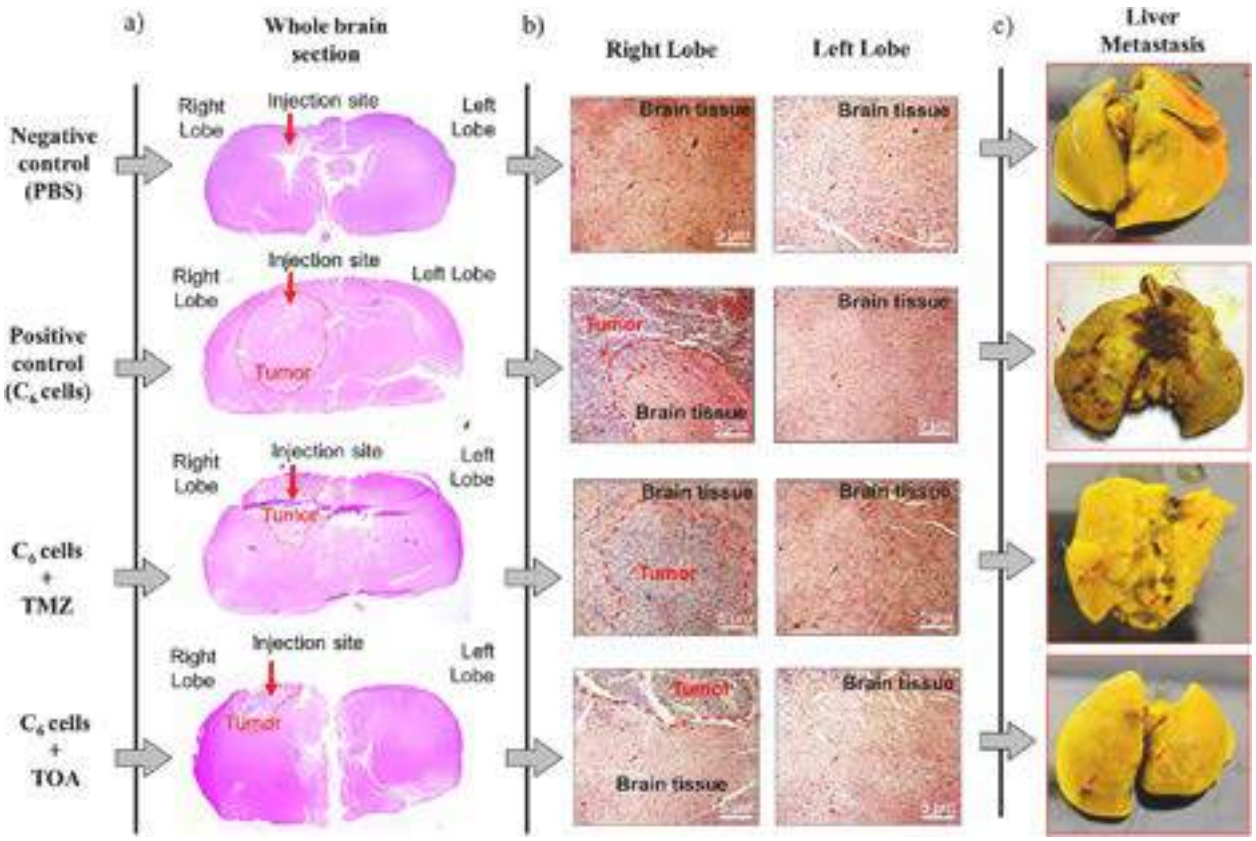

Fig. 12. *In vivo* efficacy study of TOA **(6R$_1$)** conjugate and free TMZ **(1)** in C_6 cell induced orthotropic glioma bearing SD rats, a) H&E images of the whole brain sections, b) H&E images of the tumor around the injection site (right lobe (C_6 cells injected) and left lobe (non-injected)) and c) bouin's solution-stained lungs images.

are also available in the market with the brand name Temodar. In the current research, we have not explored the oral route. This could be explored in further research to understand their oral bioavailability and, if required, could be enhanced using nanocarrier-based approaches.

6. Conclusions

Although TMZ is the standard chemotherapeutic agent for the treatment of glioblastoma multiforme, its therapeutic outcomes are constrained by its high dose of administration, short half-life, lower accumulation in brain tissue, and failure due to MGMT overexpression-dependent drug resistance. The conjugation of TMZ to fatty acids has several merits, such as (1) increased efficiency, (2) overcoming MGMT-based resistance, (3) synergism. As compared to free TMZ, its fatty acid conjugates were more efficient in killing C_6 and U87-MG cells with lower IC_{50} values. The protein expression evaluated *via* western blotting depicted that the MGMT expression gets suppressed when C_6 and U87-MG cells were treated with TMZ-fatty acid conjugates. The PK study revealed that the $t_{1/2}$ of TOA was improved 7.7 folds compared to the free drug. The *in vivo* efficacy also showed a better outcome as compared to free TMZ, wherein an improvement in survival rate and overall health, decreased tumor burden, and reduction in metastatic nodules were observed.

CRediT authorship contribution statement

Reena Jatyan: Conceptualization, Methodology, Investigation, Writing - original draft. **Deepak Kumar Sahel:** Writing – original draft, Conceptualization, Methodology. **Prabhjeet Singh:** Methodology, Formal analysis. **Rajeev Sakhuja:** Writing – review & editing, Data curation. **Anupama Mittal:** Supervision, Writing – review & editing. **Deepak Chitkara:** Supervision, Conceptualization, Funding acquisition, Resources, Writing - review & editing.

Declaration of competing Interest

The authors declare that they have no conflict of interest in the data presented in this manuscript.

Data availability

Data will be made available on request.

Acknowledgments

Financial support from Indian Council of Medical Research (ICMR), Government of India to DC *via* an extramural research grant (# 34/9/2019-TF/Nano/BMS) is duly acknowledged. Lady Tata Memorial Trust (LTMT) for their fellowship support to RJ through Junior Research Scholarship (JRS) is duly acknowledged. DST-FIST sponsored LC-MS/MS facility at the Department of Pharmacy, and DST-FIST sponsored HRMS facility at the Department of Chemistry, Birla Institute of Technology and Science, Pilani (BITS Pilani), Pilani Campus, are duly acknowledged.

References

[1] K. Rock, O. McArdle, P. Forde, M. Dunne, D. Fitzpatrick, B. O'Neill, C. Faul, A clinical review of treatment outcomes in glioblastoma multiforme–the validation in a non-trial population of the results of a randomised Phase III clinical trial: has a more radical approach improved survival? Br. J. Radiol. 85 (2012) e729–e733.

[2] J.P. Thakkar, T.A. Dolecek, C. Horbinski, Q.T. Ostrom, D.D. Lightner, J. S. Barnholtz-Sloan, J.L. Villano, Epidemiologic and molecular prognostic review of glioblastoma, Cancer Epidemiol. Biomark. Prev. 23 (2014) 1985–1996.

[3] D.N. Louis, H. Ohgaki, O.D. Wiestler, W.K. Cavenee, P.C. Burger, A. Jouvet, B.W. Scheithauer, P. Kleihues, The 2007 WHO classification of tumours of the central nervous system, Acta Neuropathol., 114 (2007) 97–109.

[4] M. Robert, M. Wastie, Glioblastoma multiforme: a rare manifestation of extensive liver and bone metastases, Biomed. Imag. Interven. J. 4 (2008), e3.

[5] O.G. Taylor, J.S. Brzozowski, K.A. Skelding, Glioblastoma multiforme: an overview of emerging therapeutic targets, Front. Oncol. 9 (2019) 963.

[6] J. Lee, K. Kay, K. Troike, M.S. Ahluwalia, J.D. Lathia, Sex differences in glioblastoma immunotherapy response, NeuroMol. Med. 24 (2022) 50–55.

[7] S.Y. Lee, Temozolomide resistance in glioblastoma multiforme, Genes Dis. 3 (2016) 198–210.

[8] H. Strobel, T. Baisch, R. Fitzel, K. Schilberg, M.D. Siegelin, G. Karpel-Massler, K. M. Debatin, M.A. Westhoff, Temozolomide and other alkylating agents in glioblastoma therapy, Biomedicines 7 (2019).

[9] M. Rubio-Camacho, J.A. Encinar, M.J. Martínez-Tomé, R. Esquembre, C.R. Mateo, The interaction of Temozolomide with blood components suggests the potential use of human serum albumin as a biomimetic carrier for the drug, Biomolecules 10 (2020).

[10] H.S. Friedman, T. Kerby, H. Calvert, Temozolomide and treatment of malignant glioma, Clin. Cancer Res.: Off. J. Am. Assoc. Cancer Res. 6 (2000) 2585–2597.

[11] M.A. Taylor, B.C. Das, S.K. Ray, Targeting autophagy for combating chemoresistance and radioresistance in glioblastoma, Apopt.: Intern. J. Progr. Cell Death 23 (2018) 563–575.

[12] M. Fresnais, S. Turcan, D. Theile, J. Ungermann, Y. Abou Zeed, J.R. Lindner, M. Breitkopf, J. Burhenne, W.E. Haefeli, R. Longuespée, Approaching sites of action of Temozolomide for pharmacological and clinical studies in glioblastoma, Biomedicines 10 (2021).

[13] K. Bouzinab, H. Summers, J. Zhang, M.F.G. Stevens, C.J. Moody, L. Turyanska, N. R. Thomas, P. Gershkovich, M.B. Ashford, E. Vitterso, L.C.D. Storer, R. Grundy, T. D. Bradshaw, In search of effective therapies to overcome resistance to Temozolomide in brain tumours, Cancer Drug Resist. (Alhambra, Calif.) vol. 2 (2019) 1018–1031.

[14] R. Jatyan, P. Singh, D.K. Sahel, Y.G. Karthik, A. Mittal, D. Chitkara, Polymeric and small molecule-conjugates of temozolomide as improved therapeutic agents for glioblastoma multiforme, J. Controll. Rel.: Off. J. Controll.Rele. Soc. 350 (2022) 494–513.

[15] J. Gao, Z. Wang, H. Liu, L. Wang, G. Huang, Liposome encapsulated of temozolomide for the treatment of glioma tumor: preparation, characterization and evaluation, Drug Discover. Therap. 9 (2015) 205–212.

[16] X. Song, L. Xie, M. Chang, X. Geng, X. Wang, T.C. Chen, X. Song, Temozolomide-perillyl alcohol conjugate downregulates O(6)-methylguanin DNA methltransferase via inducing ubiquitination-dependent proteolysis in non-small cell lung cancer, Cell Death Dis. 9 (2018) 202.

[17] L. Xie, X. Song, W. Guo, X. Wang, L. Wei, Y. Li, L. Lv, W. Wang, T.C. Chen, X. Song, Therapeutic effect of TMZ-POH on human nasopharyngeal carcinoma depends on reactive oxygen species accumulation, Oncotarget 7 (2016) 1651–1662.

[18] S.M. Ward, M. Skinner, B. Saha, T. Emrick, Polymer-Temozolomide conjugates as therapeutics for treating glioblastoma, Mol. Pharm. 15 (2018) 5263–5276.

[19] K. Du, Q. Xia, H. Heng, F. Feng, Temozolomide-doxorubicin conjugate as a double intercalating agent and delivery by Apoferritin for glioblastoma chemotherapy, ACS Appl. Mater. Interfaces 12 (2020) 34599–34609.

[20] Y. Peng, J. Huang, H. Xiao, T. Wu, X. Shuai, Codelivery of temozolomide and siRNA with polymeric nanocarrier for effective glioma treatment, Int. J. Nanomedicine 13 (2018) 3467–3480.

[21] M. Bhat, R. Jatyan, A. Mittal, R.I. Mahato, D. Chitkara, Opportunities and challenges of fatty acid conjugated therapeutics, Chem. Phys. Lipids 236 (2021), 105053.

[22] K.S. Italiya, S. Mazumdar, S. Sharma, D. Chitkara, R.I. Mahato, A. Mittal, Self-assembling lisofylline-fatty acid conjugate for effective treatment of diabetes mellitus, Nanomedicine 15 (2019) 175–187.

[23] X.Y. Ke, B.J. Zhao, X. Zhao, Y. Wang, Y. Huang, X.M. Chen, B.X. Zhao, S.S. Zhao, X. Zhang, Q. Zhang, The therapeutic efficacy of conjugated linoleic acid - paclitaxel on glioma in the rat, Biomaterials 31 (2010) 5855–5864.

[24] A. Göder, G. Nagel, A. Kraus, B. Dörsam, N. Seiwert, B. Kaina, J. Fahrer, Lipoic acid inhibits the DNA repair protein O 6-methylguanine-DNA methyltransferase (MGMT) and triggers its depletion in colorectal cancer cells with concomitant autophagy induction, Carcinogenesis 36 (2015) 817–831.

[25] D.K. Sahel, M. Salman, M. Azhar, S.G. Goswami, V. Singh, M. Dalela, S. Mohanty, A. Mittal, S. Ramalingam, D. Chitkara, Cationic lipopolymeric nanoplexes containing the CRISPR/Cas9 ribonucleoprotein for genome surgery, J. Mater. Chem. B 10 (2022) 7634–7649.

[26] S. Sharma, S.S. Pukale, D.K. Sahel, D.S. Agarwal, M. Dalela, S. Mohanty, R. Sakhuja, A. Mittal, D. Chitkara, Folate-targeted cholesterol-grafted Lipo-polymeric nanoparticles for chemotherapeutic agent delivery, AAPS PharmSciTech 21 (2020) 280.

[27] N. Clemente, B. Ferrara, C.L. Gigliotti, E. Boggio, M.T. Capucchio, E. Biasibetti, D. Schiffer, M. Mellai, L. Annovazzi, L. Cangemi, E. Muntoni, G. Miglio, U. Dianzani, L. Battaglia, C. Dianzani, Solid lipid nanoparticles carrying temozolomide for melanoma treatment. preliminary in vitro and in vivo studies, Int. J. Mol. Sci. 19 (2018).

[28] G. Tianqin, C. Chunlei, W. Jingjing, Synergistic anti-glioma effects in vitro and in vivo of Enediyne antibiotic neocarzinostatin and paclitaxel via enhanced growth delay and apoptosis-induction, Biol. Pharm. Bull. 39 (2016) 1623–1630.

[29] D.J. Lundy, K.J. Lee, I.C. Peng, C.H. Hsu, J.H. Lin, K.H. Chen, Y.W. Tien, P.C. H. Hsieh, Inducing a transient increase in blood-brain barrier permeability for improved liposomal drug therapy of glioblastoma multiforme, ACS Nano 13 (2019) 97–113.

[30] S. Chibbaro, L. Benvenuti, A. Caprio, S. Carnesecchi, F. Pulerà, F. Faggionato, D. Serino, C. Galli, M. Andreuccetti, N. Buxton, R. Gagliardi, Temozolomide as first-line agent in treating high-grade gliomas: phase II study, J. Neuro-Oncol. 67 (2004) 77–81.

[31] H. Zhang, S. Gao, Temozolomide/PLGA microparticles and antitumor activity against glioma C6 cancer cells in vitro, Int. J. Pharm. 329 (2007) 122–128.

[32] S.D. Baker, M. Wirth, P. Statkevich, P. Reidenberg, K. Alton, S.E. Sartorius, M. Dugan, D. Cutler, V. Batra, L.B. Grochow, R.C. Donehower, E.K. Rowinsky, Absorption, metabolism, and excretion of 14C-temozolomide following oral administration to patients with advanced cancer, Clin. Cancer Res.: Off. J. Am. Assoc. Cancer Res. 5 (1999) 309–317.

[33] C. Fang, K. Wang, Z.R. Stephen, Q. Mu, F.M. Kievit, D.T. Chiu, O.W. Press, M. Zhang, Temozolomide nanoparticles for targeted glioblastoma therapy, ACS Appl. Mater. Interfaces 7 (2015) 6674–6682.

[34] F. Li, C. Snow-Davis, C. Du, M.L. Bondarev, M.D. Saulsbury, S.O. Heyliger, Preparation and characterization of lipophilic doxorubicin pro-drug micelles, J. Vis. Exp. JoVE (2016).

[35] K.S. Italiya, M. Basak, S. Mazumdar, D.K. Sahel, R. Shrivastava, D. Chitkara, A. Mittal, Scalable self-assembling micellar system for enhanced oral bioavailability and efficacy of Lisofylline for treatment of type-I diabetes, Mol. Pharm. 16 (2019) 4954–4967.

[36] L. Jiang, W. Wang, Q. He, Y. Wu, Z. Lu, J. Sun, Z. Liu, Y. Shao, A. Wang, Oleic acid induces apoptosis and autophagy in the treatment of tongue squamous cell carcinomas, Sci. Rep. 7 (2017) 11277.

[37] S. Sharma, S. Mazumdar, K.S. Italiya, T. Date, R.I. Mahato, A. Mittal, D. Chitkara, Cholesterol and morpholine grafted cationic amphiphilic copolymers for miRNA-34a delivery, Mol. Pharm. 15 (2018) 2391–2402.

[38] S. Zhu, W. Jiao, Y. Xu, L. Hou, H. Li, J. Shao, X. Zhang, R. Wang, D. Kong, Palmitic acid inhibits prostate cancer cell proliferation and metastasis by suppressing the PI3K/Akt pathway, Life Sci. 286 (2021), 120046.

[39] X. Lu, H. Yu, Q. Ma, S. Shen, U.N. Das, Linoleic acid suppresses colorectal cancer cell growth by inducing oxidant stress and mitochondrial dysfunction, Lipids Health Dis. 9 (2010) 106.

[40] G.J. Kitange, B.L. Carlson, M.A. Schroeder, P.T. Grogan, J.D. Lamont, P.A. Decker, W. Wu, C.D. James, J.N. Sarkaria, Induction of MGMT expression is associated with temozolomide resistance in glioblastoma xenografts, Neuro-oncology 11 (2009) 281–291.

[41] L. Persano, F. Pistollato, E. Rampazzo, A. Della Puppa, S. Abbadi, C. Frasson, F. Volpin, S. Indraccolo, R. Scienza, G. Basso, BMP2 sensitizes glioblastoma stem-like cells to Temozolomide by affecting HIF-1α stability and MGMT expression, Cell Death Dis. 3 (2012), e412.

[42] F. Wang, K. Bhat, M. Doucette, S. Zhou, Y. Gu, B. Law, X. Liu, E.T. Wong, J.X. Kang, T.C. Hsieh, S.Y. Qian, E. Wu, Docosahexaenoic acid (DHA) sensitizes brain tumor cells to etoposide-induced apoptosis, Curr. Mol. Med. 11 (2011) 503–511.

[43] A.K. Singh, K.S. Italiya, S. Narisepalli, D. Chitkara, A. Mittal, Role of chain length and degree of unsaturation of fatty acids in the physicochemical and pharmacological behavior of drug-fatty acid conjugates in diabetes, J. Med. Chem. 64 (2021) 14217–14229.

[44] E.S. Redgate, M. Deutsch, S.S. Boggs, Time of death of CNS tumor-bearing rats can be reliably predicted by body weight-loss patterns, Lab. Anim. Sci. 41 (1991) 269–273.

[45] Y. Jin, Y. Lian, L. Du, S. Wang, C. Su, C. Gao, Self-assembled drug delivery systems. Part 6: in vitro/in vivo studies of anticancer N-octadecanoyl gemcitabine nanoassemblies, Int. J. Pharm. 430 (2012) 276–281.

[46] Y. Yu, L. Wang, J. Han, A. Wang, L. Chu, X. Xi, R. Kan, C. Sha, K. Sun, Synthesis and characterization of a series of Temozolomide esters and its anti-glioma study, J. Pharm. Sci. 110 (2021) 3431–3438.

Journal of Controlled Release 350 (2022) 494–513

Contents lists available at ScienceDirect

Journal of Controlled Release

journal homepage: www.elsevier.com/locate/jconrel

Polymeric and small molecule-conjugates of temozolomide as improved therapeutic agents for glioblastoma multiforme

Reena Jatyan, Prabhjeet Singh, Deepak Kumar Sahel, Karthik Y.G., Anupama Mittal, Deepak Chitkara*

Department of Pharmacy, Birla Institute of Technology and Science Pilani, BITS-Pilani, Vidya Vihar, Pilani 333031, Rajasthan, India

ARTICLE INFO

Keywords:
Glioblastoma Multiforme
Temozolomide
Polymer drug conjugates
Prodrugs
Small molecules

ABSTRACT

Temozolomide (TMZ), an imidazotetrazine, is a second-generation DNA alkylating agent used as a first-line treatment of glioblastoma multiforme (GBM). It was approved by FDA in 2005 and declared a blockbuster drug in 2008. Although TMZ has shown 100% oral bioavailability and crosses the blood-brain barrier effectively, however it suffers from limitations such as a short half-life (~1.8 h), rapid metabolism, and lesser accumulation in the brain (~10–20%). Additionally, development of chemoresistance has been associated with its use. Since it is a potential chemotherapeutic agent with an unmet medical need, advanced delivery strategies have been explored to overcome the associated limitations of TMZ. Nanocarriers including liposomes, solid lipid nanoparticles (SLNs), nanostructure lipid carriers (NLCs), and polymeric nanoparticles have demonstrated their ability to improve its circulation time, stability, tissue-specific accumulation, sustained release, and cellular uptake. Because of the appreciable water solubility of TMZ (~5 mg/mL), the physical loading of TMZ in these nanocarriers is always challenging. Alternatively, the conjugation approach, wherein TMZ has been conjugated to polymers or small molecules, has been explored with improved outcomes *in vitro* and *in vivo*. This review emphasized the practical evidence of the conjugation strategy to improve the therapeutic potential of TMZ in the treatment of glioblastoma multiforme.

1. Introduction

Glioblastoma (GBM) is the most prevalent and deadly primary malignant brain tumor in adults, accounting for 16% of all brain and central nervous system tumors [1]. Regardless of sophisticated diagnostic methods and finest multimodal treatment, constituting surgical resection, radiotherapy, and concurrent temozolomide chemotherapy, the major number of patients experiences nominal progression-free survival and tumor relapse. This could be attributed mainly to tumor heterogeneity, its infiltrative pattern, and location, thereby rendering it more lethal. A small molecule, temozolomide (TMZ), has demonstrated a promising effect in treating malignant gliomas and other hard-to-treat malignancies in conjugation to radiotherapy. It is a second-generation imidazotetrazine DNA alkylating prodrug, stable at acidic conditions that converts to the active alkylating agent under physiological conditions liberating 5-aminoimidazole-4-carboxamide (AIC) and a highly reactive methyl diazonium carbocation. This carbocation is responsible for the addition of the electrophilic methyl group to the susceptible nucleophilic DNA sites within the tumor cells resulting in DNA double-strand breaks, cell cycle halt, and subsequent cell death [2].

In a randomized phase III clinical study, administration of TMZ displayed the median overall survival time around 14.9–16.6 months, with progression-free survival (PFS) ranging from 5.5 to 6.7 months and a 2-year overall survival rate up to 34.2% [3], with at best 5-year survival rate up to 9.8% in newly diagnosed glioblastoma [2,4]. Furthermore, patients with MGMT methylation were found to be positively associated with improved overall survival (up to 21.4 months) and PFS (up to 8.7 months) [3]. Clinical evaluation of TMZ in GBM patients demonstrated linear wide tissue distribution pharmacokinetics with almost 100% bioavailability after oral administration to adults and children. However, the treatment with TMZ also showed multiple adverse effects. For instance, patients administered with TMZ exhibit positive effects against GBM and refractory anaplastic astrocytoma in adults, but TMZ is also known to induce negative effects towards

* Corresponding author at: Department of Pharmacy, Birla Institute of Technology and Science (BITS) Pilani, Pilani Campus, Vidya Vihar, Pilani 333 031, Rajasthan, India.
E-mail address: deepak.chitkara@pilani.bits-pilani.ac.in (D. Chitkara).

https://doi.org/10.1016/j.jconrel.2022.08.024
Received 25 March 2022; Received in revised form 31 July 2022; Accepted 12 August 2022
Available online 1 September 2022

hematopoietic stem cells, primarily due to its non-selective DNA alteration activity, resulting in dose-limiting hematological toxicity. Likewise, in a randomized clinical trial, patients treated with TMZ and radiotherapy resulted in grade 3 or grade 4 hematological toxic effects such as leukopenia, neutropenia, thrombocytopenia, anemia, etc. [5–7].

TMZ has demonstrated advancement in the treatment of the disease; however, it remains far from the optimal outcome. The reason behind such an outcome could be the degradation of the molecule under physiological conditions, thereby limiting its availability in the brain. Additionally, the inevitable development of chemoresistance results in a poor prognosis. In order to overcome the aforementioned limitations, several approaches have been adopted, such as encapsulation of TMZ in nano-carriers (including liposomes, solid lipid nanoparticles, nanostructured lipid carriers, polymeric nanoparticles, and dendrimers), gel-based systems, chemical modifications in the molecule, etc., that exhibited protection and targeting towards the GBM with minimal adverse effects [8]. For instance, TMZ loaded liposomes showed an improved pharmacokinetic profile and circulation half-life by several folds that resulted in enhanced accumulation of TMZ in the brain compared to free TMZ with a reduction in systemic toxicity and improvement in TMZ dose-toleration [9,10]. Furthermore, active functionalization with chlorotoxin onto chitosan-based nano-carrier system delivering TMZ yielded a smaller average particle size of <100 nm with improved aqueous stability under physiological pH, acidic pH, and FBS by 7.4, 31.5 and 11.8 folds, respectively. Chlorotoxin functionalization led to a marked improvement in cellular uptake by 2–6 folds with the reduction in IC_{50} by 50–90%, demonstrating targeting delivery towards the GBM cells [11]. In another set of work, peptide-functionalized nanostructured lipid carriers yielded significantly uniform and smaller particles, demonstrating improved *in vitro* cell inhibition, accumulation of the drug in tumor tissue, reduction in tumor volume, and low systemic toxicity in subcutaneously U87MG tumor-bearing mice [12,13]. Although, compared to free TMZ, nanocarrier-based TMZ delivery possess several advantages, despite this, the unique hydrophilic behavior of TMZ prevented the optimal encapsulation into the nanocarrier-based system. The development of a prodrug-based method could be used to address these constraints, wherein TMZ could be attached to either a small molecule (prodrug approach) or could be grafted to a polymer (polymer-drug conjugates (PDC)). These methods are well-known and have been widely documented in recent years, depicting improved drug loading, stability, circulation time, overcoming drug resistance. For instance, Chen and group synthesized TMZ analog with a natural monoterpene perillyl alcohol (POH). The resulting TMZ-POH exhibited improvement in stability, circulation half-life and was found to be toxic against the TMZ resistant cell lines. Furthermore, *in vivo* administration exhibited improvement in median survival half-life from 6 days to 28 days compared to free TMZ [14]. In a preclinical evaluation, the intracellular concentrations of TMZ were found to be higher after TMZ-POH (NEO212) treatment in U251TR cells compared to TMZ therapy. Further, *in vivo* levels of TMZ-POH (NEO212) in the tumor-bearing hemisphere were higher compared to the contralateral normal hemisphere in mice with a significantly higher brain: plasma ratio compared to free TMZ in syngeneic GL261 brain tumor-bearing mice [15]. Ward et al. developed a series of redox-sensitive PDCs using TMZ pendant groups with 2-methacryloyloxyethyl phosphorylcholine (MPC) viz. RAFT polymerization. Conjugation to TMZ to polyMPC improved the TMZ loading content up to 35 mol% and a half-life ranging from 2 to 19 times compared to free TMZ. *In vitro* cell-based assays also demonstrated marked improvement in cellular uptake and cytotoxicity in glioblastoma cell lines [16]. This review highlights the prospects and limitations of TMZ and key examples of conjugation strategy that improved the TMZ efficacy in treating glioblastoma multiforme.

2. Glioblastoma multiforme: Epidemiology, etiology, and pathophysiology

Glioblastoma multiforme is a malignant and aggressive form of glioma of an astrocytic lineage that is commonly found in CNS with grade IV malignancy and accounts for 80% of all malignant primary brain tumors. According to WHO standards of classification, gliomas are classified into four grades (I to IV) based upon the extent of malignancy of the tumor. Grade I and II depict the low-grade tumor with low proliferative potential, while grade III and grade IV tumors are comparatively malignant, dedifferentiated, aggressive, and lethal [17]. Moreover, multistep tumorigenesis of the malignancy of the glial cells accounts for nearly 90% of GBM IDH-wild type cases, and the rest 10% is developed from the progression of low-grade astrocytoma or oligodendrogliomas, forming secondary glioblastoma. The development of secondary glioblastoma is comparatively slower and can take around 4–5 years to develop, while primary glioblastoma usually takes around three months with nearly negligible diagnosis [1,18]. The standard treatment for GBM includes surgical removal of the tumor, wherein >95% of the tumor can be removed, followed by chemotherapy and radiotherapy. In a randomized clinical trial, patients treated with TMZ adjuvant with radiotherapy exhibited improvement in median survival rate to 14.6 months compared to 12.1 months with radiotherapy alone. In addition, 2-year progression-free survival was found to be improved up to 10.7% with TMZ plus radiotherapy compared to 1.5% in the radiotherapy alone [5]. Despite the fact that the advanced multimodal therapy, including surgical resection, radiotherapy, chemotherapy, the overall prognosis, and survival are still limited in GBM patients. Further, the associated decline in neurological function leads to a hampered quality of life of the patients and their families [19,20].

2.1. Epidemiology

Central nervous system (CNS) tumors cases have been estimated globally in multiple age groups, including children, adults, and aged individuals, with an estimation of 7–11 cases per 1 million. In a global burden of disease study, CNS cancer incidence was found to be around 330,000 cases with a significantly higher death rate of 227,000 cases worldwide. Besides, 7.7 million CNS cancer patients have been estimated to suffer from disability-adjusted life-years due to its severity of brain damage. Global age-standardized incidence rates have also been increased by 17.3% between the year 1990 to 2016, with a rate of 4.63 cases per 100,000 individuals [21,22]. According to Globocan (WHO), brain and CNS-related cancers were newly diagnosed in 308,102 cases accounting for 1.7% cases of all the cancers, and 251,329 deaths were reported worldwide in 2020 both in males and females, including all age brackets. The 5-year prevalence data also indicates the majority of cases are prevalent in Asians with 435,532 cases with a total count of 837,152 individuals worldwide. Furthermore, demographic data indicates that the majority (54.2%) of incidences and deaths were observed in Asians, followed by the European population [23]. By 2040, the incidence rate is expected to rise to 435,000 individuals. The worldwide age-standardized incidences rates were observed to be higher in males compared to females, with 3.9 to 3.4 cases per 100,000 individuals, respectively. In the US alone, all brain and CNS-related tumors with 17th position account for 24,538 new cases. Moreover, it has accounted for 3% and 18,133 deaths, acquiring the 9th rank in the list. [24]. Wherein primary GBM is uncommon in children and grows rapidly with the average patient age of 62 years, the incidence increases till the 75–84 years and decreases after 85 years, with an annual age-adjusted incidence of 5.6 compared with 3.5 per 100,000 individuals. The mean patient's age for secondary GBM is 45 years and is commonly found in children and adults [25,26]. In a hospital-based clinico-epidemiology cancer profiling, a total of 1450 glioma cases were analyzed with a mean age of 39 years, wherein glioma was more prevalent in the male population, up to 66.6%. Out of 1450 cases, 41.4% of cases were of high-

grade glioma (glioblastoma) followed by astrocytoma (22.8%), pilocytic astrocytoma (6.2%), and oligodendroglioma (4.5%) [27].

2.2. Etiology

The complete etiology of GBM has not been fully discovered by the scientific community, as no specific underlying reason for the occurrence of GBM can be identified. To date, few risk factors have been identified responsible for the development of glioblastoma. Exposing ionizing radiation is the only strongest and validated risk factor; >100 cases of glioblastoma have been diagnosed from radiation exposure with an overall risk of 2.5%. Also, the high-dose of radiotherapy and chemotherapy for treatment of the cancers are found to have a positive correlation in the development of intracranial tumors. The patients treated for acute lymphoid leukemia with radiotherapy and antimetabolite chemotherapeutic agents were more inclined to the incidence of GBM [28,29]. In retrospective cohort data, patients treated with radiation have demonstrated intensified risk of cancer in various groups. For instance, exposure to ionizing radiation due to the atomic bomb explosion in Hiroshima and Nagasaki resulted in increased incidences of all cancers, including gliomas. Furthermore, several other factors, including exposure to chemical carcinogens like pesticides, organochlorides, alkylureas, vinyl chlorides, N-nitroso compounds, aspartame, etc., are suspected to increase the risk of cancer [17,30–32]. While in a meta-analysis study, patients suffering from asthma and other allergenic conditions have shown an inverse association with the development of GBM due to activation of immune surveillance mechanisms [33]. Furthermore, the genetic predisposition syndromes are found to be associated with 5–10% of the cases associated with the development of glioblastoma, including Li–Fraumeni syndrome, Cowden's disease, and neurofibromatosis Turcot's syndrome and multiple hamartomas, providing strong, suitable candidates for understanding the possible underlying cause and molecular pathway in GBM [26,31]. Han et al. reported a supporting relationship between the head trauma and the development of glioma, describing the trauma as a cocarcinogen in the presence of initiating carcinogen [34]. Besides, the role of retroviruses and herpesviruses have been studied extensively in inducing gliomas in experimental models, suggesting a potential association between the gliomas and the viral onco-modulation in tumor malignancy [35].

2.3. Pathophysiology

Based on the histopathological evaluation, GBM cells are poorly differentiated cells with neoplasmic properties, characterized by pseudo-palisading foci, nuclear hyperchromasia, increased angiogenesis, mitotic activity, thrombosis, cellular and nuclear atypia, and reduced apoptosis, resulting in abnormal proliferation, growth, and survival of GBM cells. The most frequent location of occurrence of GBM is in the supratentorial region (95% of cases), with tumor incidences in frontal, temporal, and parietal lobes [36], followed by the cerebellum, brain stem, and spinal cord [37]. According to WHO based classification, GBM is subdivided as per the histopathological criteria wherein, Grade I tumor or juvenile pilocytic astrocytoma is characterized by benign and slow-growing tumor, Grade II or anaplastic astrocytoma is characterized by increased cellularity with minimal necrosis, Grade III tumor or anaplastic astrocytoma shows tumor hypercellularity, poorly differentiated, mitosis with a high rate of reoccurrence, and Grade IV tumor or glioblastoma is a highly deadly form of tumor possess a high rate of hypercellularity, minimal cellular differentiation, angiogenesis, and necrosis, disrupting BBB and forms a cystic and gelatinous region in the brain. GBM can be identified macroscopically with a characteristic feature of the development of gross appearance in the white matter of brain tissue. In a few cases, a portion of affected tissue appears to be necrotic or yellowish, while some of the tumor tissue appears to show angiogenesis and hemorrhage [17]. The tumor can be observed as an individual large, irregular-shaped lesion arising in the white matter that can be perceived as anaplastic astrocytoma, demonstrating the tumor heterogeneity, ranging from poorly differentiating cells to highly differentiated cells with their angiogenic, invading, proliferation, and survival feature.

The development of tumor may occasionally develop symptoms, mainly because of the site of the tumor, tissue necrosis, and increased intracranial pressure, resulting in the development of seizures (could be focal, partial, complex, or generalized seizures), cognitive, hearing, and visual impairment, gait disfigurement, headaches, etc.; which is usually be mistaken for the stroke [38]. Due to tumor heterogeneity, disruption in the brain microenvironment (BME) causes reduced tight junction proteins, loss of pericytes, and astrocytic protection, exhibiting an increased permeability and distribution of foreign substances to the BME. Furthermore, the presence of leaky, fenestrated, and damaged lymphatic vessels in GBM attributes to the accumulation of metabolic and waste proteins, resulting in the formation of edema [39] (Fig. 1(3)). Likewise, using contrast-enhanced MRI, glioma-bearing mice depicted enhanced vasculature leakage in the BME that demonstrated the formation of brain edema. Furthermore, the outflow of CSF was also found to be significantly reduced in glioma-bearing mice, depicting the damage in the lymphatic drainage in glioma cases [40].

Based on the severity and clinical evaluation, GBM is classified into primary and secondary glioblastoma. Primary glioblastoma or *de novo* grade IV glioblastoma develops into undifferentiated tumor cells without prominent evidence directly from a malignant precursor or stem cell. Molecular and gene alterations in primary glioblastoma usually includes alteration in epidermal growth factor receptor (EGFR), Phosphatase and Tensin homolog (PTEN), Telomerase Reverse Transcriptase (TERT), Mouse Double Minute 2 (MDM2), deletion of p16, and Loss of heterozygosity (LOH) at chromosome 10q, etc. Secondary GBM develops from lower-grade astrocytoma, which eventually mutates to higher-grade tumors via distinct molecular pathways, including isocitrate dehydrogenase 1 and 2 (IDH1/2), TP53 gene, platelet-derived growth factor receptor A (PDGFRA/α), Retinoblastoma (RB), and Loss of heterozygosity (LOH) at 17p, 19q, and 10q, Alpha Thalassemia/Mental Retardation Syndrome X-linked (ATRX) [17,20,41–43]. The development of glioblastoma eventually results in alteration in the endothelial tight junctions of the blood-brain barrier (BBB), leading to an increased moment of molecules, blood-borne factors, and pathogens to the brain, causing cerebral malfunctions [44] (Fig. 1). Currently going advancements in pathological techniques have attributed the correlation between the molecular downstream pathways with their clinical outcome. For instance, in a clinical high-grade glioma cohort population-based study, patients with grade III and IV glioma were evaluated for their genetic pathology. Wherein, involvement of MGMT promoter methylation, 1p19q co-deletion, IDH1 mutation, and ATRX loss was observed in HGG. Further, the prominent association of MGMT promoter methylation was found to be associated with improved overall survival and could be served as a prognostic marker in HGGs [45]. Other multiple factors, including PDGFR, Crk, p130CAS, HEF1 c-Met, HIF-α, etc., are also found to be pathologically active in the promotion of glioma survival, migration, and invasion [46].

3. Blood brain barrier (BBB): Challenges and fate of molecules

The blood-brain barrier (BBB) plays a vital role in filtering the blood components and other blood-mediated infections, critical for the normal functioning of the central nervous system and the homeostasis of the brain microenvironment. It is found in all organisms having well-developed CNS comprises multiple cellular and extracellular components such as endothelial cells, pericytes, astrocytes, and extracellular matrix [47]. The presence of claudins, occludin, junction adhesion, and cytoplasmic accessory proteins are the building blocks of the blood-brain barrier [48], forming tight junctions that primarily impede the paracellular diffusion and exhibit a low degree of transcytosis from blood to brain. In addition, cellular components, including astrocytes,

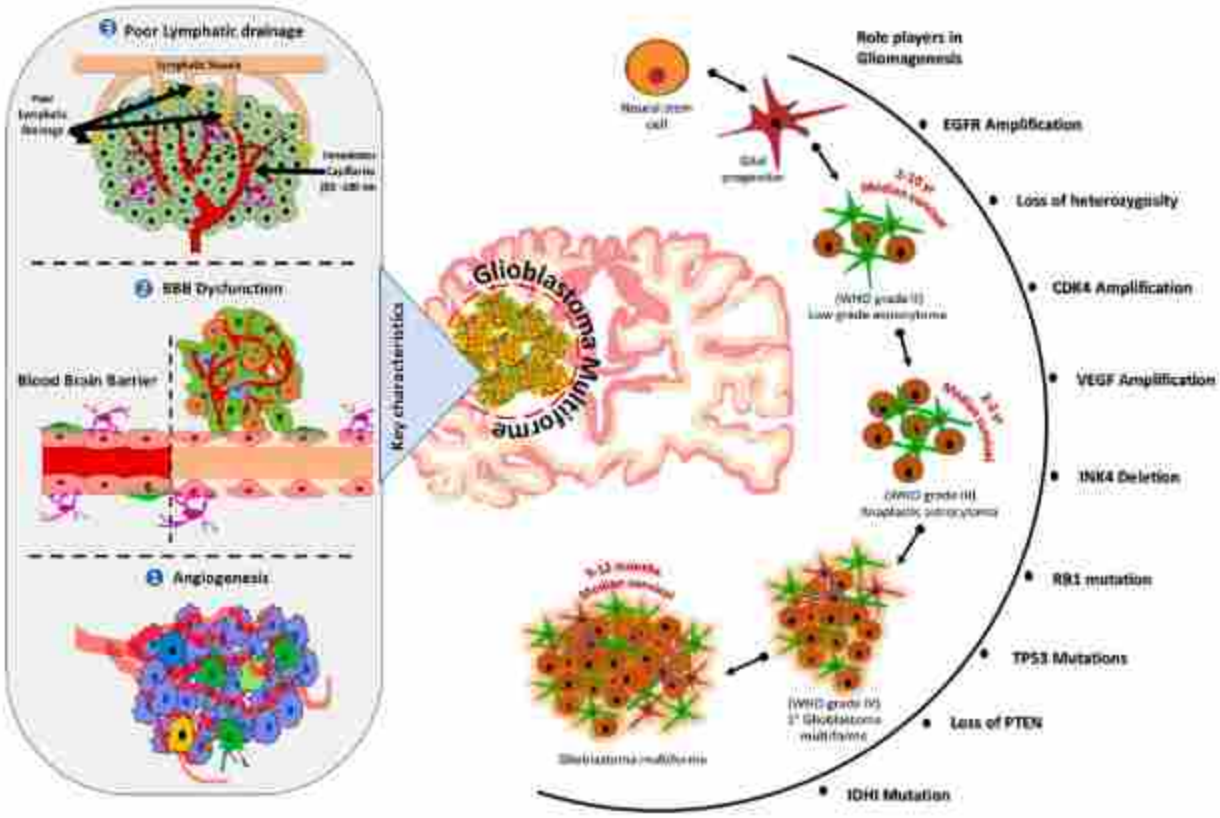

Fig. 1. Key players in the progression in Glioma genesis and the severity of the WHO grade IV glioma with key characteristics including 1) angiogenesis, 2) BBB dysfunction and 3) poor lymphatic drainage.

pericytes, and endothelial cells, work together as a single neovascular unit and release several vasoactive adhering proteins that help in the regulation of vascular tension, expression of tight junction proteins, and transport enzymes [49,50]. Such a dense network of barriers facilitates the endothelial cells to regulate the brain homeostasis, neuronal functions and protects the brain by imparting the combination of physical, transport, and the metabolic barrier between the blood and brain compartment, thus creating a high paracellular resistance for pathogens, injury, molecules, proteins, inflammatory markers, neuro-active molecules, extracellular ligands, and other blood-borne components. The BBB properties are not stringently fixed; rather, it remains dynamic, which can be physiologically and pathologically regulated by the manifestation in the endothelial cell. However, in GBM, dysfunction of the BBB results in the impairment in the tight endothelial junctions, resulting in the loss of BBB characteristics, including damage in tight junctions, depletion of adhesin proteins (tenascin, agrin claudin, occludin), increased vessel permeability, endothelial fenestrations, pericytic detachment, and alteration in the extracellular matrix and thus termed as blood-brain tumor barrier (BBTB) [51,52]. The loss in the BBB integrity causes the development of several other complications such as stroke, neuroinflammatory shock, edema, altered neuronal signaling, immune cell infiltration, eventually leading to neuronal dysregulation or degeneration. The hypercellularity and neoangiogenesis behavior of glioblastoma deals in the alteration in the integrity of tight junctions, endothelial fenestrations, perivascular space, and other components of the neovascular unit of BBB. Also, the glioma cell growth degenerates the vascular system and reduces vascular perfusion resulting in the secretion of hypoxia-related angiogenesis factors like VEGF, BFGF, IL-8, etc. Such growth factors stimulate neovascularisation and form different types of blood vessels, characterized by modulation in tight junctions and ECM [52,53]. Wherein, type I vessels depict the nominal agrin and claudin expression, type II and III exhibit either lowered or loss of expression of tenascin and claudin ECM. The type IV vessels showed complete loss of agrin and tight junctions of BBB, resulting in leaky blood vessels. Furthermore, dysfunction in BBB related ECM can be correlated with other extracellular enzymes like matrix metalloproteinase-3, matrix metalloproteinase-9, matrix metalloproteinase-12, cathepsin B, plasminogen activator, and scatter factor/ hepatocyte growth factor (SF/HGF) [54,55], which are found to be upregulated in proliferating glioma cells. Interestingly, upregulation in MMPs, TIMPs, and other proteases imparted parallel degradation in BBB integrity via, degradation of BBB, ECM growth factors, cleavage of basal laminal proteins, and remodeling of ECM, causing initiation, growth, survival, and angiogenesis of glioma cells [55]. For the effective treatment of cancer, an active moiety must be able to penetrate the barriers present alongside the tumor, including blood-borne barrier (pH, enzymes, ions, immune system), blood-brain barrier (pericytes, basal membrane, tight junctions), blood-brain tumor barrier (pH, tumor defense system), and tumor cell penetration (cellular uptake, efflux system, endosomal degradation). The aforementioned factors play a vital role directly or indirectly behind the poor delivery and treatment within the tumor. Nearly 100% of macromolecules and 98% of neurotherapeutics are not able to permeate through the presence of stringent BBB/BBTB [52,56,57]. The physiochemical properties of a molecule are as highly important as it allows the molecule to penetrate the barriers involved in the delivery to tumor cells. For instance, according to the Lipinski rule of 5, the drug can be said to be poorly absorbed when it has a molecular weight of >500 Da, log p of >5, carrying >5 hydrogen bond donors, >10 hydrogen bond acceptor, and except biological transporters dependent substrates. In conclusion, size, lipophilicity, polar surface area, charge, plasma protein interaction, rotatable bond cosunt, an affinity for uptake, and efflux of the molecule, provide a better idea in the delivery of molecules across the BBB [57,58]. Multiple approaches have been developed to deliver the molecule to the tumor tissue, *viz.*, bypassing the

physiochemical, cellular, and molecular barriers of BBB/BBTB. The chemotherapeutics otherwise are unable to cross the intact BBB, but they partially can cross the BBTB due to the EPR effect. Thus, the permeation through the disrupted BBTB does not ensure the complete accumulation near the tumor site, resulting in the mortified efficiency of chemotherapeutics in GBM therapy [52,57].

4. Clinically approved glioblastoma interventions

To date, FDA has approved several therapies for the treatment of high-grade gliomas (HGG), including Lomustine (CCNU), Carmustine (BCNU) and its wafer implants, Bevacizumab (BVZ), Optune device (utilizes tumor treating fields), and Temozolomide (TMZ) (Temodal®) [59]. CCNU was initially approved for oral administration in 1976 for recurrent HGG acting as a nonspecific alkylating agent that causes cross-linking of DNA and RNA, and is considered as the standard of care for recurrent GBM. It is administered at a dose of 80–110 mg/m^2 once every six weeks exhibited hematological toxicity with overall survival of 11.5 months in HGG. Immediately after approval of CCNU, BCNU was approved for intravenous administration in 1977 for recurrent HGG that also acts by cross-linking of DNA and RNA with modification in glutathione reductase enzyme. Further, BCNU wafer implants were approved in 1996 and 2003 for recurrent and newly diagnosed HGG, respectively. BCNU wafers were composed of a biodegradable copolymer, polifeprosan 20 (with poly[bis(p-carboxyphenoxy)]propane and sebacic acid in 20:80 M ratio) of about 1.45 cm in diameter with 1 mm thickness containing 7.7 mg of drug per unit. BCNU wafers are applied locally after the tumor resection region for improved locoregional treatment and reduced toxicity. The BCNU wafer implants have increased overall survival but with no improvement in progression-free survival compared to intravenous BCNU. Despite BCNU demonstrating its efficacy, BCNU wafers use is not considered as a standard of care for GBM, mainly because of involved high cost, clinical complications, and challenges in wafer management.

Bevacizumab (BVZ) was approved for intravenous administration in 2009 for targeted therapy *via.* binding and inhibiting the VEGF protein expression in recurrent HGG. It is given at a dose of 10 mg/kg once every two weeks. Administration of BVZ also showed common toxicities including hypertension, gastrointestinal perforation, cerebral bleeding, wound healing, proteinuria, etc. Later on, several clinical trials were performed with BVZ as a monotherapy and in combination with other molecules wherein BVZ in combination with irinotecan, etoposide, carboplatin demonstrated positive effects in clinical trials for HGG.

TMZ got approval from FDA for oral administration in 2005 along with radiotherapy and became the standard of care for recurrent HGG. It acts as a non-specific alkylating agent, showed a 6-month progression-free survival of 53.9%. Later on, detailed mechanistic pathways were studied involving tumor cell death, development of resistance, and its complications against GBM. A detailed timeline of progress in TMZ research is shown in Fig. 2. Another therapy, Optune device aka. Tumor treating field was approved by FDA in 2011 and 2015 for recurrent and new HGG, respectively. Optune device is a portable device applied to shaved scalp for a minimum of 1 month delivering low-intensity current and intermediate frequency electrical fields that disrupts mitosis in tumor cells [59].

5. Temozolomide: Potential, drawbacks, and challenges

TMZ (IUPAC: 3, 4-dihydro-3-methyl-4-oxoimidazo [5, 1-*d*]-as-tetrazine-8-carboxamide) is one of the most potent alkylating agents with anticancer activity. TMZ (Temodal®) was approved by FDA in early 1999 for the treatment of the patient with glioblastoma multiforme as second line treatment [60]. TMZ shows its action by alkylation of guanine at the O^6 and N^7 position and adenine at N^3 position during the DNA replication converting them into O^6-methylguanine (O^6-MG), N^7-methylguanine (N^7-MG), and N^3-methyladenine (N^3-MA) that results in mismatching of base pairs and breaking in DNA double strands thus inducing the cell cycle arrest at G2/M phase and cell death [61–63]. It can cross the blood-brain barrier partially and only <1% of the administered dose reaches to the brain [64]. Therefore, to achieve

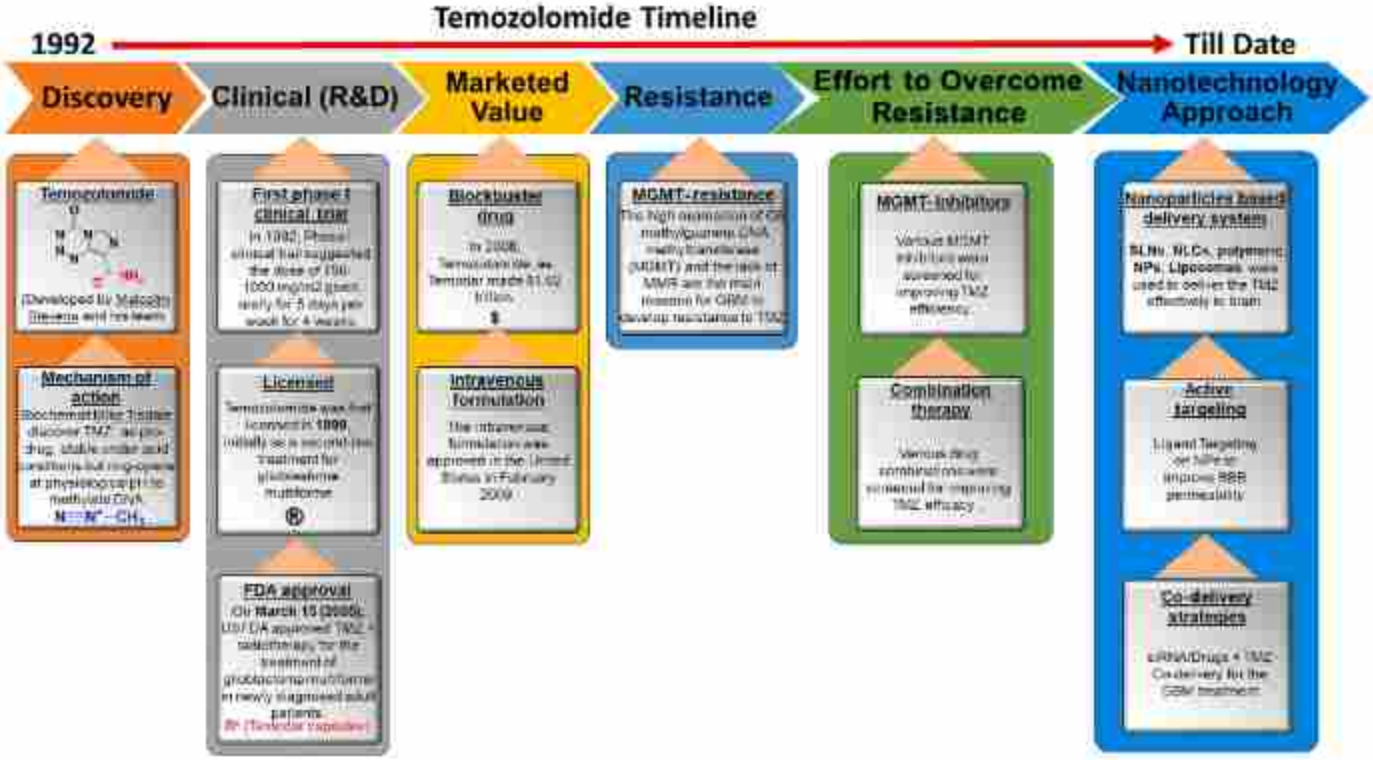

Fig. 2. History and timeline of temozolomide.

therapeutic concentration in the brain, it must be given in high doses of 200 mg/m^2/day [65]. When TMZ is given in combination with radiotherapy, it improves the median survival period slightly above a year and improves the patient's quality of life as compared to radiotherapy alone [5]. Later, the resistance was determined as a cause of failure with TMZ therapy and O^6-methylguanine-DNA methyltransferase (MGMT) played a major contribution to the development of resistance [63]. The enzyme was reported to be overexpressed in glioma cells and reverses the alkylation process done by TMZ [66,67]. Although, there are many more reported causes of TMZ resistance shown in Fig. 3, and successfully proved by experimental observations [68–70]. Although TMZ is a potent molecule, there are still several limitations resulting in its below-optimal use. Briefly, TMZ is preferred to be given *via.* oral route since it is well absorbed in the digestive tract. The reported oral bioavailability of TMZ is almost 100% [65], and the presence of food hardly affects its absorption. As reported earlier, the half-life and the volume of distribution of TMZ are 1.8 h and 17 L/m^2, respectively [65,71]. Further, after administration of 150 and 200 mg/m^2 doses, the maximum plasma concentration (Cmax) achieved was observed as 7.75 and 10.7 μg/mL, respectively [72]. TMZ is quite stable at acidic pH conditions but converts spontaneously into an active alkylating agent, MTIC (5-(3-Methyl-1-triazeno) imidazole-4-carboxamide), via decarboxylation under physiological conditions, liberating the 5-aminoimidazole-4-carboxamide (AIC) and a highly reactive methyl diazonium carbocation. This carbocation is responsible for the addition of electrophilic methyl group to the susceptible nucleophilic DNA sites within the tumor cells resulting in DNA double-strand breaks [2]. This causes cancer cell arrest from G_2 to M phase and further renders cells sensitive towards mitotic cell death. Since the pH of the blood is 7.4, the conversion of TMZ to AIC and methyl diazonium ion start immediately after the absorption of TMZ. The methyl diazonium ion has poor BBB permeability [73]. The first human pharmacokinetic studies of TMZ revealed that only 10–20% of TMZ w.r.t the plasma concentration reaches the CSF [74,75]. Additionally, a recent report revealed that a net <1% of TMZ reaches the brain efficiently [64] (Fig. 3) Thus TMZ possesses several limitations such as short half-life, dose-dependent toxicity, pH-based degradation, and *in vivo* resistance by MGMT, which limits its potency, thereby creating an unmet medical need and necessitates the use of new technologies and novel strategies for TMZ delivery.

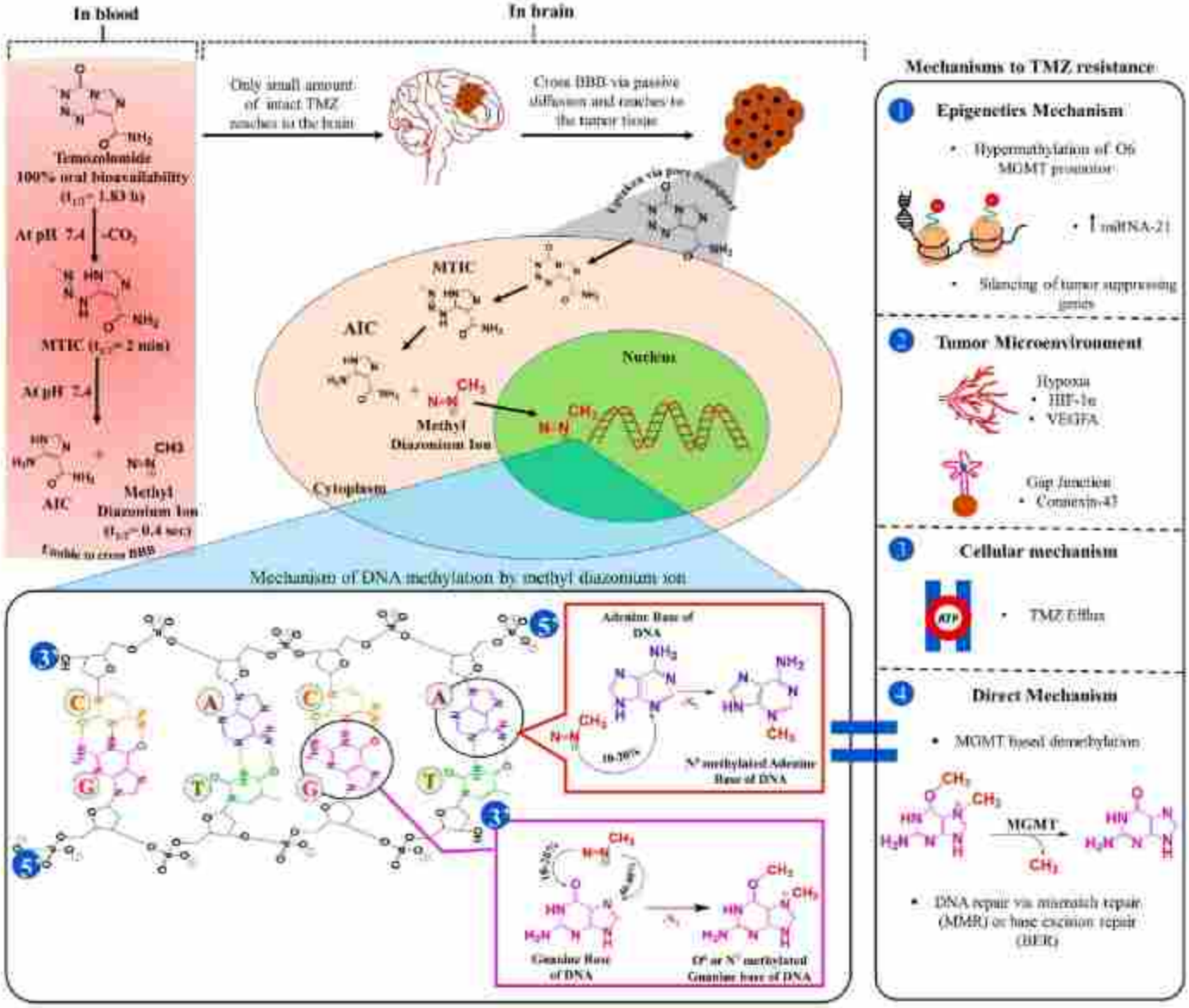

Fig. 3. Fate of TMZ in blood stream after administration and in glioma cells after reaching brain. Different mechanisms of TMZ resistance, 1) Epigenetics mechanism, 2) Tumor microenvironment, 3) Cellular mechanism, and 4) Direct mechanism.

6. Nanotechnology-based TMZ delivery

Application of nanotechnology in medicine have demonstrated an improvement in safety, efficacy, and/or compliance of the so-called "difficult-to-deliver" molecules. Strategies have also been devised to deliver TMZ in a better way so that the problems associated with this potential molecule could be avoided. Numerous treatment methods like invasive (BBB disruption, local implants, intrathecal implants) and non-invasive (intranasal, oral) have been developed to deliver the TMZ using nanocarriers to the brain. These nano-enabled medicines include a variety of systems such as polymer-based (polymeric nanoparticles, polymeric micelles, dendrimers), lipidic-based (liposomes, SLN, NLCs), and inorganic-based (iron, gold, silica) materials (Table 1) [76,77]. Compared to conventional delivery approaches, these nano-based carriers have elicited various advantages, including improved drug stability, tissue-specific delivery, biocompatibility, biodegradability with reduced systemic toxic effects, and optimal *in vitro* and *in vivo* outcomes. Several reports are available on the lipidic-based carrier system to deliver TMZ to the brain, exhibiting the biocompatibility, biodegradability, and encapsulating hydrophilic molecules as a payload [77]. Likewise, Song et al. prepared TMZ-loaded liposomes comprised of DPPC and cholesterol using a thin-film hydration method. Upon rehydration, the liposomes exhibited uniform particle size and poly dispersity index (PDI) of around 150 nm and 0.23, respectively. The resulting formulation achieved an average % encapsulation efficiency (%EE) of 52% at theoretical drug loading of 7.2% *w/w*, with a burst TMZ release up to 80% within the 6 h. Furthermore, the *in vitro* release profile demonstrated >90% of TMZ within 12 h. *In vivo* administration of TMZ-lipo demonstrated better pharmacokinetics profile and systemic circulation time, resulting in inhibition of tumor growth compared to free TMZ in orthotopic C6 tumor-bearing rats [78]. Gao et al. developed TMZ loaded liposomes using proliposomes method, yielded relatively uniform-sized particles with an average size of 156.70 ± 11.40 nm and PDI 0.29 ± 0.04 with a maximum %EE of 35.45 ± 1.48% at a drug loading capacity of 2.81 ± 0.20% *w/w*. Further, *in vitro* release assay also showed TMZ burst release up to 80% within the first hour, and release plateau was achieved at 2 h, eliciting no significant improvement in release profile. *In vivo* administration of TMZ liposomes demonstrated improvement in circulation half-life by 3.59 folds and slightly more accumulation of TMZ in brain tissue as compared to free TMZ [9]. Nordling-david et al. prepared TMZ loaded pegylated liposomes comprising DSPC, Chol, and DSPE-PEG as the lipidic carrier. The resulting liposomes exhibited an average particle size of <150 nm and PDI <0.2 with a %EE of 23% [87]. Huang et al. prepared TMZ loaded solid lipid nanoparticles of around 66 nm with %EE of 58.9% at a drug loading capacity of 0.946% *w/w*. The resulting lipid system demonstrated marked slower release up to 87.3% at 72 h. *In vivo* administration of TMZ-SLN exhibited accumulation of TMZ in the brain and improved the systemic circulation time by several folds compared to free TMZ [10]. Chen et al. reported TMZ loaded nanostructured lipidic system comprising 888 ATO, Cremophor ELP, and SPC, exhibiting particle size of 179 nm with %EE of 83% at theoretical drug loading of 7.7% *w/w* [80]. Wu et al. prepared vincristine and TMZ loaded SLN and NLC lipidic carriers yielding uniform-sized particles with an average size of 180 nm and 120 nm for SLNs and NLC, respectively. The TMZ loaded SLN and NLC systems demonstrated higher %EE of 81.2% and 89.6% at drug

Table 1
Nanocarrier systems for the delivery of TMZ with respective outcomes.

Nanocarrier	Particle Size	Zeta potential	Entrapment and Loading efficiency	Outcomes	References
scL-TMZ nanocomplex	41.4 ± 9.2 nm	30.1 ± 4.6 mV	45.23 ± 4.34%EE	1) ~2.7-fold higher antitumor activity. 2) Higher efficacy in *in-vitro* and *in-vivo* studies. 3) Significant reduction in toxicity.	[79]
Nanostructured lipid carriers	179 nm	+23 mV	91% of GL and 83% of EE	1) 3.3-fold higher reductions in tumor inhibition 2) Tumor-targeting and effective co-delivery	[80]
VCR- and TMZ-loaded SLNs (VT-SLNs) and NLCs (VT-NLCs)	160 nm for SLN 120 nm for NLC	+35.7 for SLNs +29.8 mV for NLCs	over 80% with 10.3 ± 2.3% DL for SLN and 6.8 ± 0.7% DL for NLC	1) NLCs formulation was better than SLNs 2) Dual drug loaded formulation was more efficient than single loaded drug.	[81]
Apoferritin Nanocage	13.3 ± 0.9 nm	−12.7 ± 0.3 mV	64.3 ± 5.2% encapsulation efficiency (EE) and 18.7 ± 2.3% drug loading (DL).	1) AFt was a non-toxic, biocompatible 2) Nano-sized biomaterial with in-build targeting and able to deliver concentrated TMZ in brain tumors	[82]
Liposomes	156.70 ± 11.40 nm	0.29 ± 0.04	35.45 ± 1.48% and 2.81 ± 0.20%	1) Prolonged circulation time and improved AUC. 2) TMZ-liposome decreased the accumulation in the heart and lung and increased the concentration in the brain 3) Less adverse effect and enhancement in the therapeutic effect	[9]
Dipalmitoyl phosphatidylcholine (DPPC)-based liposomes	120 nm and 160 nm	Neutral	Entrapment efficiency of 82%, with load of approximately 8.7 mg TMZ per mL	1) Inhibited tumor growth and 2) Improved tumor-growth ratio 3) Improvement in median survival 4) Improved efficacy and safety	[83]
Polymeric micelles	54 ± 4 nm	12.4 ± 1.4 mV	–	1) *In vitro* and *in vivo* studies showed efficient codelivery 2) Antiapoptotic BCL-2 gene silenced, and Bax gene activated, 3) tumor growth inhibited, and the survival rate of rats enhanced.	[84]
PAMAM-chitosan conjugate based TMZ nanoformulation (PCT)	201.4 ± 1.70 nm; (with PDI of 0.84 ± 0.105)	24.0 ± 0.17 mV	72.58 ± 0.73 with 23.40 ± 0.9% drug loading	1) Half-life increased which was 22.74 h for PCT in comparison to 15.35 h for TMZ. 2) Higher drug distribution 1) *In vitro* release for 60 days. 2) Cytotoxicity data significantly better 3) Uptake of the A2-loaded H18 nanoparticle was better	[85]
Temozolomide-loaded PLGA nanoparticles	<200 nm	−20 to −36	1.5–27% EE		[86]

loading capacity at 11.2% w/w and 7.5% w/w. The resulting lipidic system exhibited an improvement in *in vitro* cell-based assays and *in vivo* activity in U87 tumor-bearing mice [81].

Apart from the lipidic based systems, polymeric systems have also been used for the TMZ delivery. Lee et al. prepared TMZ loaded PLGA nanoparticles using emulsion solvent evaporation and nanoprecipitation method. The resulting formulation exhibited particle size >400 nm with a maximum %EE of 12.6% at a drug loading capacity of 2% *w/w* [88]. Ananta et al. prepared TMZ loaded PLGA nanoparticles using the solvent emulsification method. The resulting TMZ loaded nanoparticles demonstrated particle size of <200 nm with %EE up to 17.6% at loading efficiency of 4.4% w/w. The loaded nanoparticles demonstrated burst release of 80% within the initial six hours with no significant difference in cytotoxic effect in U87 MG glioma cells compared to free TMZ [86]. Meteoglu et al. prepared TMZ and genistein dual-loaded PLGA polymeric nanocarrier using solvent emulsification method using PVA as a stabilizer. The dual-loaded nanosystem demonstrated an average particle size of 135.5 nm with TMZ %EE up to 48.2% [89]. Further, the active functionalization with targeting ligand cetuximab to TMZ loaded PLGA nanoparticles yielded uniform-sized particles up to 162 nm with %EE of 28% at a loading capacity of 1.4% w/w. The ligand functionalized nanosystem demonstrated higher uptake in glioma cells [90]. Similarly, Song et al. prepared RGD-peptide-functionalized TMZ loaded NLCs, resulting in particle size <120 nm and PDI of <0.11. The NLCs demonstrated TMZ %EE of around 85% at a loading capacity of 7.3% and 5.6% for non-targeted and RGD-targeted systems, respectively. The *in vitro* and *in vivo* treatment with RGD-TMZ NLCs exhibited improved cell growth inhibition in U87-MG cells and reduced the tumor volume in U87-MG tumor-bearing mice [12]. Arecella et al. prepared TMZ loaded liposomes using a series of cationic lipids to improve the blood-brain barrier penetration for the treatment of glioblastoma multiforme. The cationic lipid demonstrated higher TMZ %EE ranging from 48% to 55% at drug loading capacity ranging from 16.6% to 22% w/w, demonstrating higher uptake *in vitro* and could be used as nanomedicine for the effective treatment of GBM [91]. Sharma et al. fabricated chitosan engineered PAMAM dendrimers as nanoconstructs for the delivery of TMZ for the treatment of glioma. The dendrimeric nanoconstructs exhibited an average particle size of around 200 nm with a %EE of 72.6% at drug loading capacity at 23.48% w/w. The TMZ-loaded dendrimers demonstrated improved IC_{50} in U-251 and T-98G glioma cell lines. Further, *in vivo* administration of TMZ loaded dendrimer improved the pharmacokinetic parameters with better accumulation in the brain as compared to free TMZ [85]. Although, the nanocarrier-based delivery of TMZ exhibited various advantages over free TMZ, such as improved circulation time, sustained release, better cellular uptake, less degradation, reduced systemic toxicity, improved BBB permeability, etc., still, improvement is required in terms of encapsulation and better control over drug release properties. To overcome such limitations, a prodrug strategy could be employed, wherein a small molecule could be conjugated to TMZ, or the TMZ could be grafted onto the long-chain bio-responsive polymers to form polymer-drug conjugate (PDC). These techniques are well established and reported vastly for the delivery of molecules in recent times. Inorganic-based nanoparticles such as silica nanoparticles have emerged as a promising tool for the delivery of small molecules in the management of various diseases. The silica-based crystalline form is known to cause pulmonary obstructive disease and can induce irreversible pulmonary silicosis. While the other form of silica i.e., amorphous nonporous or mesoporous silica particles, are biodegradable, biocompatible, and known for their large surface area, ease-of-functionalization, and shape modifications (such as nanohelices, nanotubes, nano-zigzags, and nanoribbons), could be deployed as a nanocarrier system for the drug delivery applications. Wherein, mesoporous silica nanoparticles (MSNPs) ranging from 2 to 200 nm depict unique physicochemical properties that could be utilized for the delivery of hard-to-deliver hydrophilic molecules. Interestingly, US-FDA has recognized colloidal silica as safe to use for biological applications. For instance, Nie et al. developed manganese (Mn)-doped mesoporous silica nanoparticles (MSNs) for the codelivery of TMZ with 10–23 DNAzyme. Delivery of Mn-MSN nanoparticles decomposed and released the payload under acidic pH and reducing conditions. The co-delivery of TMZ and 10–23 DNAzyme using Mn-MSN exhibited improvement in IC_{50} by 3.8 folds compared to free TMZ and further sensitized the T98G glioma cells and resulted in TMZ-induced cytotoxicity [92]. Bertucci et al. developed MSNPs, and incorporated Cy5 fluorophore and TMZ for the treatment of glioma. The resulting MSNPs exhibited a particle size of ~100 nm, and thereafter it was surface decorated with polyarginine-peptide nucleic acid (R8-PNA) conjugate for miR221 targeting *viz.* electrostatic interactions. The MSNPs demonstrated rapid internalization into C_6 and T87G glioma cells with intact anti-miR activity, exhibiting an improvement in apoptosis up to 70.9% in glioma cells [93]. Similarly, Zhang et al. developed TMZ-loaded MSNPs coated with polydopamine (PDA) and targeted with Asn-Gly-Arg (NGR). MSNPs-TMZ-PDA-NGR showed better autophagy and apoptosis (52.02%) in the C_6 cell line compared the TMZ alone. The induced autophagy was found to be the reason for the improved cytotoxic effect of the system [94]. Another example of the silica nanoparticle is reported by Zeng et al., wherein TMZ-loaded porous silica nanoparticles (TMZ/PSi NPs) were developed as photothermal and hyperbaric therapy for glioma. The TMZ/PSi NPs showed a particle size of 140 nm with a significantly better sensitivity towards C_6 and NCH-421 K glioma cell lines. In addition, the stem-like cell marker and hypoxia-related markers were also found to be downregulated after the treatment with TMZ/PSi NPs. The TMZ/PSi NPs were further evaluated *in vivo* in C_6 tumor-bearing mice, where the mice treated with TMZ/PSi NPs showed better outcomes in terms of tumor volume [95].

In recent years, metal-organic frameworks (MOFs) have received quite a bit of interest for their potential applications in the biomedical sciences. Considering their well-defined structure, high surface area and porosity, variable pore size, and ease of chemical functionalization, MOFs are considered a potential class of nanocarriers for the delivery of drug molecules *in vitro* and *in vivo* [96]. For instance, Wan et al. prepared TMZ loaded nanoscale MOF using UiO-66-NH_2, the UiO-66-NH2 nanoparticle is a zirconium-based framework, and the system is a composite of Zr and 2-amino-1,4-benzenedicarboxylic acid (BDC-NH2), which was able to decompose in ionic form to discharge the drug through a porous structure by low-frequency oscillation and cavitation effect. TMZ@UiO-66-NH_2 nanocomposites exhibited efficient inhibition of tumor growth along with minimal off-target toxicity. Interestingly, TMZ@UiO-66-NH2 nanocomposites were found to have biocompatibility and biosafety, which makes them ideal candidates for clinical translation [97]. Further, Pulvirenti et al. prepared a nano-metric hybrid system that consisted of Fe_3O_4 magnetic nanoparticle MNPs@MIL modified through the growth of a Fe-based Metal-organic framework. The nano-metric system has both the nanometer dimension and magnetic properties, which increases the loading capacity due to the high porosity of the system. The system showed 1.2% (i.e 12 mg/g) of loading for TMZ and was able to carry the drug into A172 cells without any degradation. Additionally, the resulting formulation efficiently suppressed human glioblastoma cell viability at the concentration of 15–20 μg/mL in comparison to free TMZ. However, the system was explored in *in vitro* cell line-based assays, and further *in vivo* investigations are required to consolidate the outcomes [98].

7. Conjugation based approach to improve TMZ delivery

Although nano-carriers have improved the TMZ delivery, however, formulation-related properties still require improvement, including TMZ stability, loading, and release characteristics from these systems. TMZ has appreciable water solubility of 5.0 mg/mL; thus, its encapsulation in polymeric or lipidic nanoparticles is always challenging. Further, its release from these systems is usually faster and associated with a burst release. Ananta et al. reported PLGA nanoparticles with a

TMZ loading of 4.4% w/w, and 80% of the TMZ was released within 6 h [86]. The same was demonstrated in work by Lee and Ooi, wherein a drug loading of 0.2–2% in folate conjugated PLGA–PEG nanoparticles was reported [88]. The conjugation strategies could be used to overcome various limitations of the parent drug; furthermore, such conjugates can be functionalized by targeting moieties to reduce the toxic effects and to distinguish the normal cell and cancer cells. For example, Patil et al. conjugated TMZ in its hydrazide form with poly(−L-malic acid) along with an anti-transferrin receptor (TfR) monoclonal antibody and pH-sensitive trileucine to disrupt endosomal membranes for tumor targeting via receptor-mediated endocytosis. These conjugates had a high TMZ payload (17% w/w) and were able to target GBM actively. Furthermore, following coupling with the polymer, the biological half-life of TMZ was dramatically increased by 3–4 folds [99]. Further, in another study, conjugation of TMZ with chitosan produced nanoparticles with an average size of around 47 nm and a TMZ loading of 4.9% w/w with the stability of up to 21 h in a physiological medium [11]. Apart from polymeric carriers, TMZ has been conjugated with small-molecule such as perillyl alcohol that demonstrated effectiveness in TMZ-resistant glioma cells *in vitro* and in orthotopic GBM tumor model [100]. Ideally, drug conjugates with the small molecule should be stable in the systemic circulation before reaching its target site with a non-cleavable linker and for cleavable spacer so that drug release could be possible at the intended site only [101]. A non-cleavable linker can also be used for the conjugation strategies to maintain the integrity of the conjugate and to maintain a single pharmacophore at the receptor/targeting site [102]. In combination therapy, two individual drugs are administered simultaneously, but drug-drug conjugation could be therapeutically advantageous and may exert synergistic action. Further, it is easier for the patient to take a single drug as compared to two drugs, thus facilitating patient compliance [102]. During the designing of conjugates, their stability and efficacy should be carefully considered and the conjugate having the cleavable linker must release the drug at the specific site maintaining its efficiency exhibiting minimal adverse effects [103].

7.1. Linkers for conjugation: Role and characteristics

A linker could be a simple chain of carbons, an ether bond, ester bond, amide bond, hydrazones linkage, and disulfide linkage, or could be a small chain of peptides [103–105]. Tunable linkers play a significant role in achieving targeting, for instance, the hydrazone linkage is stable in physiologic conditions (pH 7.4) but gets hydrolyzed at the acidic environment of the tumor, thus releasing the active in the tumor environment. However, this type of linker could be unstable in the presence of acidic buffers, excipients, or gastric environment [106,107]. While synthesizing nano/bioconjugates of any drug molecule, the role of a linker is significant in order to achieve the release of the drug in a predetermined physiological environment. For example, the tumor

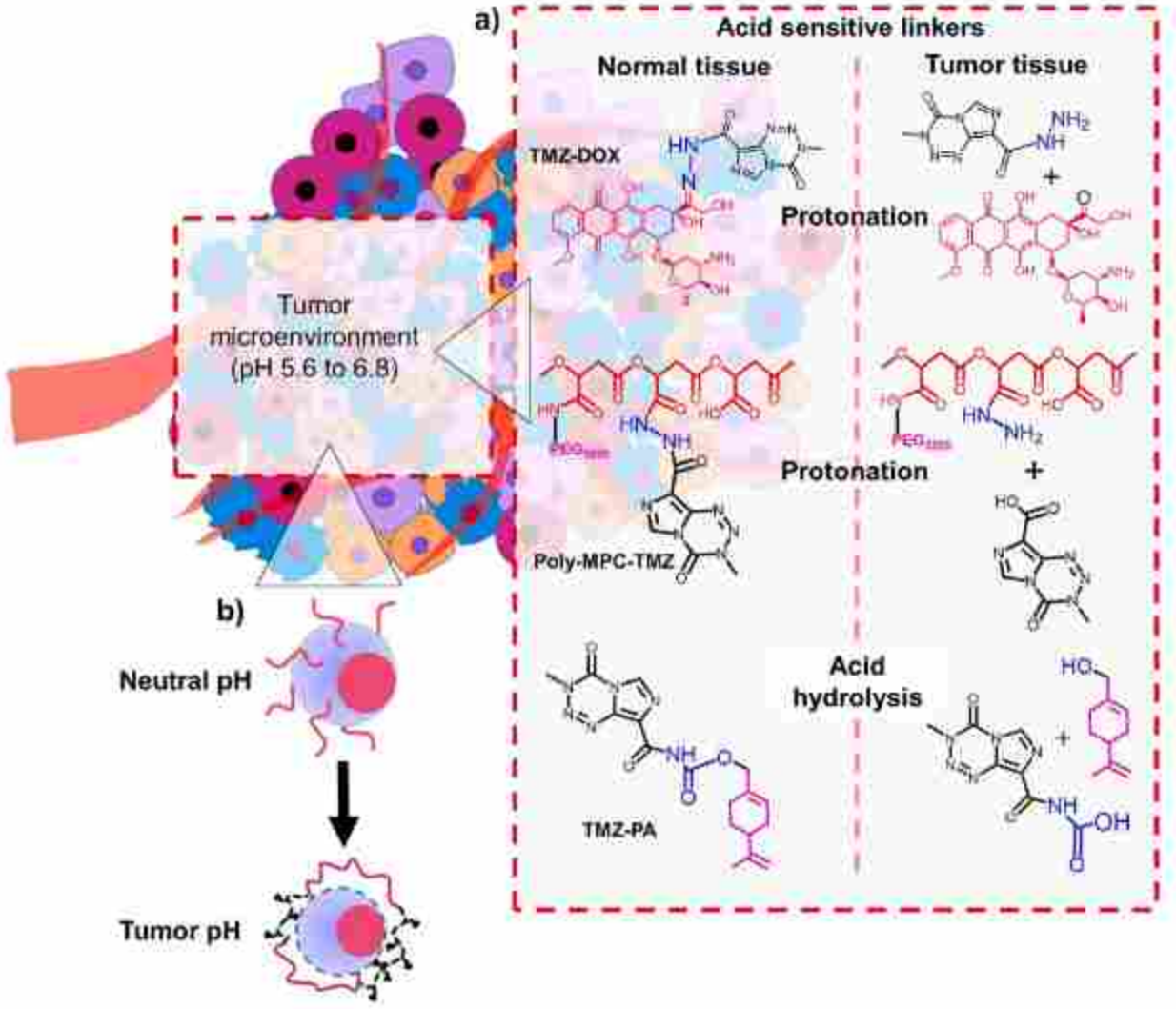

Fig. 4. a) Fate of acid sensitive linkers in tumor microenvironment having acidic pH due to the presence of high lactate concentration, and b) the fate of acid sensitive nanoparticles in tumor microenvironment.

microenvironment is acidic, and thus an acid-sensitive linker could release the therapeutic agent only in the tumor compartment. Similarly, the intended route of administration could be kept considered during the selection of the linker. For example, acidic pH (~3.5) of the stomach could degrade the linkers such as ester, hydrazone, silyl ethers, etc. (Fig. 4). Interestingly, the thiol linker has been explored for the delivery of several macromolecules and small molecule because of its self-targeting property. Since the level of GSH is >10 uM in the cytoplasm, more than anywhere else in the body, which leads to the release of the molecule from the nanocarrier after reaching the cytoplasm. However, this linker possesses limitations as it is heat sensitive and can be broken down during the heat sterilization process [105,108]. Further, the linker should not possess any intrinsic property and toxicity. Collectively, the linker should be designed such that it can degrade in the presence of bio-

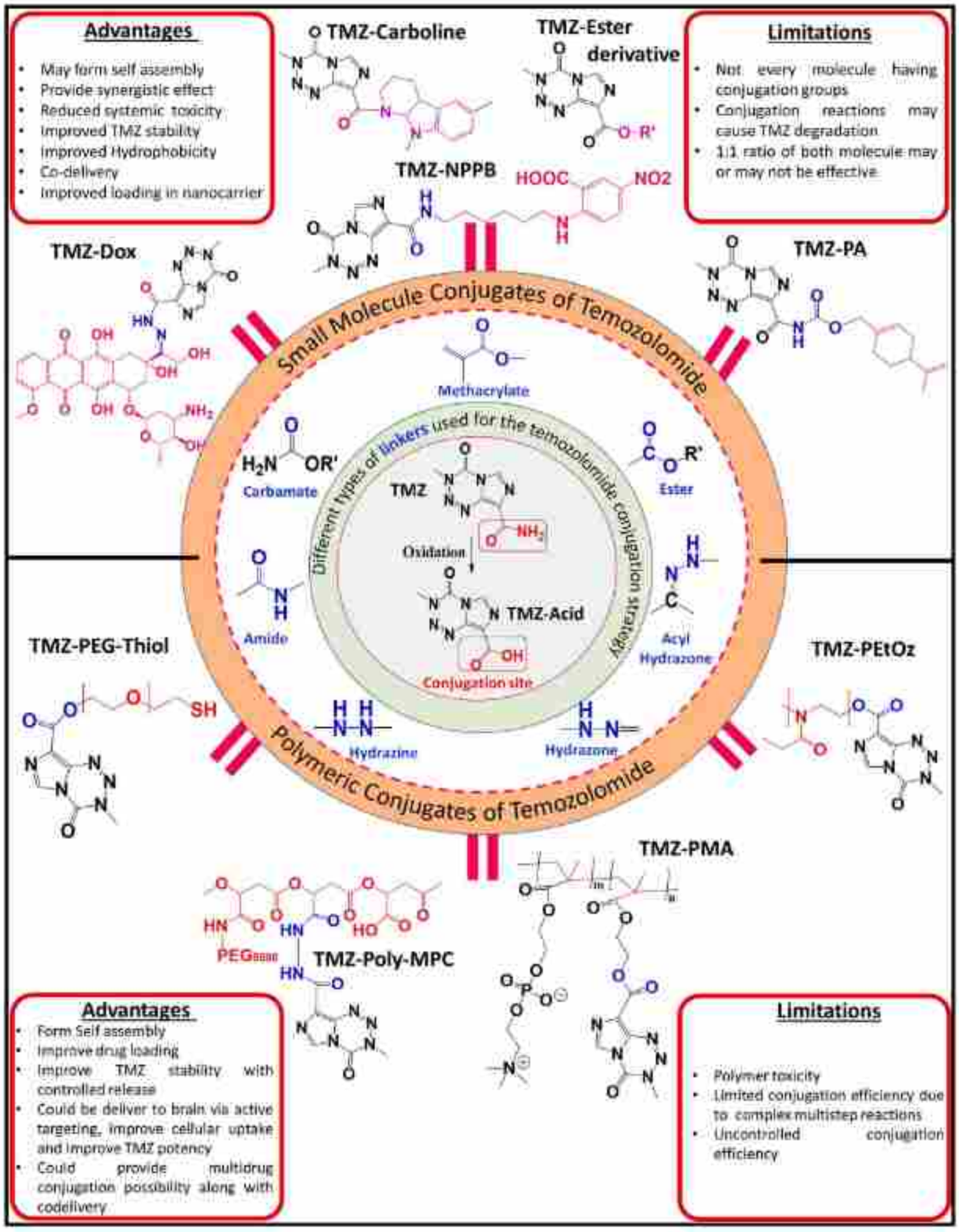

Fig. 5. Conjugation strategies of Temozolomide with small molecules (upper half) and polymers (lower half).

stimuli such as enzyme or pH within cancer cells for targeted drug delivery and to avoid premature release during the circulation under physiological conditions [106]. Besides the type of linkage, the conjugation site should also be focused on based on their structure-activity relationship to maintain the functionality of the two constituents [109]. Various linkers reported for TMZ conjugation are illustrated in Fig. 5.

7.2. Polymer conjugates of Temozolomide

Polymer conjugates, aka polymeric prodrugs, have acquired special attention in the delivery of both small and macromolecules, as they have demonstrated improved safety profile and desired clinical outcome [110–112]. In the 1950s, the synthesis of the first polymer-drug conjugate was reported by von Horst Jatzkewitz using a dipeptide linker of leucine and glycine [111]. Thereafter, the concept of polymer-drug conjugates was detailed by Helmut Ringsdorf in the mid-1970s, characterized by the presence of polymeric backbone to which low molecular bioactive molecule (for bioactivity), solubilizer (for imparting hydrophilicity), and a targeting moiety (for biological targeting) are covalently attached through a bioresponsive linker. The concept of the ideal Ringsdorf model of polymeric therapeutics provides various chemical modalities that can be modified, including the polymeric backbone, bioresponsive spacer, and functionality of a drug molecule for the desired application [110,113,114]. The polymeric backbone provides the platform to the nanomedicine, which can be modified with free and selective end group functionalities, while the presence of end group functionalities provides a basic ground for the attachment of spacers and bioactive molecules. Another area of interest is the attachment of the bioactive molecule *via*. spacer to the polymeric backbone itself. The nature of free end group functionalities of polymeric backbone, bioactive molecule and spacer are of primary interest in the designing of such system. Certain functionalities including amines, carboxylic acids, hydrazone, acyl, alcohols, and thiols, provide better support in the conjugation process, resulting in a stimuli-based system responsive to pH, enzyme, light, external field, etc. [115,116]. On the other hand, some molecules do not possess such free end group functionalities, in such cases attachment to the backbone is a difficult task. For such molecules, initially, free functionalities are generated which were subsequently conjugated to the polymeric backbone using a specialized linker, yielding the polymeric prodrug. The third area of interest is the presence of ligand or a transport system that directs the movement of the conjugate to the specific targeted site of action with minimal non-specific binding. Specific targeting can be achieved by the presence of the homing (receptor active) components including enzymes, hormones, peptides, immunoglobulins, etc., resulting in tissue-specific targeting with minimal toxicity [117]. Since then, multiple works based on Ringsdorf model have been carried out by various researchers in the development process, eliciting advancements in the translational process. For instance, in 1990, Adagen, the first clinical approval of a polymer protein conjugate was acquired for the enzyme replacement therapy for adenosine deaminase deficiency (ADA) [111]. Several other polymeric prodrugs including NKTR-118, CT-2106, AP5346, AP5280, Xyotax, IT-101, PK1, PK2, etc., are in the clinical development stage and require detailed clinical evaluation [117,118]. The hydrophilic drugs are hard to load in the hydrophobic core of the nanocarriers; therefore, the concept of polymer drug-conjugate came in the scenario for such molecules, wherein the drug is being conjugated or grafted in the backbone of the polymer with a bioresponsive spacer. Various reported polymer drug conjugates are shown in Table 2. The delivery of TMZ payload by encapsulation techniques has demonstrated significantly lowered carrying capacity to the target site, resulting in the administration of a significantly large amount of carrier with the drug to achieve the desired effect. For instance, PLGA based nanoparticles encapsulating TMZ using solvent evaporation technique exhibited drug load ranging 0.4 to 4.4% *w/w* with maximum encapsulation efficiency up to 27%, along with the burst release in the first 6 h [86]. Lee et al. prepared folate-targeted PEG-PLGA nanoparticles using solvent evaporation, and nanoprecipitation method showed drug loading up to 2% *w/w* with encapsulation efficiency ranging 2.6 to 12.6% [88]. Dilnawaz et al. prepared TMZ and curcumin-loaded magnetic nanoparticles delivery system. Wherein, drugs were allowed to partition into the glyceryl monooleate shells surrounding the magnetic nanoparticles, exhibiting encapsulation efficiency of 75% and 30% at drug loading <5% *w/w* for curcumin and TMZ, respectively [119]. On the other hand, the polymer-drug conjugates (PDC) have shown significant improvement in drug payload with controlled physico-biochemical properties, not only ensuring the stability, biocompatibility, non-toxic behavior but also ensuring the targeted delivery and release to a specific site [111,116,120]. The polymer-TMZ conjugate has exhibited numerous benefits, including improvement in TMZ stability, efficacy, improved pharmacokinetics, systemic circulation half-life, and reduced toxicity. Likewise, Patil et al. synthesized multifunctional targetable conjugates of TMZ with poly(β-L-malic acid) polymeric backbone, containing targeting monoclonal transferrin receptor antibody (TfR), trileucine (LLL) for pH-dependent endosomal escape, Alexa fluor 680 for identification,

Table 2
Polymeric conjugates of Temozolomide.

Polymer Conjugate	Linker	IC_{50}	Formulation	Outcomes	References
Poly MPC polymer	Methacrylate linker	396–1282 μM 1477–9260 μM	Micelles	1) Enhanced drug stability 2) Half-life improved 2–19 times from free TMZ	[16]
Poly(β-L-malic acid)	Hydrazine linker	–	Nanoconjugate	1) Half-life improved from 1.8 h to 5–7 h 2) Cell viability reduced	[93]
Poly(2-ethyl-2-oxazoline)	Ester	$PEtOz_{47}$-TMZ – 22.43 μg/ml. PEG_{113}-TMZ- 26.08 μg/ml.	Nano conjugation micelles	1) Enhanced the stability of TMZ 2) Prolonged the circulation time in vivo 3)Increased the TMZ accumulation in glioblastoma	
Conjugated Gold Nanoparticles	Ester	5.74 0.02 μmol/L 64.06 ± 0.16 μmol/L	Gold nano formulation	1) IC_{50} of anti-EphA3-TMZ@GNPs (64.06 ± 0.16 μM) was 18.5-fold 2) Down-modulated expression of O6 -methylguanine-DNA methyltransferase 3) Increased chemosensitivity of 198G to TMZ 4) Prolonged the median survival time to 42 days and increased tumor-cell apoptosis	[121]
$PEtOz_{47}$-TMZ polymer micelles	Ester	22.43 μg/ml. for $PEtOz_{47}$-TMZ 26.08 μg/ml. for PEG_{113}-TMZ	Micelles	1) Reduces TMZ degradation rate with half-life upto 13.7 h compared to free TMZ with $t_{1/2}$ of 1.1 h in plasma 2) Median survival of polymer-drug conjugates significantly improved upto 45 days 3) no significant morphological change or tissue damage in toxicity analysis	[122]

and PEG for protection. The water-soluble multifunctional TMZ nanoconjugates exhibited hydrodynamic diameter ranging from 6.5 to 14.8 nm with zeta potential ranging −6.3 to −17.7 mV. Further, the nanoconjugates had significant improvement in TMZ payload up to 30% *w/w* in the form of TMZ hydrazide, demonstrating improved stability by 3–4 times and uptake in glioma cells, especially in the presence of TfR targeted conjugate [99]. In another study, Fang et al. prepared chlorotoxin-targeted TMZ conjugated chitosan-based delivery system (NP-TMZ-CTX), exhibiting stable and significantly higher TMZ loading with an average particle size of <100 nm. The actively functionalized TMZ-conjugated nanosystem was able to target and penetrate 2–6 folds efficiently and reduce the IC_{50} by 50–90%, compared to non-targeted nanoparticles against GBM cells [11]. Emrick group developed a series of TMZ conjugated poly(2-methacryloyloxyethyl phosphorylcholine) (polyMPC-TMZ) using controlled free-radical copolymerization of MPC and TMZ-substituted methacrylate. The resulting conjugate showed TMZ loading >50 mol%, which may require tissue specific bio-recognition using targeting molecules like peptides, targeting ligands, and antibodies to facilitate BBB trans permeability [123]. Afterward, the polyMPC-TMZ was prepared via RAFT polymerizntion and used to prepare the nanoformulation with a size ranging from 7 to 40 nm that enhanced the half-life of TMZ by 19 folds compared to free TMZ [16]. The attachment on drug conjugates with targeting ligand has a significant role in the delivery of TMZ to the specific site of action with minimum adverse effects *in vivo*. Likewise, Wang et al. fabricated anti-ephrin type-A receptor functionalized TMZ-PEG-Gold nanoparticle conjugates, wherein, TMZ was conjugated to PEG thiol, which was further reacted with gold nanoparticles to yield TMZ-PEG-GNPs. The prepared anti-EphA3-TMZ-PEG-GNPs exhibited loading efficiency up to 7% *w/w* with an average particle size of 46.12 nm. The results showed enhanced cellular uptake, apoptosis, and reduced IC_{50} by 18.5 folds compared to free TMZ in glioma cell lines. Furthermore, *in vivo* administration of targeted nanoparticles improved the median survival time to 42 days, found to be safe and biocompatible as compared to TMZ treatment [121]. Recently Xu et al. synthesized poly(2-ethyl-2-oxazoline) (PEtOz)–TMZ conjugate using ester linker, with the TMZ loading up to 4% *w/w* of

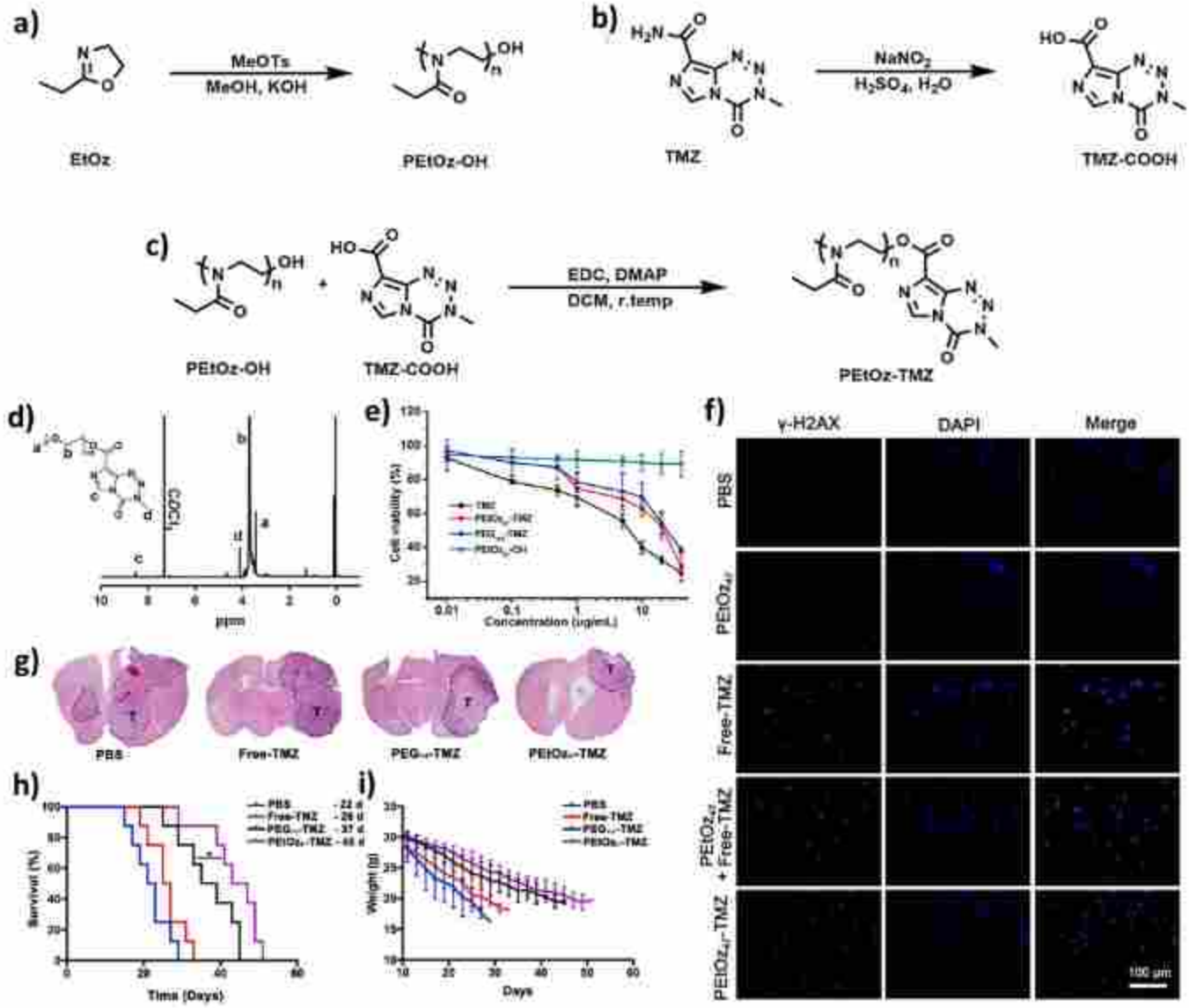

Fig. 6. Synthesis scheme of PEtOz-TMZ conjugate-a) conversion of EtOz to PEtOz, b) conversion of TMZ to its -COOH derivative i.e. TMZ-COOH, c) conjugation of TMZ-COOH with PEtOz by the means of EDC/DMAP coupling chemistry, d) ^{1}HNMR spectra of EtOz to PEtOz conjugate, e) cell viability (%) after treatment with EtOz to PEtOz w.r.t free TMZ and blank polymers, g) H&E staining of tumor area in brain after different treatments, h and i) % survival and average body weight change (%) respectively, after different treatment groups. Reprinted with permission from [123].

the conjugate. The nanoconjugates yielded micelles, exhibiting a significant improvement in the stability by 5.5 folds up to 13.8 h compared to free TMZ. *In vivo* systemic administration resulted in reduction in the degradation rate of TMZ and extended the systemic half-life from 1.1 h to 13.7 h in plasma with improvement in survival time to 45 days compared to 26 days in the free TMZ treatment group in the C_6 orthotopic xenograft mouse model [122] (Fig. 6).

7.3. Small molecule conjugates of temozolomide

Despite polymers, small molecules such as lipids, drugs, alcohols, etc., were also explored for conjugation with TMZ to improve its therapeutic efficiency *in vitro* and *in vivo* (Table 3). In 2014, Chen et al. conjugated perillyl alcohol (POH) with TMZ using a carbamate linker to form TMZ-POH. The linkage of TMZ with POH improved the half-life of the drug and made it stable as compared to free TMZ, which get hydrolyzed instantly at the physiological pH. The cytotoxic potential of the conjugate was evaluated by colony-forming assay in different cell lines such as estrogen receptor-positive cells MCF7 and T47D, the triple-negative lines MDA-MB-231, MDA-MB-468, and HCC-1937, and a brain-seeking variant of the 231-cell line. The conjugate was found to be potent and prevented colony formation in all the cell lines at 15 uM concentration. For instance, 95% of reduction in colony formation was observed in the cells treated with TMZ-POH conjugate, while only 50% reduction was observed with the parent drug at a 10 uM concentration. Further, in comparison to free TMZ, the TMZ-POH conjugate was 6.3 to 15.5-fold more potent in MGMT-expressing cells while the potency in MGMT negative cells was 3.2 to 4.3-fold, suggesting the effectiveness of conjugate against resistant glioma. Further, western blotting data showed a significant decrease in MGMT expression in the MGMT expressing cells treated with TMZ-POH conjugate. *In vivo* performance of the conjugate was determined in a mouse-bearing intracranial tumor-induced using triple-negative breast cancer cells (D3H2LN cells). The survival time of animals treated with TMZ-POH conjugate was improved up to 50 days, while the TMZ- treated animals showed a survival time of 30 days. Altogether, the results demonstrated that TMZ-POH conjugate was more anticancer potential as compared to free TMZ in both *in-vitro* and *in-vivo* conditions [14]. Later, Chang et al. explored the effectiveness of TMZ-POH conjugate by means of autophagy. The study aimed at determining the relationship between TMZ-POH conjugate and the autophagy process with its underlying mechanism. To show the autophagy effect of TMZ-POH conjugate, four cell lines of non-small cell lung cancer (NSCLC), including A549, SPC-A1, NCI-H460 (H460), and NCI-H520 (H520), were incubated with 100 μM of free TMZ, POH, physical mixture and TMZ-POH conjugate. The results showed that there was significantly more autophagy index when the cells were treated with TMZ-POH with respect to other treatment groups. The expression of autophagosome was significantly higher in the cells treated with TMZ-POH. Further the proteomic studies indicated that there was an effect on phosphorylation of mTOR, P70S6K, after TMZ-POH treatment. Meanwhile, the expression of the downstream effector of mTOR i.e., BECN1, significantly deviated. Such findings concluded that the process of autophagosome formation after TMZ-POH was mTOR independent. The findings also suggested the change in mitochondrial length to shorter with few branches when the cells were treated with TMZ-POH, and the reason could be the lack of mitochondrial fusion, inhibiting

Table 3
Small molecule conjugates of Temozolomide.

Drug Conjugate	Linker	Cell line	IC_{50}	Outcome	References
Doxorubicin	Biodegradable arylhydrazone linkage	U87MG	Killed 94% cells at 8 μM	1) Stable under physiological Conditions 2)Drug release was activatable in the presence of glutathione	[124]
5-nitro-2-(3-phenylpropylamino)-benzoate (NPPB)	Covalent	U373MG, U87MG, BV-2 and LN18	112 ± 7 μM for U373MG 130 ± 20 μM for U87MG 129 ± 10 μM for LN18 77 ± 6 μM for BV-2	1) MZ-NPPB blocked chloride currents 2) Suppressed migration and invasion of U373MG 3) Enhanced cytotoxicity inducing apoptotic cell death via DNA damage.	[125]
Perillyl alcohol	Carbamate linkage	HUT78, HUT-102 MyLa cells	8 μM for HUT78, 9 μM for HUT-102 130 μM for MyLa	1) Inhibited proliferation, diminished viability, and stimulated apoptosis 2) Triggered endoplasmic reticulum stress and activation of caspases.	[126]
Perillyl Alcohol	Carbamate linkage	MDA-MB-231-br MDA-MB-231 T47D HCC-1937 MDA-MB-468 MCF7	1.2 μmol/L 2.3 μmol/L 4.6 μmol/L 31 μmol/L 31 μmol/L 33 μmol/L	1) Increased anticancer activity inclusive of TMZ-resistant ones. 2) DNA damage and cell death more efficient than its parental compound TMZ 3) Biologic half-life improved 3) Greater therapeutic efficacy than TMZ	[14]
Perillyl Alcohol	carbamate linkage	LN229TR2 U251 U251 TR T98G LN229	45 μmol/L 8 μmol/L 40 μmol/L 50 μmol/L 5 μmol/L	1) Reduced intracranial tumor growth 2) Increases animal survival without significant toxicity.	[100]
Perillyl Alcohol	carbamate linkage	A549 H460 H520	–	1) Induced mitochondrial transmembrane potential (MTP) decrease and ROS accumulation, 2) Activated mitogen-activated protein kinase (MAPKs) signaling and mitochondrial apoptosis, and exhibited cytotoxicity	[127]
Perillyl Alcohol	carbamate linkage	TW1 TW4	32 μM 37 μM	1) Inactivated the MGMT as results in significant chemo sensitization 2) NEO212 reduced tumor growth	[128]
Perillyl Alcohol	carbamate linkage	U251 LN229 T98G	–	1) Higher brain:plasma ratio, 2) long-lived metabolites, in particular AIC and PA	[153]

mitophagy. Conversely, tubular mitochondria were observed in the case of free drug treatment. Staining of anti-TOM20 demonstrated the fragmented mitochondria in the cells treated with TMZ-POH conjugate. The expression of LC3B was also significantly higher after TMZ-POH treatment along with their colocalization with autophagosome, which consolidated the fact that the TMZ-POH conjugate causes mitochondrial fission. [129]. In another study, Ramos et al. demonstrated that the conjugate downregulates the angiogenesis and invasiveness in glioma cells via endothelial-to-mesenchymal transition (EndMT) blockage. Immunofluorescence evaluation in GSC and brain endothelial cells (BEC) co-cultures depicted upregulation of mesenchymal markers α-SMA and SM22-α expression and reduction in endothelial markers endoglin and VWF expression in a time-dependent manner. Subculturing of USC04 + BEC and U251 + BEC showed the cell dependency for EndMT induction and found that α-SMA expression was increased in both the glioma and non-glioma cell lines. The co-culture of GSC + BEC treated with 5 μM of NEO212 (TMZ-POH), demonstrated a decrease in the number of BEC that undergo EndMT that leads to a decrease in α-SMA expression and increase in endothelial markers after treating the tumor associated-BEC (TuBEC). NEO212 effect in intracranial co-implantation of BEC and GSC in athymic mice was also analyzed wherein it potentially blocked the EndMT [130].

Further, Chen et al. used the TMZ-POH for the treatment of nasopharyngeal carcinoma. The IC_{50} of NEO212 was 32 and 37uM in TW1 and TW4 while free TMZ showed weaker cytotoxicity with IC_{50} of 85 and > 100 μM and free POH did not display any cytotoxicity at a concentration up to 100 uM. The MGMT expression was strongly downregulated at the concentration of 50 uM of NEO212, and the inhibitory effect was more prominent, especially in combination with MGMT-inhibitor O6-BG. *In vivo* administration of NEO212 exhibited an obvious antitumor effect with no detectable luciferase signal in TW4 cells tumor-bearing mice. [128].

Cho et al. explored the NEO212 conjugate for the treatment of a broad range of temozolomide-resistant glioma. The cytotoxic effect on five different TMZ-sensitive human glioma cell lines, i.e., U251, U251TR, LN229, LN229TR2, and T98G by colony formation assay, demonstrated that NEO212 was 2 to 3-fold more potent than free TMZ. Further, NEO212 was strongly cytotoxic to U251-resistant (TR) and LN229TR2 with the IC_{50} of 40 and 45 uM, respectively. Also, NEO212 was not cytotoxic to a normal cell, human brain-derived endothelial cells (BEC), and normal human astrocytes. In an intracranial athymic nude mouse model for temozolomide-resistant glioma cells (U251TR), NEO212 delayed tumor growth and survival time was improved over 50% from 25 to 37 days [100]. Hirschberg et al. explored the anticancer activity of NEO212, on primary cutaneous lymphoma cell lines (HUT78, HUT102, and MyLa). The result showed that even 1 uM concentration of NEO212 was sufficient for the proliferation-inhibitory effects, but the effect was prominent in HUT78 followed by HUT102 and weaker in MyLa cell line. [126]. Song et al. explored the TMZ-POH conjugate for induction of ROS accumulation that was mainly responsible for the cytotoxic activity against non-small cell lung cancer. The inhibitory effect of TMZ-POH in the murine xenograft tumors model suggested that the weight and volume of the tumor were smaller in the case of the conjugate as compared to other treated groups. It was also demonstrated that TMZ-POH induced the phosphorylation of ATM at the ser1981 site, phosphorylation of H2AFX and CHEK 1, and CHEK 1 phosphorylated at ser345 and Thr68 site, respectively [127]. The half-life of NEO212 was found to be 94 min in mouse plasma. Further, the amount of NEO212 was more in the tumor-bearing hemisphere than in the contralateral normal hemisphere in GL261 brain tumors in mice. Also, the brain to plasma ratio was more for conjugate as compared to the parent drug [15].

TMZ has also been conjugated with doxorubicin via. acylhydrazone linkage and characterized using FTIR, NMR, Mass, and UV spectroscopy. TMZ-DOX conjugate acted as a non-classical double intercalating agent and the same was revealed by viscosity and spectroscopy studies, exhibiting a reduction in DNA viscosity and hypochromicity in the presence of ctDNA and TMZ-DOX conjugate. Furthermore, DNA interaction behavior of the conjugate was predicted using the Schrödinger molecular modeling, revealing the anthracycline of DOX penetrated the major groove of the double helix of DNA, which promoted intercalation of the imidazole ring of the TMZ and the acyl hydrazone linker of TMZ-DOX provided sufficient freedom for twisting. Hydrogen bonds formed between DNA base and TMZ-DOX on various sites to favor TMZ-DOX and DNA interaction. Further, TMZ-DOX conjugate was loaded into apoferritin scaffold in the presence of copper (II) gluconate (CuGlu) at pH 8.5. The loading efficiency of the nanoplatforms for TMZ-DOX was found to be 83%, with the stability of up to 2 weeks at physiological pH. The cytotoxicity assay in U87MG cells at the dose of 8 uM showed the cell viability of 6%, 8%, and 20% by TMZ-DOX, CNP, and free DOX, respectively [124] (Fig. 7). In another study, Park et al. conjugated TMZ with NPPB for the treatment of glioblastoma multiforme. TMZ-NPPB conjugate has an IC_{50} of 112 uM, which was 10 fold less than that of free TMZ, which showed IC_{50} of 1164 uM in U373MG cells. A similar result was obtained in U87-MG and LN18 cell lines. The DNA damage efficiency of TMZ-NPPB was also 10-fold greater as compared to free TMZ. The stability study's results demonstrated that after 130 min of incubation, free TMZ degraded up to 88%, while only 20% degradation of parent drug was observed in TMZ-NPPB conjugate. Further, TMZ-NPPB was able to decrease cell migration and invasion as compared to free drugs and their physical mixture [125]. For instance, Chu et al. developed ephrin type-A receptor 3 (EPHA3) tyrosine kinase antibody-modified polylactide-*co*-glycolide (PLGA) nanoparticles (NPs) for nose-to-brain delivery of TMZ-butylated ester for the treatment of GBM. After intranasal delivery, the NPs showed an improved accumulation in glioma tissues due to targeting. [131].

In 2016, Rai et al. synthesized new analogs of TMZ, wherein a carboline moiety was conjugated with an 8-acid analog of TMZ to form carboline-TMZ analogs. The purpose of this study stems from the fact that carboline has a superior BBB permeability, and conjugating carboline with TMZ increases the overall permeability of TMZ to the brain. To screen this hypothesis, β- and γ-carbolines were explored for conjugation with TMZ (as shown in Fig. 8a). In the γ-carboline analogs of TMZ, the TMZ was attached to the 2^{nd} and 5^{th} position of carboline with an amino ethyl linker. As a result, three γ-carbolines analogs were synthesized namely 1, 2, and 3. The TMZ is connected to the c-carboline at the 5-position in compound 1, whereas it is attached at the 2-position in compounds 2 and 3. The efficiency was evaluated in terms of the brain/plasma (B/P) ratio of each analog after 30, 90, and 180 min following *i.v* injection in rats. The free TMZ showed a B/P ratio of 0.34, which was quite small as per the therapeutic requirements. On the other hand, compounds 1, 2, and 3 showed a B/P ratio of 0.34, 0.67, and 0.75, respectively. Similarly, the β-carbolines analogs of TMZ (namely 4, 5 and 6) were synthesized but this time modifications were done in the conjugation such as a) length of the linker was shortened, b) basic amines were converted into neutral amide and c) two chlorine groups were introduced in carboline moiety (as shown in Fig. 8). The B/P ratio of 4, 5, and 6 compounds were 1.36, 3.17, and 10.42, respectively. To support these results, it was stated that the cLogP value of 1.5 to 2.7 is optimal for BBB permeability, and the improvement in cLogP value of compound 4 (cLogP-1.21), 5 (cLogP-1.04), and 6 (cLogP-1.77) was the reason for the improvement in B/P ratio. Further, *in vitro* assays revealed that compounds 1, 3, and 4 did not show any significant inhibition in the proliferation of U87-MG cells but compound 4 inhibited the proliferation up to 27.3%. Further, the compounds were evaluated for their efficacy in the U87-MG cell-induced orthotopic mouse xenograft model of glioblastoma. As per the observation, the compound showed no significant improvement in activity despite improved brain penetration [132].

In 2020, Shirvington et al., synthesized a novel series of ester/amide derivatives of TMZ by modification at the 8^{th} position of the imidazole ring. Firstly, the $-CONH_2$ group of TMZ was converted into a -COOH

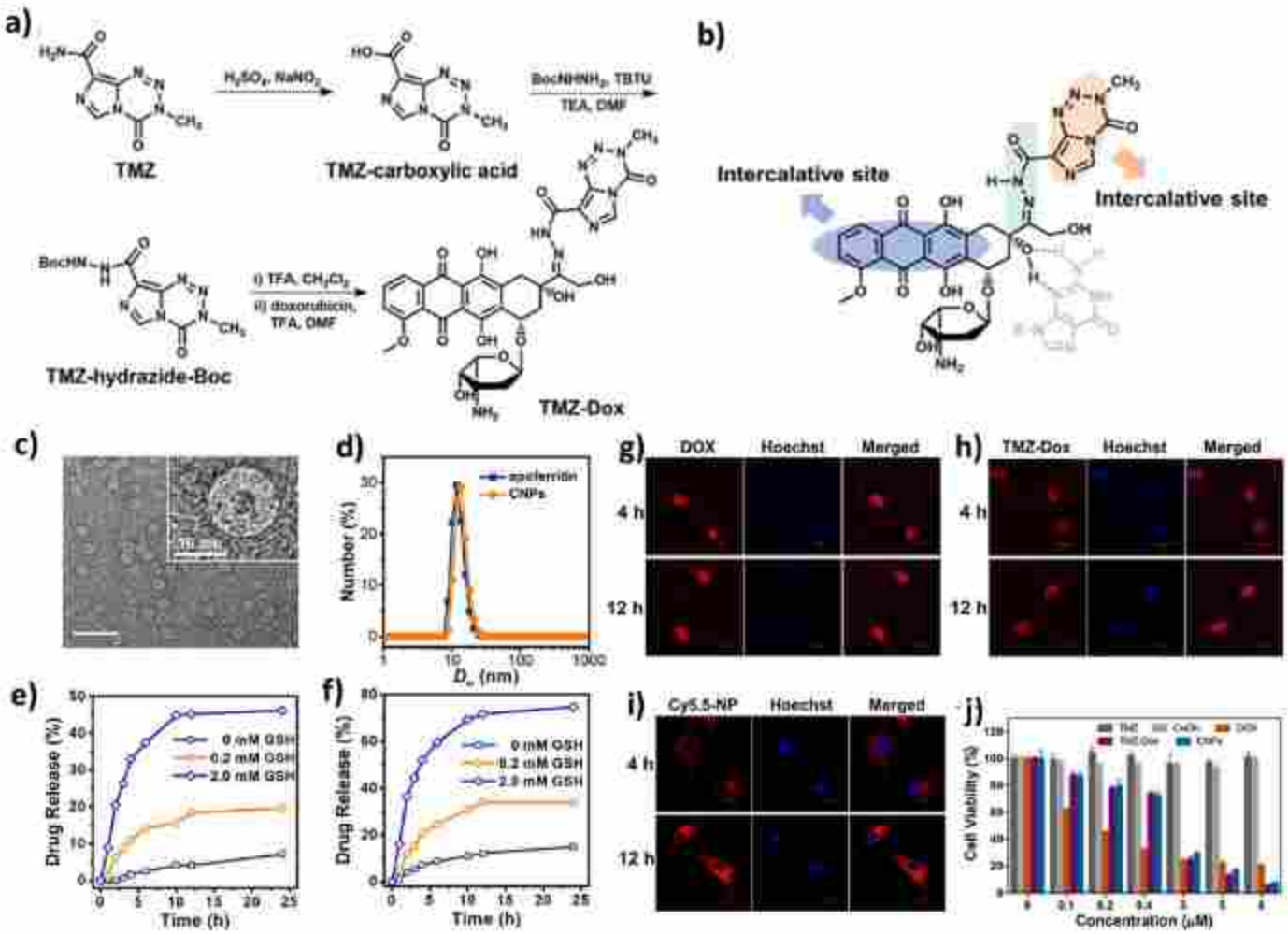

Fig. 7. a) Synthesis scheme of TMZ-Dox conjugate, b) illustration of dual intercalative sites in TMZ-Doc conjugate, c) TEM images of TMZ-Dox CNPs, d) particle size distribution of apoferritin and CNPs, e&f) release profile of TMZ-Dox from CNPs at 7.4 and 6.5 pH respectively, g, h &i) cellular uptake of free Dox, TMZ-Dox and CNPs, respectively, and j) cell viability assay of different treatment groups. Reprinted with permission from [124].

group to form TMZ-acid *via.* oxidation in the presence of nitrous acid. Further, the TMZ-acid was converted into TMZ acyl chloride (-COCl) through reflux in the presence of thionyl chloride using vilsmeier salt as a catalyst (formed by the addition of DMF). Further, a series of alcohols and amines were conjugated with TMZ acyl chloride *via.* nucleophilic reaction. This strategy was found to have poor yield due to the steric effect. Therefore, EDC/DMAP coupling reaction was utilized to synthesize the ester derivative of TMZ. The synthesized derivatives were screened for their cytotoxicity effect in different glioma cells. The ester derivatives of TMZ were found to have significantly lower IC_{50} values w.r.t TMZ and TMZ-acid. Since the ester bond is liable to degrade within the plasma due to the presence of the esterase enzyme, therefore stability study was performed. Results showed that 50% of ester derivatives containing para methoxy and nitrile groups get hydrolyzed within 7.3 and 13.7 min, respectively [133].

8. Challenges and future prospects

TMZ chemotherapy has several limitations that need addressal for its optimal utilization. Further, the long-term use of TMZ leads to resistance to chemotherapy, and the survival rate of less than a year persists the consequences. Despite the use of various nanocarrier-based approaches such as polymers, lipids, surfactants, inorganic materials, etc. that showed an improved cytotoxic effect, potency, and BBB permeability, TMZ's water solubility results in lower loading efficiency and faster release. Although TMZ-based nanocarriers like dendrimers, polymeric nanoparticles, solid lipid nanoparticles, nanostructured lipid carriers, silica/gold nanoparticles, metal-organic framework, etc. have exhibited significant improvements in TMZ chemotherapy in GBM. However, more relevant advancement is still required to facilitate the GBM-specific penetration and efficiency of TMZ. The conjugation approach has yielded the opportunity to further improvise on the formulation characteristics wherein both the small molecule and polymeric conjugates of TMZ have been explored with promising results. Nevertheless, these conjugates are considered new chemical entities, thus requiring a whole array of clinical testing before reaching the market. Continuous study into the designing of conjugates will, without a doubt, lead to the development of very effective medicines. Interestingly, novel approaches such as nose to brain delivery could be explored extensively in the near future. On the other hand, the oral delivery of TMZ conjugates is expected to encounter challenges in terms of stability of the linker in the gastrointestinal environment, their oral absorption, and permeation through BBB to reach the target site, thus limiting their applicability *via.* the oral route. This remains an interesting area, and any innovation in this regard could not only benefit patient compliance but also impact the overall development of small molecule conjugates in a broader sense. Although the toxicity of the polymers could limit the technology, the use of readily available biodegradable polymers could overcome such constraints.

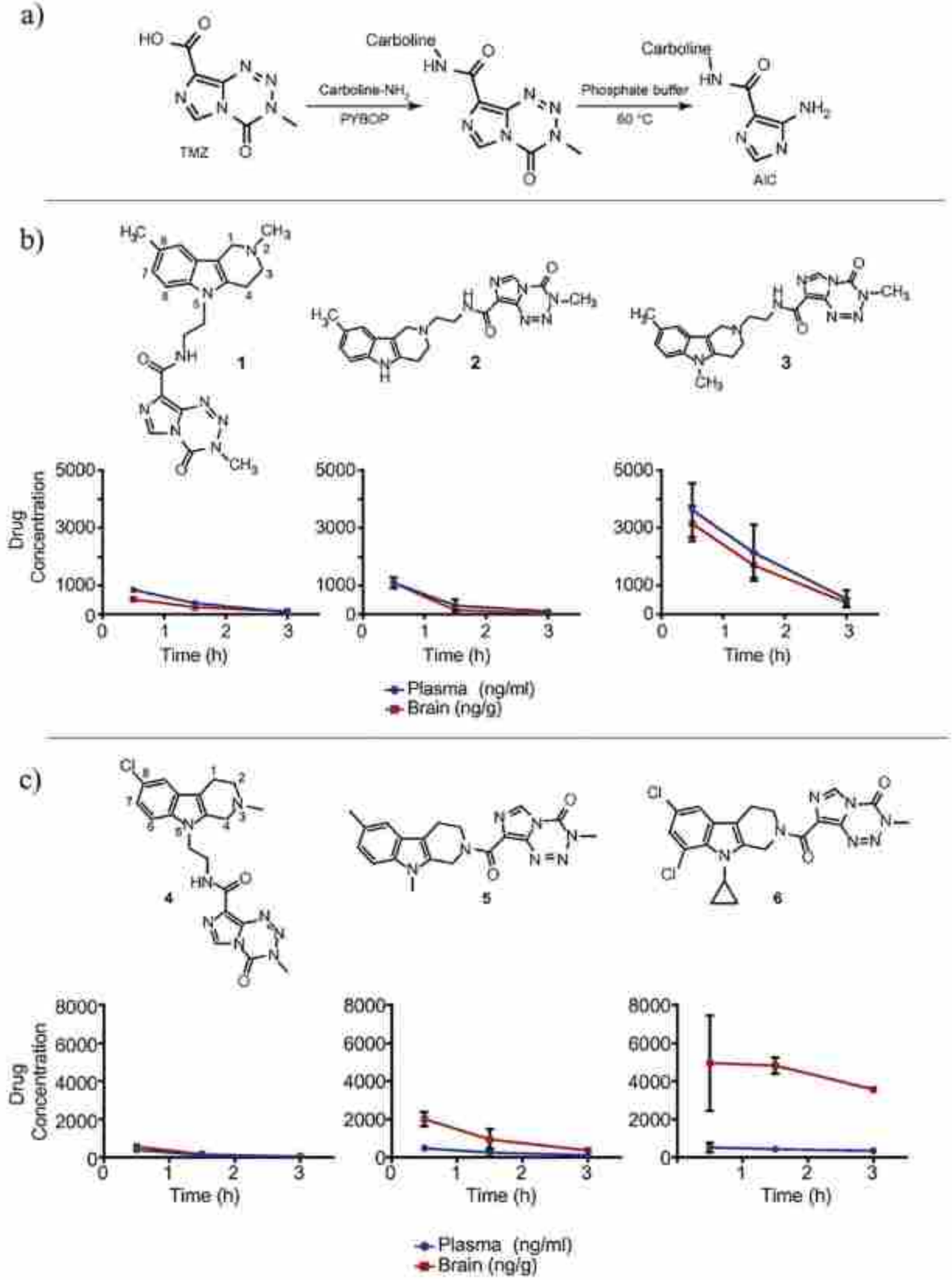

Fig. 8. a) Synthesis scheme of TMZ-Carboline analogue, b) blood and plasma concentrations of γ-carbolines analogs (1, 2 and 3) of TMZ and c) blood and plasma concentration of β-carbolines analogs of TMZ (4, 5 and 6). Reprinted with permission from [132].

CRediT authorship contribution statement

Reena Jatyan: Writing – original draft, Conceptualization. **Prabhjeet Singh:** Writing – original draft, Conceptualization. **Deepak Kumar Sahel:** Writing – original draft. **Karthik Y.G:** Writing – original draft. **Anupama Mittal:** Supervision, Writing – review & editing. **Deepak Chitkara:** Supervision, Conceptualization, Writing – review & editing.

Declaration of Competing Interest

The authors declare no conflict of interest.

Acknowledgment

We sincerely acknowledge the financial support from the Department of Biotechnology (DBT), Ministry of Science and Technology, to DC through a research grant (BT/PR22123/NNT/28/1120/2016). We would like to acknowledge Lady Tata Memorial Trust (LTMT) for their financial support through Junior Research Scholarship (JRS) to RJ. We would like to thank Department of Science and Technology (DST) for their financial support to PS through DST-INSPIRE fellowship (Code No-DST/ INSPIRE Fellowship/ 2018/ IF180652).

References

[1] J.P. Thakkar, T.A. Dolecek, C. Horbinski, Q.T. Ostrom, D.D. Lightner, J. S. Barnholtz-Sloan, J.L. Villano, Epidemiologic and molecular prognostic review of glioblastoma, Cancer Epidemiol. Biomark. Prev. 23 (2014), https://doi.org/10.1158/1055-9965.EPI-14-0275, 1985 LP – 1996.

[2] J. Zhang, M.F.G. Stevens, T.D. Bradshaw, Temozolomide: mechanisms of action, repair and resistance, Curr. Mol. Pharmacol. 5 (2012) 102–114, https://doi.org/10.2174/1874467211205010102.

[3] M.R. Gilbert, M. Wang, K.D. Aldape, R. Stupp, M.E. Hegi, K.A. Jaeckle, T. S. Armstrong, J.S. Wefel, M. Won, D.T. Blumenthal, A. Mahajan, C.J. Schultz, S. Erridge, B. Baumert, K.I. Hopkins, T. Tzuk-Shina, P.D. Brown, A. Chakravarti, W.J. Curran, M.P. Mehta, Dose-dense temozolomide for newly diagnosed glioblastoma: a randomized phase III clinical trial, J. Clin. Oncol. 31 (2013) 4085–4091, https://doi.org/10.1200/JCO.2013.49.6968.

[4] R. Stupp, M.E. Hegi, W.P. Mason, M.J. van den Bent, M.J.B. Taphoorn, R. C. Janzer, S.K. Ludwin, A. Allgeier, B. Fisher, K. Belanger, P. Hau, A.A. Brandes, J. Gijtenbeek, C. Marosi, C.J. Vecht, K. Mokhtari, P. Wesseling, S. Villa, E. Eisenhauer, T. Gorlia, M. Weller, D. Lacombe, J.G. Cairncross, R.-O. Mirimanoff, Effects of radiotherapy with concomitant and adjuvant temozolomide versus radiotherapy alone on survival in glioblastoma in a randomised phase III study: 5-year analysis of the EORTC-NCIC trial, Lancet Oncol. 10 (2009) 459–466, https://doi.org/10.1016/S1470-2045(09)70025-7.

[5] R. Stupp, W.P. Mason, M.J. van den Bent, M. Weller, B. Fisher, M.J.B. Taphoorn, K. Belanger, A.A. Brandes, C. Marosi, U. Bogdahn, J. Curschmann, R.C. Janzer, S. K. Ludwin, T. Gorlia, A. Allgeier, D. Lacombe, J.G. Cairncross, E. Eisenhauer, R. O. Mirimanoff, Radiotherapy plus concomitant and adjuvant temozolomide for glioblastoma, N. Engl. J. Med. 352 (2005) 987–996, https://doi.org/10.1056/NEJMoa043330.

[6] J.A. Quinn, S.X. Jiang, D.A. Reardon, A. Desjardins, J.J. Vredenburgh, J.N. Rich, S. Gururangan, A.H. Friedman, D.D. Bigner, J.H. Sampson, R.E. McLendon, J. E. Herndon, A. Walker, H.S. Friedman, Phase II trial of temozolomide plus O6-benzylguanine in adults with recurrent, temozolomide-resistant malignant glioma, J. Clin. Oncol. 27 (2009) 1262–1267, https://doi.org/10.1200/JCO.2008.18.8417.

[7] H.S. Friedman, T. Kerby, H. Calvert, Temozolomide and treatment of malignant glioma, Clin. Cancer Res. 6 (2000), 2585 LP – 2597, http://clincancerres.aacrjournals.org/content/6/7/2585.abstract.

[8] C.-H. Chien, W.-T. Hsueh, J.-Y. Chuang, K.-Y. Chang, Dissecting the mechanism of temozolomide resistance and its association with the regulatory roles of intracellular reactive oxygen species in glioblastoma, J. Biomed. Sci. 28 (2021) 18, https://doi.org/10.1186/s12929-021-00717-7.

[9] J. Gao, Z. Wang, H. Liu, L. Wang, G. Huang, Liposome encapsulated of temozolomide for the treatment of glioma tumor: preparation, characterization and evaluation, Drug Discov. Ther. 9 (2015) 205–212, https://doi.org/10.5582/ddt.2015.01026.

[10] G. Huang, N. Zhang, X. Bi, M. Dou, Solid lipid nanoparticles of temozolomide: potential reduction of cardial and nephric toxicity, Int. J. Pharm. 356 (2008) 314–320, https://doi.org/10.1016/j.ijpharm.2007.12.013.

[11] C. Fang, K. Wang, Z.R. Stephen, Q. Mu, F.M. Kievit, D.T. Chiu, O.W. Press, M. Zhang, Temozolomide nanoparticles for targeted glioblastoma therapy, ACS Appl. Mater. Interfaces 7 (2015) 6674–6682, https://doi.org/10.1021/am509216a.

[12] S. Song, G. Mao, J. Du, X. Zhu, Novel RGD containing, temozolomide-loading nanostructured lipid carriers for glioblastoma multiforme chemotherapy, Drug Deliv. 23 (2016) 1404–1408, https://doi.org/10.3109/10717544.2015.1064160.

[13] J. Zhang, X. Xiao, J. Zhu, Z. Gao, X. Lai, X. Zhu, G. Mao, Lactoferrin- and RGD-comodified, temozolomide and vincristine-coloaded nanostructured lipid carriers for gliomatosis cerebri combination therapy, Int. J. Nanomedicine 13 (2018) 3039–3051, https://doi.org/10.2147/IJN.S161163.

[14] T.C. Chen, H.-Y. Chu, W. Wang, M. Barath, N. Shimma, F.M. Hofman, A. H. Schönthal, A Novel Temozolomide–Perillyl Alcohol Conjugate Exhibits Superior Activity against Breast Cancer Cells In Vitro and Intracranial Triple-Negative Tumor Growth In Vivo, Mol. Cancer Ther. 13 (2014), https://doi.org/10.1158/1535-7163.MCT-13-0862, 1183 LP – 1193.

[15] H.-Y. Chu, S. Swenson, T.Z. Thein, W. Wang, N.B. Wijeratne, N.I. Marin-Ramos, J. E. Katz, F.M. Hofman, A.H. Schönthal, T.C. Chen, Pharmacokinetic properties of the temozolomide perillyl alcohol conjugate (NEO212) in mice, Neuro-Oncol. Adv. 2 (2020) vdaa160, https://doi.org/10.1093/noajnl/vdaa160.

[16] S.M. Ward, M. Skinner, B. Saha, T. Emrick, Polymer–temozolomide conjugates as therapeutics for treating glioblastoma, Mol. Pharm. 15 (2018) 5263–5276, https://doi.org/10.1021/acs.molpharmaceut.8b00766.

[17] T. Hanif, K. Muzaffar, K. Perveen, S.M. Malhi, S.U. Simjee, Glioblastoma Multiforme: a review of its epidemiology and pathogenesis through clinical presentation and treatment, Asian Pac. J. Cancer Prev. 18 (2017) 3–9, https://doi.org/10.22034/APJCP.2017.18.1.3.

[18] K. Urbańska, J. Sokołowska, M. Szmidt, P. Sysa, Glioblastoma multiforme - an overview, Contemp. Oncol. (Poznan, Poland). 18 (2014) 307–312, https://doi.org/10.5114/wo.2014.40559.

[19] A.C. Tan, D.M. Ashley, G.Y. López, M. Malinzak, H.S. Friedman, M. Khasraw, Management of glioblastoma: state of the art and future directions, CA. Cancer J. Clin. 70 (2020) 299–312, https://doi.org/10.3322/caac.21613.

[20] B. Batash, N. Asna, P. Schaffer, N. Francis, M. Schaffer, Glioblastoma Multiforme, diagnosis and treatment; recent literature review, Curr. Med. Chem. 24 (2017) 3002–3009, https://doi.org/10.2174/0929867324666170516123206.

[21] E. Mohammadi, E. Ghasemi, S. Azadnajafabad, N. Rezaei, S. Saeedi Moghaddam, S. Ebrahimi Meimand, N. Fattahi, Z. Habibi, K. Karimi Yazdi, A. Amirjamshidi, F. Nejat, F. Kompani, A.H. Mokdad, B. Larijani, F. Farzadfar, A global, regional, and national survey on burden and quality of care index (QCI) of brain and other central nervous system cancers, global burden of disease systematic analysis 1990-2017, PLoS One 16 (2021), e0247120, https://doi.org/10.1371/journal.pone.0247120.

[22] E. Beghi, G. Giussani, E. Nichols, F. Abd-Allah, J. Abdela, A. Abdelalim, H. N. Abraha, M.G. Adib, S. Agrawal, F. Alahdab, A. Awasthi, Y. Ayele, M. A. Barboza, A.B. Belachew, B. Biadgo, A. Bijani, H. Bitew, F. Carvalho, Y. Chaiah, A. Daryani, H.P. Do, M. Dubey, A.Y.Y. Endries, S. Eskandarieh, A. Faro, F. Farzadfar, S.-M. Fereshtehnejad, E. Fernandes, D.O. Fijabi, I. Filip, F. Fischer, A.K. Gebre, A.G. Tsadik, T.G. Gebremichael, K.E. Gone, M. Ghasemi-Kasman, K. G. Weldegwergs, M.G. Degefa, E.V. Grudzevskaya, T.B. Hagos, A. Haj-Mirzaian, A. Haj-Mirzaian, H.Y. Hasaneen, S.I. Hay, M. Jakovljevic, A. Kasaeian, T.D. Koyu, Y. S. Khader, I. Khalil, E.A. Khan, J. Khubchandani, A. Kisa, K.J. Krohn, C. Kulkarni, Y.L. Nirayo, M.T. Mackay, M. Majdan, A. Majeed, T. Manhertz, M. M. Mehndiratta, T. Mekonen, H.G. Meles, G. Mengistu, S. Mohammed, M. Naghavi, A.H. Mokdad, G. Mustafa, S.S.N. Irvani, L.H. Nguyen, M.R. Nixon, F. A. Ogbo, A.T. Olagunju, T.O. Olagunju, M.O. Owolabi, M.R. Phillips, G.D. Pinilla-Monsalve, M. Qorbani, A. Radfar, A. Rafiy, V. Rahimi-Movaghar, N. Rezaei, P. S. Sachdev, H. Safari, S. Safari, S. Safiri, M.A. Sahraian, A.M. Samy, S. Sarvi, M. Sawhney, M.A. Shaikh, M. Sharif, G. Singh, M. Smith, C.E.I. Sunoko, R. Tabarés-Seisdedos, M.-H. Tehrani, O. Temsah, M. Torralpa-Girbes, B.X. Tran, A.A.T. Tsegay, I. Ullah, N. Venketasubramanian, R. Westerman, A.S. Winkler, E. M. Yimer, N. Yonemoto, V.L. Feigin, T. Vos, C.J.L. Murray, Global, regional, and national burden of epilepsy, 1990–2016: a systematic analysis for the global burden of disease study 2016, Lancet Neurol. 18 (2019) 357–375, https://doi.org/10.1016/S1474-4422(18)30454-X.

[23] W. Globocan, International Agency for Research on cancer, Brain, Central Nervous System, https://gco.iarc.fr/today/data/factsheets/cancers/31-Brain-central-nervous-system-fact-sheet.pdf, 2020.

[24] Q.T. Ostrom, G. Cioffi, K. Waite, C. Kruchko, J.S. Barnholtz-Sloan, CBTRUS statistical report: primary brain and other central nervous system tumors diagnosed in the United States in 2014-2018, Neuro-Oncology 23 (2021), https://doi.org/10.1093/neuonc/noab200 iii1–iii105.

[25] K.D. Miller, Q.T. Ostrom, C. Kruchko, N. Patil, T. Tihan, G. Cioffi, H.E. Fuchs, K. A. Waite, A. Jemal, R.L. Siegel, J.S. Barnholtz-Sloan, Brain and other central nervous system tumor statistics, 2021, CA. Cancer J. Clin. 71 (2021) 381–406, https://doi.org/10.3322/caac.21693.

[26] A.F. Tamimi, M. Juweid, in: S. De Vleeschouwer (Ed.), Epidemiology and outcome of glioblastoma, 2017, https://doi.org/10.15586/codon.glioblastoma.2017.ch8, Brisbane (AU).

[27] S. Singh, H. Deora, A. Nayaz, K.K. Das, A. Mehrotra, A.K. Srivastava, S. Behari, A. K. Jaiswal, S. Jaiswal, Trends in clinico-epidemiology profile of surgically operated glioma patients in a tertiary care center over 12 years—through the looking glass!, Egypt. J. Neurosurg. 36 (2021) 32, https://doi.org/10.1186/s41984-021-00118-w.

[28] M. Salvati, A. Frati, N. Russo, E. Cervoni, F.M. Pelli, G. Minniti, R. Delfini, Radiation-induced gliomas: report of 10 cases and review of the literature, Surg. Neurol. 60 (2003) 60–67, https://doi.org/10.1016/S0090-3019(03)00127-X.

[29] M.V. Relling, J.E. Rubnitz, G.K. Rivera, J.M. Boyett, M.L. Hancock, C.A. Felix, L. E. Kun, A.W. Walter, W.E. Evans, C.-H. Pui, High incidence of secondary brain

tumours after radiotherapy and antimetabolites, Lancet. 354 (1999) 34–39, https://doi.org/10.1016/S0140-6736(98)11094-6.
[30] C. Wingren, P. James, C.A.K. Borrebaeck, Strategy for surveying the proteome using affinity proteomics and mass spectrometry, Proteomics. 9 (2009) 1511–1517, https://doi.org/10.1002/pmic.200800822.
[31] C. Adamson, O.O. Kanu, A.I. Mehta, C. Di, N. Lin, A.K. Mattox, D.D. Bigner, Glioblastoma multiforme: a review of where we have been and where we are going, Expert Opin. Investig. Drugs 18 (2009) 1061–1083, https://doi.org/10.1517/13543780902952764.
[32] A. Omuro, L.M. DeAngelis, Glioblastoma and other malignant gliomas: a clinical review, JAMA. 310 (2013) 1842–1850, https://doi.org/10.1001/jama.2013.280319.
[33] J.A. Schwartzbaum, J.L. Fisher, K.D. Aldape, M. Wrensch, Epidemiology and molecular pathology of glioma, Nat. Clin. Pract. Neurol. 2 (2006) 494–503, https://doi.org/10.1038/ncpneuro0289.
[34] Z. Han, Y. Du, H. Qi, W. Yin, Post-traumatic malignant glioma in a pregnant woman: case report and review of the literature, Neurol. Med. Chir. (Tokyo) 53 (2013) 630–634, https://doi.org/10.2176/nmc.cr2013-0020.
[35] A. Kofman, L. Marcinkiewicz, E. Dupart, A. Lyubchev, B. Martynov, A. Byvaltsev, E. Kutelevskaya, J. Brown, D. Schiff, R. Abounader, The roles of viruses in brain tumor initiation and oncomodulation, J. Neuro-Oncol. 105 (2011) 451–466, https://doi.org/10.1007/s11060-011-0606-6.
[36] I. Chakravarti, M. Cockburn, W. Cozen, Y.-P. Wang, S. Preston-Martin, A population-based description of glioblastoma multiforme in Los Angeles County, 1974–1999, Cancer. 104 (2005) 2798–2806, https://doi.org/10.1002/cncr.21529.
[37] M. Nakada, D. Kita, T. Watanabe, Y. Hayashi, L. Teng, I.V. Pyko, J.-I. Hamada, Aberrant signaling pathways in glioma, Cancers 3 (2011), https://doi.org/10.3390/cancers3033242.
[38] F. Hanif, K. Muzaffar, Kahkashan Perveen, S. Malhi, S. Simjee, Glioblastoma multiforme: a review of its epidemiology and pathogenesis through clinical presentation and treatment, Asian Pac. J. Cancer Prev. 18 (2017).
[39] H.S. Sharma, D.F. Muresanu, R.J. Castellani, A. Nozari, J.V. Lafuente, Z.R. Tian, S. Sahib, I. Bryukhovetskiy, A. Bryukhovetskiy, A.D. Buzoianu, R. Patnaik, L. Wiklund, A. Sharma, Chapter One - Pathophysiology of blood-brain barrier in brain tumor. Novel therapeutic advances using nanomedicine, H.S.B.T.-I.R. of N. Sharma, in: I. Bryukhovetskiy, A. Sharma, X. Zhang, Academic Press (Eds.), Nov. Ther. Adv. Glioblastoma, 2020, pp. 1–66, https://doi.org/10.1016/bs.irn.2020.03.003.
[40] Q. Ma, F. Schlegel, S.B. Bachmann, H. Schneider, Y. Decker, M. Rudin, M. Weller, S.T. Proulx, M. Detmar, Lymphatic outflow of cerebrospinal fluid is reduced in glioma, Sci. Rep. 9 (2019) 14815, https://doi.org/10.1038/s41598-019-51373-9.
[41] E. Veini, P. Ofek, N. Alheck, D. Rodriguez Ajamil, L. Neufeld, A. Eldar-Boock, R. Kleiner, D. Vaskovich, S. Koshrovski-Michael, S.I. Dangoor, A. Krivitsky, C. Bergo Luna, G. Shenhach-Koltin, M. Goldenfeld, O. Hadad, G. Tiram, R. Satchi-Fainaro, Targeting glioblastoma: advances in drug delivery and novel therapeutic approaches, Adv. Ther. 4 (2021) 2000124, https://doi.org/10.1002/adtp.202000124.
[42] C.-L. Tso, W.A. Freije, A. Day, Z. Chen, B. Merriman, A. Perlina, Y. Lee, E.Q. Dia, K. Yoshimoto, P.S. Mischel, L.M. Liau, T.F. Cloughesy, S.F. Nelson, Distinct transcription profiles of primary and secondary glioblastoma subgroups, Cancer Res. 66 (2006), https://doi.org/10.1158/0008-5472.CAN-05-0077, 159 LP – 167.
[43] H. Ohgaki, P. Dessen, B. Jourde, S. Horstmann, T. Nishikawa, P.-L. Di Patre, C. Burkhard, D. Schüler, N.M. Probst-Hensch, P.C. Maiorka, N. Baeza, P. Pisani, Y. Yonekawa, M.G. Yasargil, U.M. Lütolf, P. Kleihues, Genetic pathways to glioblastoma, Cancer Res. 64 (2004), https://doi.org/10.1158/0008-5472.CAN-04-1337, 6892 LP – 6899.
[44] S.S.C. Papadopoulos, D.C. Davies, B.A. Bell, Emerging molecular mechanisms of brain tumour oedema, Br. J. Neurosurg. 15 (2001) 101–108, https://doi.org/10.1080/02688690120036775.
[45] S.Y.L. Ang, L. Lee, A.A.Q. See, T.Y. Ang, B.T. Ang, N.K.K. King, Incidence of biomarkers in high-grade gliomas and their impact on survival in a diverse SouthEast Asian cohort - a population-based study, BMC Cancer. 20 (2020) 79, https://doi.org/10.1186/s12885-020-6536-x.
[46] C.L. Gladson, R.A. Prayson, W.M. Liu, The pathobiology of glioma tumors, Annu. Rev. Pathol. Mech. Dis. 5 (2010) 33–50, https://doi.org/10.1146/annurev.pathol.121808.102109.
[47] N.J. Abbott, Dynamics of CNS barriers: evolution, differentiation, and modulation, Cell. Mol. Neurobiol. 25 (2005) 5–23, https://doi.org/10.1007/s10571-004-1374-y.
[48] P. Ballabh, A. Braun, M. Nedergaard, The blood-brain barrier: an overview: structure, regulation, and clinical implications, Neurobiol. Dis. 16 (2004) 1–13, https://doi.org/10.1016/j.nbd.2003.12.016.
[49] C.M. Van Itallie, J.M. Anderson, Claudins and epithelial paracellular transport, Annu. Rev. Physiol. 68 (2006) 403–429, https://doi.org/10.1146/annurev.physiol.68.040104.131404.
[50] C.M. Van Itallie, J. Holmes, A. Bridges, J.L. Gookin, M.R. Coccaro, W. Proctor, O. R. Colegio, J.M. Anderson, The density of small tight junction pores varies among cell types and is increased by expression of claudin-2, J. Cell Sci. 121 (2008) 298–305, https://doi.org/10.1242/jcs.021485.
[51] G. Rascher, A. Fischmann, S. Kröger, F. Duffner, E.-H. Grote, H. Wolburg, Extracellular matrix and the blood-brain barrier in glioblastoma multiforme: spatial segregation of tenascin and agrin, Acta Neuropathol. 104 (2002) 85–91, https://doi.org/10.1007/s00401-002-0534-y.
[52] C.D. Arvanitis, G.B. Ferraro, R.K. Jain, The blood–brain barrier and blood–tumour barrier in brain tumours and metastases, Nat. Rev. Cancer 20 (2020) 26–41, https://doi.org/10.1038/s41568-019-0205-x.
[53] Y. Wang, P. Zhang, N. Xiong, H. Xu, S. Chai, H. Wang, J. Wang, H. Zhao, X. Jiang, P. Fu, W. Xiang, Remodelling and treatment of the blood-brain barrier in glioma, Cancer Manag. Res. 13 (2021) 4217–4232, https://doi.org/10.2147/CMAR.S289020.
[54] S.W. Schneider, T. Ludwig, L. Tatenhorst, S. Braune, H. Oberleithner, V. Senner, W. Paulus, Glioblastoma cells release factors that disrupt blood-brain barrier features, Acta Neuropathol. 107 (2004) 272–276, https://doi.org/10.1007/s00401-003-0811-2.
[55] H. Wolburg, S. Noell, P. Fallier-Becker, A.F. Mack, K. Wolburg-Buchholz, The disturbed blood–brain barrier in human glioblastoma, Mol. Asp. Med. 33 (2012) 579–589, https://doi.org/10.1016/j.mam.2012.02.003.
[56] N.J. Abbott, A.A.K. Patabendige, D.E.M. Dolman, S.R. Yusof, D.J. Begley, Structure and function of the blood–brain barrier, Neurobiol. Dis. 37 (2010) 13–25, https://doi.org/10.1016/j.nbd.2009.07.030.
[57] D. Wang, C. Wang, L. Wang, Y. Chen, A comprehensive review in improving delivery of small-molecule chemotherapeutic agents overcoming the blood-brain/brain tumor barriers for glioblastoma treatment, Drug Deliv. 26 (2019) 551–565, https://doi.org/10.1080/10717544.2019.1622235.
[58] A. Dréan, L. Goldwirt, M. Verreault, M. Canney, C. Schmitt, J. Guehennec, J.-Y. Delattre, A. Carpentier, A. Idbaih, Blood-brain barrier, cytotoxic chemotherapies and glioblastoma, Expert. Rev. Neurother. 16 (2016) 1385–1400, https://doi.org/10.1080/14737175.2016.1202761.
[59] J.P. Fisher, D.C. Adamson, Current FDA-approved therapies for high-grade malignant gliomas, Biomed. 9 (2021), https://doi.org/10.3390/biomedicines9030324.
[60] J. Dirnes, C. Cave, S. Huang, R. Milne, A rapid and systematic review of the effectiveness of temozolomide for the treatment of recurrent malignant glioma, Br. J. Cancer 86 (2002) 501–505, https://doi.org/10.1038/sj.bjc.6600135.
[61] Y. Yan, Z. Xu, S. Dai, L. Qian, L. Sun, Z. Gong, Targeting autophagy to sensitive glioma to temozolomide treatment, J. Exp. Clin. Cancer Res. 35 (2016) 23, https://doi.org/10.1186/s13046-016-0303-5.
[62] T. Kanzawa, J. Bedwell, Y. Kondo, S. Kondo, I.M. Germano, Inhibition of DNA repair for sensitizing resistant glioma cells to temozolomide, J. Neurosurg. 99 (2003) 1047–1052, https://doi.org/10.3171/jns.2003.99.6.1047.
[63] G. Perazzoli, J. Prados, R. Ortiz, O. Caba, L. Cabeza, M. Berdasco, B. Gónzalez, C. Melguizo, Temozolomide resistance in glioblastoma cell lines: implication of MGMT, MMR, P-glycoprotein and CD133 expression, PLoS One 10 (2015), e0140131, https://doi.org/10.1371/journal.pone.0140131.
[64] K. Bourzinah, H. Summers, J. Zhang, M.F.G. Stevens, C.J. Moody, L. Turyanska, N. E. Thomas, P. Gershkovich, M.B. Ashford, E. Virmani, L.C.D. Storer, R. Grundy, T. D. Bradshaw, In search of effective therapies to overcome resistance to Temozolomide in brain tumours, Cancer Drug Resist. 2 (2019) 1018–1031, https://doi.org/10.20517/cdr.2019.84.
[65] S.D. Baker, M. Wirth, P. Statkevich, P. Reidenberg, K. Alton, S.E. Sartorius, M. Dugan, D. Cutler, V. Batra, L.B. Grochow, R.C. Donehower, E.K. Rowinsky, Absorption, Metabolism, and Excretion of ¹⁴C-Temozolomide following Oral Administration to Patients with Advanced Cancer, Clin. Cancer Res. 5 (1999), 309 LP – 317, http://clincancerres.aacrjournals.org/content/5/2/309.abstract.
[66] M.S. Bobola, S.H. Tseng, A. Blank, M.S. Berger, J.R. Silber, Role of O6-methylguanine-DNA methyltransferase in resistance of human brain tumor cell lines to the clinically relevant methylating agents temozolomide and streptozotocin, Clin. Cancer Res. 2 (1996), 735 LP – 741, http://clincancerres.aacrjournals.org/content/2/4/735.abstract.
[67] K. Xu, L. Wang, H.-K.G. Shu, COX-2 overexpression increases malignant potential of human glioma cells through kl1, Oncotarget. 5 (2014) 1241–1252, https://doi.org/10.18632/oncotarget.1570.
[68] M.E. Hegi, A.-C. Diserens, T. Gorlia, M.-F. Hamou, N. de Tribolet, M. Weller, J. M. Kros, J.A. Hainfellner, W. Mason, L. Mariani, J.E.C. Bromberg, P. Hau, R. O. Mirimanoff, J.G. Cairncross, R.C. Janzer, R. Stupp, MGMT gene silencing and benefit from temozolomide in glioblastoma, N. Engl. J. Med. 352 (2005) 997–1003, https://doi.org/10.1056/NEJMoa043331.
[69] S. Jiapaer, T. Furuta, S. Tanaka, T. Kitabayashi, M. Nakada, Potential strategies overcoming the temozolomide resistance for glioblastoma, Neurol. Med. Chir. (Tokyo) 58 (2018) 405–421, https://doi.org/10.2176/nmc.ra.2018-0141.
[70] G.J. Kitange, B.L. Carlson, M.A. Schroeder, P.T. Grogan, J.D. Lamont, P. A. Decker, W. Wu, C.D. James, J.N. Sarkaria, Induction of MGMT expression is associated with temozolomide resistance in glioblastoma xenografts, Neuro. Oncology 11 (2009) 281–291, https://doi.org/10.1215/15228517-2008-096.
[71] E.S. Newlands, M.F.G. Stevens, S.B. Wedge, R.T. Wheelhouse, C. Brock, Temozolomide: a review of its discovery, chemical properties, pre-clinical development and clinical trials, Cancer Treat. Rev. 23 (1997) 35–61, https://doi.org/10.1016/s0305-7372(97)90019-0.
[72] G.V. Koukourakis, V. Kouloulias, G. Zacharias, C. Papadimitriou, P. Pantelakos, G. Maravelis, A. Potiwas, I. Bell, D. Chaldeopoulos, J. Kouvaris, Temozolomide with radiation therapy in high grade brain gliomas: pharmaceuticals consideration and efficacy:a review article, Mol. 14 (2009), https://doi.org/10.3390/molecules14041561.
[73] H. Strobel, T. Baisch, R. Fitzel, K. Schilberg, M.D. Siegelin, G. Karpel-Massler, K.-M. Debatin, M.-A. Westhoff, Temozolomide and other alkylating agents in glioblastoma therapy, Biomed. 7 (2019), https://doi.org/10.3390/biomedicines7020069.

[74] R.E. Kast, Use of FDA approved methamphetamine to allow adjunctive use of methylhaltrexone to mediate core anti-growth factor signaling effects in glioblastoma, J. Neuro-Oncol. 94 (2009) 163–167, https://doi.org/10.1007/s11060-009-9853-y.
[75] S. Ostermann, C. Csajka, Y. Buclin, S. Leyvraz, F. Lejeune, L.A. Decosterd, B. Stupp, Plasma and cerebrospinal fluid population pharmacokinetics of temozolomide in malignant glioma patients, Clin. Cancer Res. 10 (2004), https://doi.org/10.1158/1078-0432.CCR-03-0807, 3728 LP – 3736.
[76] P.S. Yavvari, K. Shetty, K.S. Yadav, Temozolomide nano enabled medicine: promises made by the nanocarriers in glioblastoma therapy, J. Control. Release 336 (2021) 549–571, https://doi.org/10.1016/j.jconrel.2021.07.003.
[77] M.J. Ramalho, M.A.N. Coelho, M.C. Pereira, Chapter 18 - Nanocarriers for the delivery of temozolomide in the treatment of glioblastoma: A review, in: A.M.B. T.-D. and D. of N.N. Grumezescu (Ed.), William Andrew Publishing, 2018, pp. 687–722, https://doi.org/10.1016/B978-0-12-813927-0.00018-1.
[78] Z. Song, X. Huang, J. Wang, F. Cai, P. Zhao, F. Yan, Targeted delivery of liposomal temozolomide enhanced anti-glioblastoma efficacy through ultrasound-mediated blood-brain barrier opening, Pharm. 13 (2021), https://doi.org/10.3390/pharmaceutics13081270.
[79] S.-S. Kim, A. Rait, E. Kim, J. DeMarco, K.F. Pirollo, E.H. Chang, Encapsulation of temozolomide in a tumor targeting nanocomplex enhances anti-cancer efficacy and reduces toxicity in a mouse model of glioblastoma, Cancer Lett. 369 (2015) 250–256, https://doi.org/10.1016/j.canlet.2015.08.022.
[80] Z. Chen, X. Lai, S. Song, X. Zhu, J. Zhu, Nanostructured lipid carriers based temozolomide and gene co-encapsulated nanomedicine for gliomatosis cerebri combination therapy, Drug Deliv. 23 (2016) 1369–1373, https://doi.org/10.3109/10717544.2015.1088857.
[81] M. Wu, Y. Fan, S. Lv, B. Xiao, M. Ye, X. Zhu, Vincristine and temozolomide combined chemotherapy for the treatment of glioma: a comparison of solid lipid nanoparticles and nanostructured lipid carriers for dual drugs delivery, Drug Deliv. 23 (2016) 2720–2725, https://doi.org/10.3109/10717544.2016.1058434.
[82] K. Boussiah, H.S. Summers, M.F.G. Stevens, C.J. Moody, N.R. Thomas, P. Gershkovich, N. Weston, M.B. Ashford, T.D. Bradshaw, L. Turyanska, Delivery of temozolomide and N3-propargyl analog to brain tumors using an apoferritin nanocage, ACS Appl. Mater. Interfaces 12 (2020) 12669–12617, https://doi.org/10.1021/acsami.9b21518.
[83] C.-Y. Lin, R.-J. Li, C.-Y. Huang, K.-C. Wei, P.-Y. Chen, Controlled release of liposome-encapsulated temozolomide for brain tumour treatment by convection-enhanced delivery, J. Drug Target. 26 (2018) 325–332, https://doi.org/10.1080/1061186X.2017.1379526.
[84] Y. Peng, J. Huang, H. Xiao, T. Wu, X. Shuai, Codelivery of temozolomide and siRNA with polymeric nanocarrier for effective glioma treatment, Int. J. Nanomedicine 13 (2018) 3467–3480, https://doi.org/10.2147/IJN.S164611.
[85] A.K. Sharma, L. Gupta, H. Sahu, A. Qayum, S.K. Singh, K.T. Nakhate, U. Gupta Ajazuddin, Chitosan engineered PAMAM dendrimers as nanoconstructs for the enhanced anti-cancer potential and improved in vivo brain pharmacokinetics of temozolomide, Pharm. Res. 35 (2018) 9, https://doi.org/10.1007/s11095-017-2224-y.
[86] J.S. Ananta, B. Paulmurugan, T.F. Massoud, Temozolomide-loaded PLGA nanoparticles to treat glioblastoma cells: a biophysical and cell culture evaluation, Neurol. Res. 38 (2016) 51–59, https://doi.org/10.1080/01616412.2015.1120925.
[87] M.M. Nordling-David, R. Yaffe, D. Guez, H. Meirow, D. Last, E. Grad, S. Salomon, S. Sharabi, Y. Levi-Kalisman, G. Golomb, Y. Mardor, Liposomal temozolomide drug delivery using convection enhanced delivery, J. Control. Release 261 (2017) 138–146, https://doi.org/10.1016/j.jconrel.2017.06.028.
[88] C.Y. Lee, I.H. Ooi, Preparation of temozolomide-loaded nanoparticles for glioblastoma multiforme targeting—ideal versus reality, Pharm. 9 (2016), https://doi.org/10.3390/ph9030054.
[89] I. Metcoglu, A. Erdemir, Genistein and temozolomide-loaded polymeric nanoparticles: a synergistic approach for improved anti-tumor efficacy against glioblastoma, Process Biochem. 110 (2021) 9–18, https://doi.org/10.1016/j.procbio.2021.07.015.
[90] R. Duwa, A. Banstola, F. Emami, J.-H. Jeong, S. Lee, S. Yook, Cetuximab conjugated temozolomide-loaded poly (lactic-co-glycolic acid) nanoparticles for targeted nanomedicine in EGFR overexpressing cancer cells, J. Drug Deliv. Sci. Technol. 60 (2020), 101928, https://doi.org/10.1016/j.jddst.2020.101928.
[91] A. Arcelli, S. Palchetti, L. Digiacomo, D. Pozzi, A.L. Capriotti, L. Frati, M.A. Oliva, G. Tsaousi, R. Riza, I. Screpanti, M. Mahmoudi, G. Caracciolo, Brain targeting by liposome–biomolecular corona boosts anticancer efficacy of temozolomide in glioblastoma cells, ACS Chem. Neurosci. 9 (2018) 3166–3174, https://doi.org/10.1021/acschemneuro.8b00339.
[92] C. Nie, X. Chu, Q. Pan, J. Zhang, Y. Hu, J. Yi, M. He, M. He, T. Chen, X. Chu, Engineering a biodegradable nanocarrier for enhancing the response of T98G cells to temozolomide, ACS Appl. Bio Mater. 3 (2020) 3337–3344, https://doi.org/10.1021/acsabm.0c00253.
[93] A. Bertucci, E.A. Prasetyanto, D. Septiadi, A. Manicardi, E. Brognara, R. Gambari, R. Corradini, L. De Cola, Combined delivery of temozolomide and anti-miR221 PNA using mesoporous silica nanoparticles induces apoptosis in resistant glioma cells, Small. 11 (2015) 5687–5695, https://doi.org/10.1002/smll.201501540.
[94] P. Zhang, M. Tang, Q. Huang, G. Zhao, N. Huang, X. Zhang, Y. Tan, Y. Cheng, Combination of 3-methyladenine therapy and Asn-Gly-Arg (NGR)-modified mesoporous silica nanoparticles loaded with temozolomide for glioma therapy in vitro, Biochem. Biophys. Res. Commun. 509 (2019) 549–556, https://doi.org/10.1016/j.bbrc.2018.12.158.
[95] X. Zeng, Q. Wang, X. Tan, L. Jia, Y. Li, M. Hu, Z. Zhang, X. Bai, Y. Zhu, X. Yang, Mild thermotherapy and hyperbaric oxygen enhance sensitivity of TMZ/PSi nanoparticles via decreasing the stemness in glioma, J. Nanobiotechnol. 17 (2019) 47, https://doi.org/10.1186/s12951-019-0483-1.
[96] Y. Sun, L. Zheng, Y. Yang, X. Qian, T. Fu, X. Li, Z. Yang, H. Yan, C. Cui, W. Tan, Metal–organic framework nanocarriers for drug delivery in biomedical applications, Nano-Micro. Lett. 12 (2020) 103, https://doi.org/10.1007/s40820-020-00423-3.
[97] X. Wan, C. Li, J. Gu, J. Qian, J. Zhu, J. Wang, Y. Li, J. Zhang, H. Chen, C. Luo, Accurately controlled delivery of temozolomide by biomimetic DHA-66-NHS through ultrasound to enhance the antitumor efficacy and attenuate the toxicity for treatment of malignant glioma, Int. J. Nanomedicine 16 (2021) 1995.
[98] L. Polvirenti, F. Monforte, F. Lo Presti, G. Li Volti, G. Carota, F. Sinatra, G. Bongiorno, G. Mannino, M.T. Cambria, G.G. Condorelli, Synthesis of MIL-modified Fe3O4 magnetic nanoparticles for enhancing uptake and efficiency of temozolomide in glioblastoma treatment, Int. J. Mol. Sci. 23 (2022), https://doi.org/10.3390/ijms23052874.
[99] R. Patil, J. Portilla-Arias, H. Ding, S. Inoue, R. Konda, J. Hu, K.A. Wawrowsky, P. K. Shin, K.L. Black, E. Holler, J.Y. Ljubimova, Temozolomide delivery to tumor cells by a multifunctional nano vehicle based on poly(β-L-malic acid), Pharm. Res. 27 (2010) 2317–2329, https://doi.org/10.1007/s11095-010-0091-6.
[100] H.-Y. Cho, W. Wang, N. Jhaveri, D.J. Lee, N. Sharma, L. Dubeau, A.H. Schönthal, F.M. Hofman, T.C. Chen, NEO212, temozolomide conjugated to perillyl alcohol, is a novel drug for effective treatment of a broad range of temozolomide-resistant gliomas, Mol. Cancer Ther. 13 (2014), https://doi.org/10.1158/1535-7163.MCT-13-0964, 2004 LP – 2017.
[101] M. Durywalska, P. Strup, J.A. Melton-Witt, A. Hasa-Moreno, S.E. Farias, M. Galindo Casas, K. Delaria, V. Lai, K. Poulsen, J. Sutton, G. Bolton, D. Zhou, L. Moise, R. Dushin, T.-T. Tran, S.-H. Liu, M. Rickert, D. Foletti, D.L. Shelton, J. Pons, A. Rajpal, Site-dependent degradation of a non-cleavable Auristatin-based linker-payload in rodent plasma and its effect on ADC efficacy, PLoS One 10 (2015), e0132282, https://doi.org/10.1371/journal.pone.0132282.
[102] D.J. Marshall, S.S. Harried, J.L. Murphy, C.A. Hull, M.S. Shekhani, C. Pors, C. A. Lyons, A. Chillemi, F. Malavasi, H.L. Pearce, J.S. Thorson, J.R. Prudent, Extracellular antibody drug conjugates exploiting the proximity of two proteins, Mol. Ther. 24 (2016) 1760–1770, https://doi.org/10.1038/mt.2016.119.
[103] H. Donaghy, Effects of antibody, drug and linker on the preclinical and clinical toxicities of antibody-drug conjugates, MAbs. 8 (2016) 659–671, https://doi.org/10.1080/19420862.2016.1158829.
[104] J.R. McCombs, S.C. Owen, Antibody drug conjugates: design and selection of linker, payload and conjugation chemistry, AAPS J. 17 (2015) 339–351, https://doi.org/10.1208/s12248-014-9710-8.
[105] M. Hasan, R.K. Lesk, R.E. Stratford, D.F. Ziotos, P.A. Witt-Enderby, Drug conjugates—an emerging approach to treat breast cancer, Pharmacol. Res. Perspect. 6 (2018), e00417, https://doi.org/10.1002/prp2.417.
[106] L. Ducry, B. Stump, Antibody–drug conjugates: linking cytotoxic payloads to monoclonal antibodies, Bioconjug. Chem. 21 (2010) 5–13, https://doi.org/10.1021/bc900211f.
[107] A.A. Kale, V.P. Torchilin, Design, synthesis, and characterization of pH-sensitive PEG–PE conjugates for stimuli-sensitive pharmaceutical nanocarriers: the effect of substitutes at the hydrazone linkage on the pH stability of PEG–PE conjugates, Bioconjug. Chem. 18 (2007) 363–370, https://doi.org/10.1021/bc060328t.
[108] E.R. Lowe, S.G. Anema, A. Bienvenue, M.J. Boland, L.K. Creamer, R. Jiménez-Flores, Heat-induced redistribution of disulfide bonds in milk proteins. 2. Disulfide bonding patterns between bovine β-Lactoglobulin and κ-casein, J. Agric. Food Chem. 52 (2004) 7669–7680, https://doi.org/10.1021/jf049124x.
[109] K. Nepali, S. Sharma, M. Sharma, P.M.S. Bedi, K.L. Dhar, Rational approaches, design strategies, structure activity relationship and mechanistic insights for anticancer hybrids, Eur. J. Med. Chem. 77 (2014) 422–487, https://doi.org/10.1016/j.ejmech.2014.03.018.
[110] J. Khandare, T. Minko, Polymer–drug conjugates: progress in polymeric prodrugs, Prog. Polym. Sci. 31 (2006) 359–397, https://doi.org/10.1016/j.progpolymsci.2005.09.004.
[111] I. Ekladious, Y.L. Colson, M.W. Grinstaff, Polymer–drug conjugate therapeutics: advances, insights and prospects, Nat. Rev. Drug Discov. 18 (2019) 273–294, https://doi.org/10.1038/s41573-018-0005-0.
[112] I. Ansari, P. Singh, A. Mittal, R.I. Mahato, D. Chitkara, 2,2-Bis(hydroxymethyl) propionic acid based cyclic carbonate monomers and their (co)polymers as advanced materials for biomedical applications, Biomaterials. 275 (2021), 120953, https://doi.org/10.1016/j.biomaterials.2021.120953.
[113] S. Wadhwa, R.J. Mumper, Polymer-drug conjugates for anticancer drug delivery, Crit. Rev. Ther. Drug Carrier Syst. 32 (2015) 215–245, https://doi.org/10.1615/critrevtherdrugcarriersyst.2015010174.
[114] A. Duro-Castano, J. Movellan, M.J. Vicent, Smart branched polymer drug conjugates as nano-sized drug delivery systems, Biomater. Sci. 3 (2015) 1321–1334, https://doi.org/10.1039/C5BM00104H.
[115] M.L. Girase, P.G. Patil, P.P. Ige, Polymer-drug conjugates as nanomedicine: a review, Int. J. Polym. Mater. Polym. Biomater. 69 (2020) 990–1014, https://doi.org/10.1080/00914037.2019.1653748.
[116] S. Alven, X. Nqoro, B. Buyana, B.A. Aderibigbe, Polymer-drug conjugate, a potential therapeutic to combat breast and lung cancer, Pharm. 12 (2020), https://doi.org/10.3390/pharmaceutics12050908.
[117] C. Fante, F. Greco, in: I.F. Uchegbu, A.G. Schätzlein, W.P. Cheng, A. Lalatsa (Eds.), Polymer-Drug Conjugates BT - Fundamentals of Pharmaceutical Nanoscience, Springer, New York, New York, NY, 2013, pp. 159–182, https://doi.org/10.1007/978-1-4614-9161-4_7.

[118] R. Duncan, M.J. Vicent, F. Greco, R.I. Nicholson, Polymer-drug conjugates: towards a novel approach for the treatment of endrocine-related cancer, Endocr. Relat. Cancer 12 (Suppl. 1) (2005) S189–S199, https://doi.org/10.1677/erc.1.01045.

[119] F. Dilnawaz, S.K. Sahoo, Enhanced accumulation of curcumin and temozolomide loaded magnetic nanoparticles executes profound cytotoxic effect in glioblastoma spheroid model, Eur. J. Pharm. Biopharm. 85 (2013) 452–462, https://doi.org/10.1016/j.ejpb.2013.07.013.

[120] M. Chang, F. Zhang, T. Wei, T. Fan, Y. Guan, G. Lin, W. Shao, Smart linkers in polymer-drug conjugates for tumor-targeted delivery, J. Drug Target. 24 (2016) 475–491, https://doi.org/10.3109/1061186X.2015.1108724.

[121] L. Wang, S. Tang, Y. Yu, Y. Lv, A. Wang, X. Yan, N. Li, C. Sha, K. Sun, Y. Li, Intranasal delivery of temozolomide-conjugated gold nanoparticles functionalized with anti-EphA3 for glioblastoma targeting, Mol. Pharm. 18 (2021) 915–927, https://doi.org/10.1021/acs.molpharmaceut.0c00911.

[122] K. Xu, L. Zhang, Y. Gu, H. Yang, B. Du, H. Liu, Y. Li, Increased the TMZ concentration in brain by poly(2-ethyl-2-oxazoline) conjugated temozolomide prodrug micelles for glioblastoma treatment, Eur. Polym. J. 145 (2021), 110232, https://doi.org/10.1016/j.eurpolymj.2020.110232.

[123] M. Skinner, S.M. Ward, T. Emrick, Versatile synthesis of polymer-temozolomide conjugates, ACS Macro Lett. 6 (2017) 215–218, https://doi.org/10.1021/acsmacrolett.7b00007.

[124] K. Du, Q. Xia, H. Heng, F. Feng, Temozolomide–doxorubicin conjugate as a double intercalating agent and delivery by apoferritin for glioblastoma chemotherapy, ACS Appl. Mater. Interfaces 12 (2020) 34599–34609, https://doi.org/10.1021/acsami.0c08531.

[125] M. Park, C. Song, H. Yoon, K.-H. Choi, Double blockade of glioma cell proliferation and migration by temozolomide conjugated with NPPB, a chloride channel blocker, ACS Chem. Neurosci. 7 (2016) 275–285, https://doi.org/10.1021/acschemneuro.5b00178.

[126] G. Silva-Hirschberg, H. Hartman, S. Stark, S. Swenson, R.O. Mirza, M.A. Davies, T.C. Chen, A.H. Schonthal, Cytotoxic impact of a perillyl alcohol–temozolomide conjugate, NEO212, on cutaneous T-cell lymphoma in vitro, Ther. Adv. Med. Oncol. 11 (2019), https://doi.org/10.1177/1758835919891567, 1758835919891567.

[127] X. Song, L. Xie, X. Wang, Q. Zeng, T.C. Chen, W. Wang, X. Song, Temozolomide-perillyl alcohol conjugate induced reactive oxygen species accumulation contributes to its cytotoxicity against non-small cell lung cancer, Sci. Rep. 6 (2016) 22762, https://doi.org/10.1038/srep22762.

[128] T.C. Chen, H.-Y. Cho, W. Wang, S.J. Wenzel, A. Singh, J. Nguyen, F.M. Hofman, A. H. Schonthal, Chemotherapeutic effect of a novel temozolomide analog on nasopharyngeal carcinoma in vitro and in vivo, J. Biomed. Sci. 22 (2015) 71, https://doi.org/10.1186/s12929-015-0175-6.

[129] M. Chang, X. Song, X. Geng, X. Wang, W. Wang, T.C. Chen, L. Xie, X. Song, Temozolomide-Perillyl alcohol conjugate impairs Mitophagy flux by inducing lysosomal dysfunction in non-small cell lung Cancer cells and sensitizes them to irradiation, J. Exp. Clin. Cancer Res. 37 (2018) 250, https://doi.org/10.1186/s13046-018-0905-1.

[130] N.I. Marín-Ramos, N. Jhaveri, T.Z. Thein, R.A. Payngor, T.C. Chen, F.M. Hofman, NEO212, a conjugate of temozolomide and perillyl alcohol, blocks the endothelial-to-mesenchymal transition in tumor-associated brain endothelial cells in glioblastoma, Cancer Lett. 442 (2019) 170–180, https://doi.org/10.1016/j.canlet.2018.10.034.

[131] L. Chu, A. Wang, L. Ni, X. Yan, Y. Song, M. Zhao, K. Sun, H. Mu, S. Liu, Z. Wu, C. Zhang, Nose-to-brain delivery of temozolomide-loaded PLGA nanoparticles functionalized with anti-EPHA3 for glioblastoma targeting, Drug Deliv. 25 (2018) 1634–1641, https://doi.org/10.1080/10717544.2018.1494228.

[132] R. Rai, M. Banerjee, D.H. Wong, E. McCullagh, A. Gupta, S. Tripathi, E. Riquelme, R. Jangir, S. Yadav, M. Raja, P. Melkani, V. Dixit, U. Patil, R. Shrivastava, S. Muddyu, F. Olivares, J. Guerrero, A. Surya, S.M. Pham, S. Bernales, A.A. Protter, D.T. Hung, S. Chakravarty, Temozolomide analogs with improved brain/plasma ratios – exploring the possibility of enhancing the therapeutic index of temozolomide, Bioorg. Med. Chem. Lett. 26 (2016) 5103–5109, https://doi.org/10.1016/j.bmcl.2016.08.064.

[133] L. Shervington, O. Ingham, A. Shervington, A novel series of phenolic temozolomide (TMZ) esters with 4 to 5-fold increased potency, compared to TMZ, against glioma cells irrespective of MGMT expression, BSC Adv. 10 (2020) 17561–17570, https://doi.org/10.1039/D0RA02886G.